U.S. Department
of Transportation
Federal Railroad
Administration

Office of Research,
Development and Technology
Washington, DC 20590

Relationship of Inspection Methods to Ballast Degradation Models: Phase I

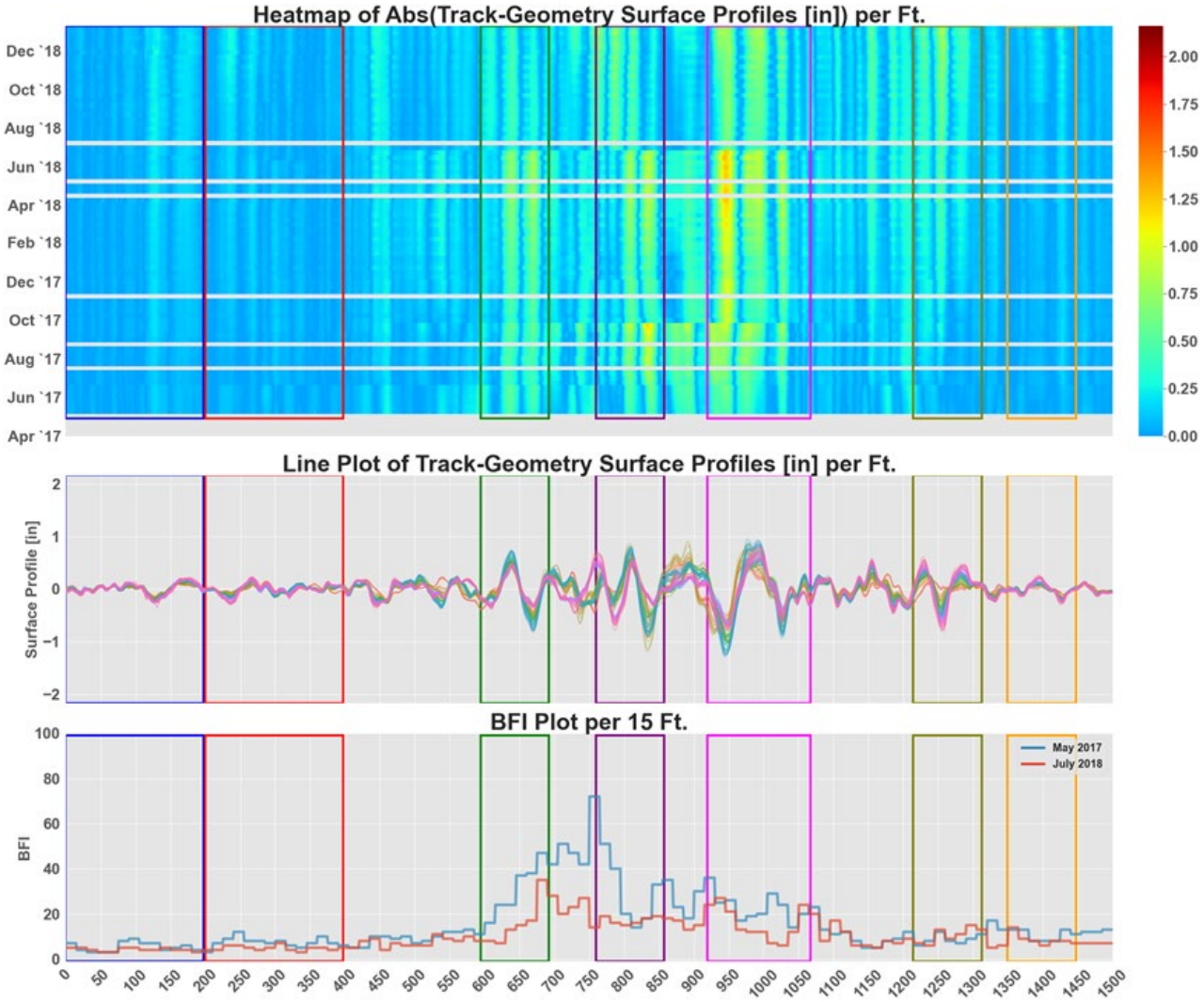

REPORT DOCUMENTATION PAGE

Form Approved
OMB No. 0704-0188

1. REPORT DATE *(DD-MM-YYYY*	**2. REPORT TYPE**	**3. DATES COVERED** *(From - To)*
January 2023	Technical Report	August 1, 2020–July 31, 2021

4. TITLE AND SUBTITLE
Relationship of Inspection Methods to Ballast Degradation Models: Phase I

5a. CONTRACT NUMBER
DTFR5311D00008L

5b. GRANT NUMBER

5c. PROGRAM ELEMENT NUMBER

6. AUTHOR(S)
Stephen Wilk – 0000-0001-5347-569X
Dingqing Li – 0000-0001-5891-839X

5d. PROJECT NUMBER

5e. TASK NUMBER
TO 693JJ620F000030

5f. WORK UNIT NUMBER

7. PERFORMING ORGANIZATION NAME(S) AND ADDRESS(ES)
Transportation Technology Center, Inc.
55500 DOT Road
Pueblo, CO 81001

8. PERFORMING ORGANIZATION REPORT NUMBER

9. SPONSORING/MONITORING AGENCY NAME(S) AND ADDRESS(ES)
U.S. Department of Transportation
Federal Railroad Administration
Office of Railroad Policy and Development
Office of Research, Data and Innovation
Washington, DC 20590

10. SPONSOR/MONITOR'S ACRONYM(S)

11. SPONSOR/MONITOR'S REPORT NUMBER(S)
DOT/FRA/ORD-23/04

12. DISTRIBUTION/AVAILABILITY STATEMENT
This document is available to the public through the FRA website.

13. SUPPLEMENTARY NOTES
COR: Hugh Thompson

14. ABSTRACT

This report compiles the first phase of a Federal Railroad Administration (FRA)-sponsored project to evaluate lateral ballast behavior and how mechanics-based track geometry deterioration models forecast field behavior. The lateral ballast behavior section analyzed historical and recent single tie push test (STPT) results, compared the influence various ballast parameters, and evaluated the potential ability of a model to estimate lateral track strength from outputs of track inspection vehicles. The results suggest that a track location could eventually be placed into broad risk categories based on the measurable ballast condition.

The second aspect investigated the ability of mechanics-based track geometry deterioration models to forecast field behavior. Field data that included aligned track geometry records and ground penetrating radar (GPR) was analyzed and relationships were developed between the ballast condition and track geometry deterioration rate. The existing mechanics-based models were compared against the statistically fit models and recommendations on how to improve the models were made.

15. SUBJECT TERMS
Ballast, track geometry, lateral strength, lateral resistance, single tie push test, STPT, ballast condition, forecasting, track, ground penetrating radar, GPR

16. SECURITY CLASSIFICATION OF:			**17. LIMITATION OF ABSTRACT**	**18. NUMBER OF PAGES**	**19a. NAME OF RESPONSIBLE PERSON**
a. REPORT	**b. ABSTRACT**	**c. THIS PAGE**			Stephen Wilk, Senior Engineer
Unclassified	Unclassified	Unclassified		142	**19b. TELEPHONE NUMBER** *(Include area code)* 719- 584-0736

Standard Form 298 (Rev. 8/98)
Prescribed by ANSI Std. Z39.18

METRIC/ENGLISH CONVERSION FACTORS

ENGLISH TO METRIC

LENGTH (APPROXIMATE)

1 inch (in)	=	2.5 centimeters (cm)
1 foot (ft)	=	30 centimeters (cm)
1 yard (yd)	=	0.9 meter (m)
1 mile (mi)	=	1.6 kilometers (km)

AREA (APPROXIMATE)

1 square inch (sq in, in^2)	=	6.5 square centimeters (cm^2)
1 square foot (sq ft, ft^2)	=	0.09 square meter (m^2)
1 square yard (sq yd, yd^2)	=	0.8 square meter (m^2)
1 square mile (sq mi, mi^2)	=	2.6 square kilometers (km^2)
1 acre = 0.4 hectare (he)	=	4,000 square meters (m^2)

MASS - WEIGHT (APPROXIMATE)

1 ounce (oz)	=	28 grams (gm)
1 pound (lb)	=	0.45 kilogram (kg)
1 short ton = 2,000 pounds (lb)	=	0.9 tonne (t)

VOLUME (APPROXIMATE)

1 teaspoon (tsp)	=	5 milliliters (ml)
1 tablespoon (tbsp)	=	15 milliliters (ml)
1 fluid ounce (fl oz)	=	30 milliliters (ml)
1 cup (c)	=	0.24 liter (l)
1 pint (pt)	=	0.47 liter (l)
1 quart (qt)	=	0.96 liter (l)
1 gallon (gal)	=	3.8 liters (l)
1 cubic foot (cu ft, ft^3)	=	0.03 cubic meter (m^3)
1 cubic yard (cu yd, yd^3)	=	0.76 cubic meter (m^3)

TEMPERATURE (EXACT)

[(x-32)(5/9)] °F = y °C

METRIC TO ENGLISH

LENGTH (APPROXIMATE)

1 millimeter (mm)	=	0.04 inch (in)
1 centimeter (cm)	=	0.4 inch (in)
1 meter (m)	=	3.3 feet (ft)
1 meter (m)	=	1.1 yards (yd)
1 kilometer (km)	=	0.6 mile (mi)

AREA (APPROXIMATE)

1 square centimeter (cm^2)	=	0.16 square inch (sq in, in^2)
1 square meter (m^2)	=	1.2 square yards (sq yd, yd^2)
1 square kilometer (km^2)	=	0.4 square mile (sq mi, mi^2)
10,000 square meters (m^2)	=	1 hectare (ha) = 2.5 acres

MASS - WEIGHT (APPROXIMATE)

1 gram (gm)	=	0.036 ounce (oz)
1 kilogram (kg)	=	2.2 pounds (lb)
1 tonne (t)	=	1,000 kilograms (kg)
	=	1.1 short tons

VOLUME (APPROXIMATE)

1 milliliter (ml)	=	0.03 fluid ounce (fl oz)
1 liter (l)	=	2.1 pints (pt)
1 liter (l)	=	1.06 quarts (qt)
1 liter (l)	=	0.26 gallon (gal)
1 cubic meter (m^3)	=	36 cubic feet (cu ft, ft^3)
1 cubic meter (m^3)	=	1.3 cubic yards (cu yd, yd^3)

TEMPERATURE (EXACT)

[(9/5) y + 32] °C = x °F

QUICK INCH - CENTIMETER LENGTH CONVERSION

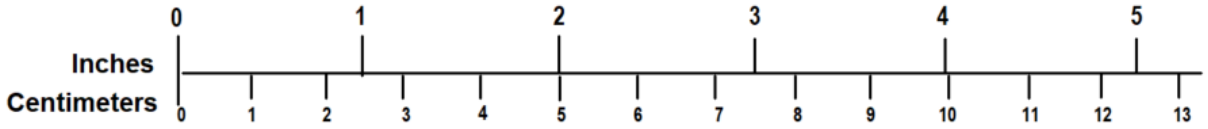

QUICK FAHRENHEIT - CELSIUS TEMPERATURE CONVERSION

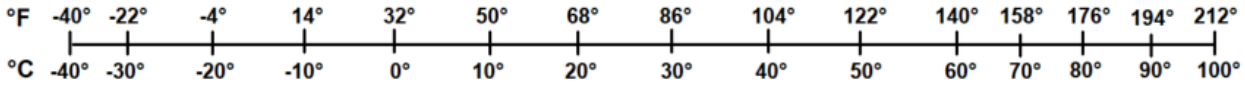

For more exact and or other conversion factors, see NIST Miscellaneous Publication 286, Units of Weights and Measures. Price $2.50 SD Catalog No. C13 10286

Updated 6/17/98

Contents

Illustrations

Tables

Executive Summary

Forecasting ballast-induced track geometry degradation or loss of stability in a ballast section is a difficult task because of complex ballast degradation mechanisms and challenges characterizing the ballast in a manner that can accurately forecast settlement. Multiple mechanics-based track geometry degradation models exist, including models previously developed by Transportation Technology Center, Inc. (TTCI), but these models have not been updated recently and do not incorporate current principles in the understanding of fundamental ballast behavior, ballast inspection technologies, and data analytics. From August 1, 2020, to July 31, 2021, the Federal Railroad Administration (FRA) requested that TTCI build on and extend earlier work on mechanics-based ballast condition forecasting models to support improved safety and reliability of ballast tracks. This work took place at the Transportation Technology Center (TTC).

The goal of this project was to update previous mechanics-based models so that the model inputs align with outputs from the inspection technologies that are either currently in use or in development. The updated model(s) will be used to help develop indicators of track reliability and potentially identify locations of high risk of degradation or failure.

Researchers expect a general improvement of the ability to forecast track geometry behavior. This could include both short-term risk assessments and projections on how track behavior may change depending on ballast maintenance and long-term forecasts to incorporate changes in track structure, tonnage, or climate.

The Phase I portion of this project involved investigating lateral ballast behavior, analyzing field data, and applying existing mechanics-based track geometry deterioration models to the analyzed field data. The following information describes a high-level summary from each of these tasks.

The lateral ballast behavior task investigated the ability of track inspection vehicle ballast condition outputs to estimate lateral tie strength. The results of the lateral ballast behavior task showed that multiple parameters including, but not necessarily limited to, ballast density, ballast shape characteristics, ballast shoulder width, ballast crib height, tie type, tie-ballast interface, and maintenance can influence the lateral tie strength of clean ballast. Risk-based assessments could be made using general knowledge of the ballast parameters, but more work is required before forecasting models can be used with high confidence.

The field data analysis reviewed track geometry and ground penetrating radar (GPR) records at multiple locations within a single Class I track subdivision. The goal of this analysis was to 1) understand key parameters that affect track geometry degradation, 2) develop relationships for future projections, and 3) assess parameters and trends that could be incorporated into a forecasting model.

The results showed that relationships between track geometry degradation and the Ballast Fouling Index (BFI) can be developed based on the collected field data. In addition, unique statistical curves appear to exist for each track section. These unique curves for each specific track section are likely due to the unique ballast maintenance history, and also possibly local variations in drainage, subgrade, tonnage, and tie type. The locations where the track geometry degradation was vastly over- or under-projected from the BFI could be explained through the parameters that characterized the track roughness, but more work is needed to investigate the meaning behind these potential trends. In addition, most track geometry degradation trends were

linear or close enough to assume a linear trend and the post-surfacing track geometry state could be estimated based on the pre-surfacing track geometry state.

The mechanics-based model development aspect involved compiling existing track geometry deterioration models and demonstrating their ability to project future track geometry conditions by comparing the projections versus field data results. The goal of this analysis was to gain a current assessment of the ability of these models to project future track geometry conditions and how the models can be improved in the future. The end objective is to develop track geometry forecasting models robust enough to perform: 1) short-term risk assessments on current track risk, 2) medium-term projections on how track behavior may change depending on ballast maintenance, and 3) long-term forecasts to incorporate potential changes in track structure, tonnage, and/or climate.

The results showed that each of the three previously developed models were significantly different from each other in terms of ability and scope. For example, one model projected the range in behavior at a specific location due to the range of possible moisture levels at that location while another model projected the median track response of an entire track section depending on the climate region. The future forecasting model would aim to incorporate both of those factors, as well as the variation in the median response of a specific track section due to climate differences and the variation of response at a specific location due to varying site-specific moisture levels, along with other important factors. It is envisioned that a forecasting model could initially give broad projections based on track structure, tonnage, climate, and other potential factors. The projected information could be useful for forecasting at a location with little data or exploring how changes of these factors (e.g., tie type) would affect track geometry degradation. Then, eventually, as track data is collected and analyzed, the model could be developed into a site-specific model based on statistic fits of the track section and even potentially project future behavior at highly localized, high-risk locations.

1. Introduction

Forecasting ballast-induced track geometry degradation or loss of stability in a ballast section is a difficult task because of the complex ballast degradation mechanisms and challenges that characterize the ballast to accurately forecast settlement. Multiple mechanics-based track geometry degradation models exist, including models previously developed by Transportation Technology Center, Inc. (TTCI), but these models have not been updated recently and do not incorporate current principles in the understanding of fundamental ballast behavior, ballast inspection technologies, and data analytics. From August 1, 2020, to July 31, 2021, the Federal Railroad Administration (FRA) requested that TTCI build on and extend earlier work on mechanics-based ballast condition forecasting models to support improved safety and reliability of ballast tracks.

The goal of this project was to update previous mechanics-based models so that the model inputs align with outputs from the inspection technologies that are either currently in use or in development. The updated model(s) will be used to help develop indicators of track reliability and potentially identify locations of high risk of degradation or failure.

The potential outcome of this research is a general improvement of the ability to forecast track geometry behavior. This could include short-term risk assessments and projections on how track behavior may change depending on ballast maintenance to long-term forecasts to incorporate changes in track structure, tonnage, or climate.

1.1 Background

Forecasting ballast-induced track geometry degradation is a difficult task because of the complex ballast degradation mechanism and difficulty characterizing the ballast. Multiple mechanics-based track geometry degradation models exist, including previous TTCI-developed models, but these models have not been updated, and they do not incorporate significant recent improvements in understanding fundamental ballast behavior, ballast inspection technologies, and data analytics.

This report summarizes the results from mechanics-based track geometry deterioration models so that the model inputs align with outputs from the inspection technologies that are either currently used or currently in development. This research will potentially improve the ability to forecast track geometry behavior and could include short-term risk assessments, projections on how track behavior may change depending on ballast maintenance, and long-term forecasts to incorporate changes in track structure, tonnage, or climate.

1.2 Objectives

The Phase I work involved two different topics: lateral ballast behavior and track geometry deterioration behavior. The objectives and scope of these two projects will be discussed separately in this report.

The objectives of the lateral ballast behavior project included:

- Improving the understanding of how lateral track strength is related to variables such as ballast density, ballast fine levels, track modulus, and shoulder width

- Performing a literature review of previous single tie push tests (STPTs) and categorizing the results based on ballast conditions such as ballast density, ballast fine levels, moisture, and track modulus
- Performing additional measurements alongside an existing lateral strength test plan that is led by the Association of American Railroads (AAR) under the Strategic Research Initiatives (SRI) program. These additional measurements include track modulus and ballast modulus
- Conducting statistical correlation analyses to compare the influence of the various ballast parameters
- Determining the potential use of ballast inspection technologies to estimate lateral track strength

The objectives of the track geometry deterioration behavior, which incorporate both field data collection and mechanics-based model forecasting, included:

- Providing a background of existing ballast testing literature, categorizing the parameters that influence ballast performance and relating those parameters to current inspection technology outputs
- Providing a background of existing track geometry deterioration models with an emphasis on mechanics-based models
- Collecting and processing FRA-provided field data
- Analyzing field data using available track geometry degradation techniques and comparing track geometry trends with available parameters such as BFI and others
- Conducting an analysis to determine the ability to forecast track geometry degradation using the data available from track-based inspection vehicles
- Demonstrating how each mechanics-based model compares to field behavior

1.3 Overall Approach

This project used multiple approaches including a literature review, field testing, computer modeling, and data analytics. The research team used literature to compile and analyze data and mechanics-based models. Field testing was used to expand the dataset for analysis and test the capabilities of new inspection technologies. Computer models implemented the mechanics-based models to compare the model projections against field behavior and better understand model performance. Using data analytics allowed the team to process large datasets gathered from inspection technologies and develop forecasting models based on this information. In addition, the work was done in conjunction with an existing AAR SRI program project.

1.4 Scope

The scope of the lateral ballast behavior project included collecting additional data to expand on the lateral ballast behavior test being conducted by the AAR SRI program. This additional data included track modulus from AAR's Track Loading Vehicle (TLV) and ballast modulus from third-party contractors. The data analysis included a comparison of the lateral strength with all

relevant ballast parameters and comparing them to historical tests. Lastly, this project explored how current ballast inspection technologies could be used to help estimate lateral tie strength.

The scope of the track geometry deterioration project includes a comprehensive background on the topics that would be relevant to the field data analysis and mechanic-based model demonstration. This included, but was not limited to, fundamental ballast behavior and an introduction into track geometry representations. The scope of the field analysis was, first, to determine the ability to forecast track geometry deterioration using basic correlation and regression analysis. This included developing projection models and determining if patterns existed in the outlier data. The second part of the scope was to generalize the track geometry behavior so it can be simplified for forecasting models. The scope of the model demonstration was to test the general attributes of the mechanics-based models and recommend improvements.

Future phases of the project are planned to expand on Phase I with field tests, additional field data analysis, and forecasting model development.

1.5 Organization of the Report

Phase I contains six sections as briefly described below.

Section 1 introduces the work performed during this project.

Section 2 contains all the lateral ballast behavior topics and is considered a completely independent section from the remainder of the report. This includes a background and introduction to the test matrix, tie push results, relationships with additional parameters, and discussion on vertical versus lateral behavior and how current inspection methods can characterize important lateral strength parameters.

Section 3 provides all the necessary background information to interpret the field data analysis and mechanics-based model demonstration. This information includes a full background of fundamental ballast behavior, track geometry representation, and existing track geometry deterioration models.

Section 4 consists of the field data analysis. This includes details on the data processing procedures, BFI-track geometry degradation regression curves, correlations with additional parameters, outlier and pattern analysis, and maintenance and surfacing.

Section 5 includes the model demonstration of the mechanistic models introduced in Section 3 with the field data analyzed in Section 4. A discussion of the model performance and future recommendations are also included.

Section 6 summarizes the results and conclusions.

2. Lateral Ballast Behavior

The goal of the lateral ballast behavior testing was to improve the understanding of how lateral track strength is related to variables such as ballast density, ballast fine levels, track modulus, and shoulder width. This may improve estimates of lateral track strength and identify at-risk conditions for track buckling from ballast condition assessments that are already being collected in track-based inspection devices for general track health assessment and track geometry degradation.

2.1 Introduction to Lateral Track Strength

With the widespread replacement of jointed rail with continuously welded rail (CWR) in the late 20th century, the ability for track to resist lateral movement and track buckling became important. When the rail temperature increases to a high enough level from the rail neutral temperature (RNT), or no-thermal stress temperature, compressive thermal stresses can cause the track to move laterally or even "buckle" outwards. Figure 1 shows an example of a track buckle. It can occur when the driving lateral forces from the track (thermal stress and sometimes vehicle-induced stresses) exceeds the resisting forces from the track structure. One of the important regions to resist lateral failure is the tie-ballast interface.

Figure 1: Photograph of a Symmetric Track Buckle

One of the early identifying factors of reduced lateral resistance at the tie-ballast interface was the loosening of ballast attributed to surfacing events. This led to the use of slow orders (typically 0.1 MGT) after surfacing and ballast maintenance events, or dynamic track stabilizers (DTS), which attempted to strengthen the ballast through vibrations from the DTS. Additionally, ensuring a strong ballast section with full shoulder and full ballast crib height was considered key to minimizing the negative lateral strength reduction from surfacing/maintenance events.

Multiple research studies have been conducted over the years to characterize the lateral strength and the influence of some parameters, namely ballast density. Typically, these have involved single-tie push tests (STPTs), which involved removing the fastening system to isolate the tie-ballast interface and physically push the individual tie with a load device [1] [2] [3] [4] [53] [54]. The results of these tests generally showed that tonnage does consistently increase the lateral strength, and DTS and slow-order tonnage generally have a similar positive contribution to

lateral strength. In addition, it has been observed that STPT resulted in a wide range of values that were highly dependent on the tie type and ballast condition.

Other testing methods that simulate a track panel shift instead of the resistance of a single tie have been performed [5] [54]. While the outputs of the track panel shift could be directly compared to the STPT test results, there was general agreement between the two testing methods.

The objectives of the testing presented in this report were to perform STPTs on track with a wide range of tie and ballast parameters to quantify their influence and compare them against the influence of slow order tonnage. In addition, the important parameters would be aligned with potential inspection devices that are currently used or planned to be used in the future.

The potential outcome of improved characterization of ballast lateral strength and the ballast parameters that affect the lateral strength is that this improved characterization and knowledge could be used to better define the track buckle risk since the tie-ballast resistance was one of the key parameters in track buckle calculations [1]. The applications of this work could range from current assessments of track buckle risk to long-term assessments. An example of a long-term assessment would be investigating the effect of increasing extreme temperature ranges (i.e., extreme hot and cold) from climate change at some geographic regions in the United States.

2.2 Test Matrix

In fall 2020, researchers conducted a comprehensive lateral tie push study that involved measuring the increase of lateral strength after a surfacing event. The test had multiple goals and AAR and FRA funded it jointly under the SRI program.

2.2.1 Test Goals and Objectives

The stated goals of the project included but were not limited to:

- Comparing the lateral strength of wood and concrete tie sections
- Measuring the increase in lateral strength after surfacing from tonnage accumulation
- Improving understanding of pre-peak and peak lateral strength behavior:
    - To determine similarities and/or differences between lateral and vertical ballast behavior
    - To develop/refine/verify inputs parameters that could be used in advanced lateral strength models
- Developing correlations between multiple measured parameters to understand the influences of lateral strength
- Determining the ability to predict lateral strength from track-based measurement systems

In the past, multiple lateral tie push tests were conducted that showed the increase in lateral strength with tonnage accumulation. However, future testing will both add another scenario to the existing tests and perform a more in-depth analysis of the pre-peak behavior, statistical distributions, and correlations between parameters.

2.2.2 Site Location and Component Details

The research team conducted the tests on the High Tonnage Loop (HTL) at the Facility for Accelerated Service Testing (FAST), located at the Transportation Technology Center (TTC) in Pueblo, CO. Using this site allowed the use of the freight railroad test bed that could provide a replica of the freight rail environment but with a focus on track testing. More specifically, the test was located on Section 36 of the HTL. This location involved tangent track on a double mainline section of track and had both wood and concrete tie sections.

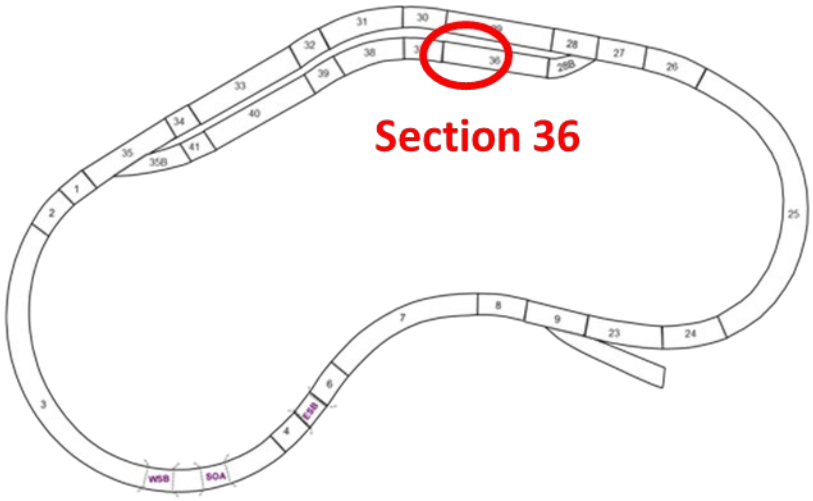

Figure 2: Site Map of HTL with Test Location Emphasized

Figure 2 shows both diagrams of the track layout and photographs of the wood and concrete ties. Both the wood and concrete tie section tested had about 25 ties each. The wood tie section involved tie numbers 367 to 445. These ties were 7 inches high, 9 inches wide, and 8.5 feet long and appeared to be decades old. The ties were in good condition, but the sides were smooth and did not allow for much ballast indentation. The ballast was granite and the ballast condition itself appeared to have rounded or smoothed ballast particles. The shoulder in this section were about 8 inches wide and would be considered narrow. The ballast crib was considered full, but the ballast height was about 2 inches below the top of the tie. The ballast conditions appeared consistent throughout the wood section.

The concrete tie section involved tie numbers 447 to 525. These ties were 8 inches high, 7 inches wide, and 8.5 feet-foot long and have been in track since early 1990s (~30 years in service). The tie vendor was unknown, but the tie was untextured (unscalloped) and still appeared to be in good condition. The ballast was again granite, but the ballast condition appeared better with more angular and rougher ballast particles. The shoulder would be considered typical with a consistent regulated shoulder of about 18 inches wide. A section of the shoulder was reduced to 8 inches (number ties 505 to 525) to make the shoulder condition of that section of concrete ties similar to the wood tie section. The crib height varied between full and low crib conditions, and the crib height was measured for each measured tie.

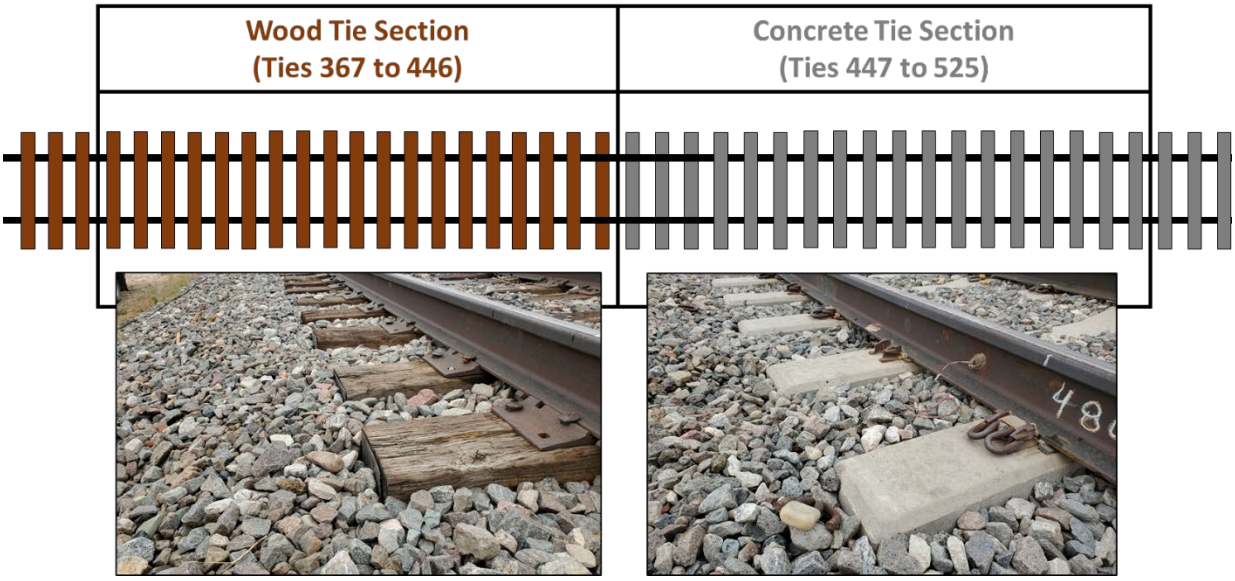

Figure 3: Diagram of the Wood and Concrete Test Section

After the STPT tests were completed, samples of ballast were taken from the wood and concrete tie sections. At each section, five ties were selected and a bucket of ballast from the tie end was collected at each location. The goal of the sampling was to select ballast that would be representative of the shoulder ballast resisting the tie push. Figure 4 shows the ballast gradations. The results showed very similar gradations, and that both sections appeared to fall within AREMA #4a specifications [7].

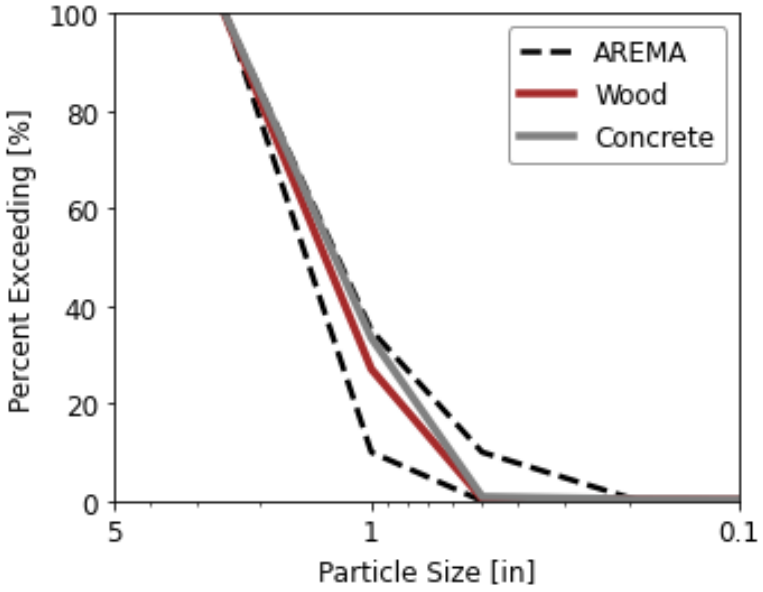

Figure 4: Ballast Gradations of the Wood and Concrete Tie Sections

Figure 5 shows the changes in shoulder and crib height condition. The results showed consistency within the wood tie section and variation within the concrete tie section, especially in crib height. The narrow shoulder regions had shoulder widths of about 8 inches while the good

shoulder was about 18 inches wide. The depth of crib ballast below the top of tie ranged from 0 to 3 inches.

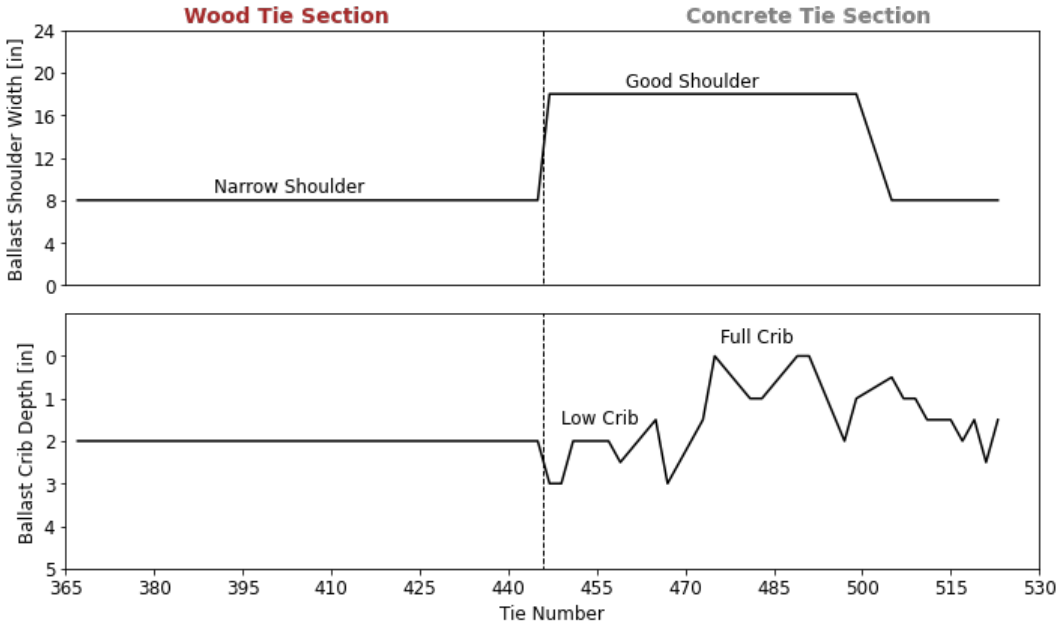

Figure 5: Shoulder and Crib Height with Tie Number

2.2.3 Test Measurements

The testing involved collecting multiple measurements over three tonnage conditions: 0, 0.1, and 22.3 MGT. These tonnage conditions represent the post-tamped condition (0 MGT), the slow order release condition (0.1 MGT), and a consolidated condition (22.3 MGT). Descriptions of the measurements are summarized as follows:

Single Tie Push Test (STPT): The STPT is the most commonly used method of measuring lateral tie strengths, and the results from these tests can be used in advanced track buckling models [1]. The test setup was similar for both wood and concrete ties and involves unclipping the fastening system and lifting the rail to isolate the tie-ballast behavior. A load cell attached to the tie pushes the rail and creates a reaction force on the tie. For concrete ties, track equipment was used to ensure no rail movement occurred when lifting the rail by providing a reaction force. When loaded laterally, the tie will move laterally, and the lateral displacement is measured using a string potentiometer (string pot). The final output is a full load-displacement curve. Figure 6 shows a photograph of the STPT.

Figure 6: Photograph of the STPT

Rail Elevations: Rail settlement is measured using elevation surveys that measure the top of rail (TOR) on both the inside and outside rail at select tie locations. The rail settlement and tamping lift height can be calculated by taking the difference in elevations at a single location. The advantage of this measurement over track geometry carts or vehicles is that the settlement can be measured instead of inferred from a mid-chord offset surface profile.

Track Loading Vehicle (TLV): The TLV is a TTCI-owned and operated research testing vehicle that has many track measurement capabilities, and, for this test, the static loading capabilities were used to measure loaded rail defections and calculate track modulus. The loading occurred statically and at a select location both the inside and outside rail displacement was measured at 0-, 10-, 20-, 30-, and 40-kip wheel loads. These measurements can be used to characterize the vertical ballast behavior under load.

Track stiffness and modulus are two measurements that can characterize the vertical track stiffness. Track stiffness and modulus are similar but track stiffness accounts for the entire track while track modulus removes the influence of the rails. Both track stiffness and modulus can be calculated from the 10- and 40-kip measurements using the following equations:

$$k = \frac{P_2 - P_1}{y_2 - y_1} \quad (1)$$

Where:

k = track stiffness

P_2 = heavy car wheel load (178 kN/40 kips)

P_1 = light car wheel load (44 kN/10 kips)

Y_2 = rail deflection from heavy car

Y_1 = rail deflection from light car

To calculate track modulus, the following equation is used:

$$u = \frac{k^{4/3}}{64EI^{1/3}} \quad (2)$$

Where:

u = track modulus

E = rail modulus of elasticity (200 GPa/2.9E7 psi)

I = rail section modulus (3,900 cm^4/93.7 in^4)

FRA Research Vehicles: The FRA research vehicle is an FRA-owned, ENSCO-operated vehicle that collects a wide range of measurements in both dynamic and static conditions. For this test, a wide range of track-based measurements were collected while the vehicle was moving at 10, 20, and 30 mph in both directions. The analysis was outside the scope of the project but can be used for future applications. In addition, the loading frame was tested on a few ties. Figure 7a shows a photograph of FRA research vehicle compared to the TLV (Figure 7b).

(a) (b)

Figure 7: Photographs, FRA Research Vehicle TLV (a) and TLV Track Loading Setup (b)

Seismic Ballast Inspection Tool (SeiBIT): In development by Earth Science Systems under an FRA research project, the SeiBIT could have the capability of using seismic waves to measure ballast modulus over a 10-tie track length. The data from this test was collected to potentially gain insight into the ballast condition but is currently considered experimental.

2.2.4 Test Matrix

The test matrix involved performing multiple tests over three tonnage conditions: post-tamped (0.0 MGT), slow order (0.1 MGT), and consolidated (22.3 MGT). STPTs, rail elevations, and track modulus were performed for all three tonnage conditions, while additional information from the FRA research vehicle and ballast modulus measurements were taken at the slow order (0.1 MGT) tonnage condition. Table 1 shows the final test matrix, and tie locations are found in Table 2.

Table 1: Fall 2020 Lateral Strength Testing Test Matrix

Measurements	0.0 MGT	0.1 MGT	22 MGT
STPT	✓	✓	✓
Rail elevations	✓	✓	✓
TLV	✓	✓	✓
FRA inspection vehicle		✓	
SeiBIT		✓	

Table 2: Tie Locations of Each Measurement

	STPT	Rail Elevations	TLV	FRA	SeiBIT
Tie Range	367 to 525	367 to 525	367 to 525	Varied	371 to 421 and 511 to 541
Tie Intervals	Varied intervals	Every other tie	Every fourth tie	Varied	10 ties

2.3 Tie Push Results

This section summarizes the results from the STPT tests. This includes an introduction to how the data outputs are calculated from the force-displacement curve (Section 2.3.1), test results (Sections 2.3.2 to 2.3.4), correlations between the various STPT output parameters (Section 2.3.5), and a basic statistical analysis of the results (Section 2.3.6).

2.3.1 Tie Push Measurement Outputs

A typical STPT force-displacement curve is highly non-linear with an initially high stiffness that rounds out to either a defined peak or a residual peak [1]. Three outputs were characterized from each STPT force-displacement curve to emphasize different aspects of the lateral behavior. These include peak lateral force (resistance), initial lateral stiffness, and lateral displacement at a specified force. Figure 8 shows a typical load-displacement curve and the three outputs. The subsections describe the outputs.

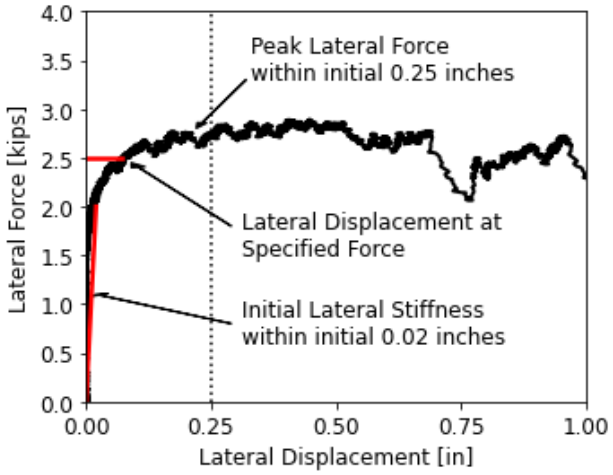

Figure 8: Typical STPT Load-Displacement Curve with Outputs of Peak Lateral Force, Initial Lateral Stiffness, and Lateral Displacement at Specified Force

Peak Lateral Resistance

Historically, peak lateral resistance (or strength) is the most commonly used STPT output and represents a particular tie's buckling resistance. The resistance is defined as the peak force within 0.25 inch of initial lateral tie displacement. The research team uses 0.25 inches because any lateral tie movement greater than 0.25 inches is considered significant movement.

Initial Lateral Stiffness

Initial lateral stiffness is a second output based on the STPT, and it is calculated by taking the stiffness (slope of force-displacement curve) for the initial 0.02 inches. The benefit of this measurement is that it characterizes the small-displacement resistance to track geometry issues, such as track shift, track alignment, and curve breathing, rather than the large-displacement resistance to buckling.

Lateral Displacement at Specified Force

Lateral displacement at a specified force is the third output from the STPT force-displacement curve. This output would be most relevant for predicting lateral movement if the lateral force acting on the tie were known. For example, if the rail experiences a lateral force of 5 kips and a half of that (2.5 kips) gets distributed to the center tie, this measurement could estimate the anticipated lateral movement from that 2.5-kip lateral force on the tie. Figure 9 shows how this displacement measurement can be calculated for an assumed lateral force of 2.5 kips.

2.3.2 Force-Displacement Curves

All the force-displacement curves for both the wood and concrete tie sections at all three tonnage intervals are displayed in Figure 9 with the thick black line representing a tie that was close to the median. Any tie push that experienced binding from the STPT setup was removed from the data set. The overall results showed generally higher lateral tie resistance values for the concrete tie section and increasing resistance with MGT. The variation in the force-displacement response at each tonnage interval could also be observed.

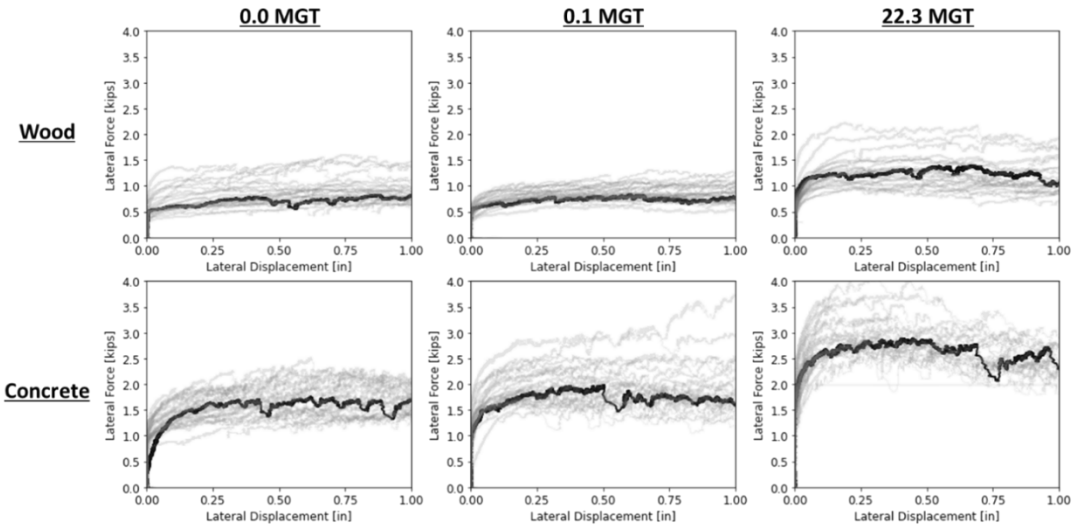

Figure 9: Force-Displacement Curves, Wood and Concrete Tie Sections at 0, 0.1, and 22.3 MGT

2.3.3 Visual Observations

During the push tests, the ballast in the wood and concrete tie sections behaved differently from each other, which may partly explain the large difference between the results from the two sections beyond what would be expected from differences in tie weight and tie surface texture. The ballast particles in the concrete tie section were able to better interlock with each other, forming a resistance bulb of two full ballast cribs. The ballast particles in the wood tie section did not interlock to the same degree, appearing to slide off each other and formed a resistance bulb of two half ballast cribs. This ability/non-ability for the ballast particles to interlock appeared to significantly affect the resistance to the tie push.

The resistance bulbs were easily identified after the tie push because the ballast particles had dilated and uplifted, forming a clear area where the ballast particles had engaged.

(a) **(b)**

Figure 10: Resistance Bulbs for the Wood (a) and Concrete (b) Yellow Shaded Region is the Region Where the Ballast Particles Dilated and Uplifted From the Tie Push

2.3.4 Results

The subsequent subsection summarizes the results from the STPT tests.

Peak Lateral Tie Resistance

Figure 11a shows the peak lateral resistance of each tie at 0, 0.1, and 22.3 MGT and Figure 11b shows the median values for the wood section and various ballast conditions in the concrete section. The ballast conditions included a low crib region, good shoulder and crib, and a narrow shoulder region. Figure 11c shows the increase in lateral resistance from the 0.0 MGT condition as a ratio.

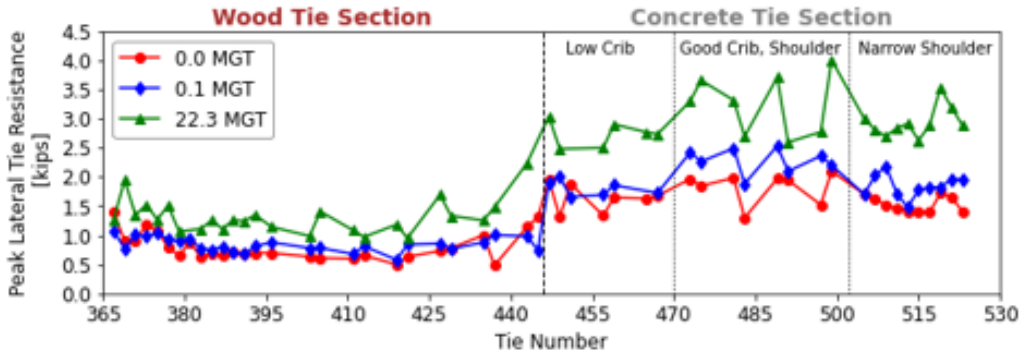

(a)

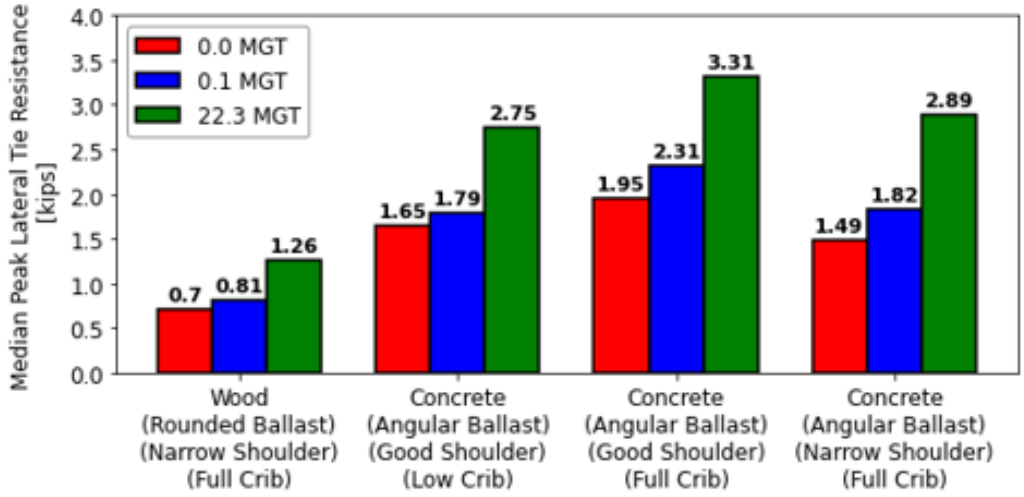

(b)

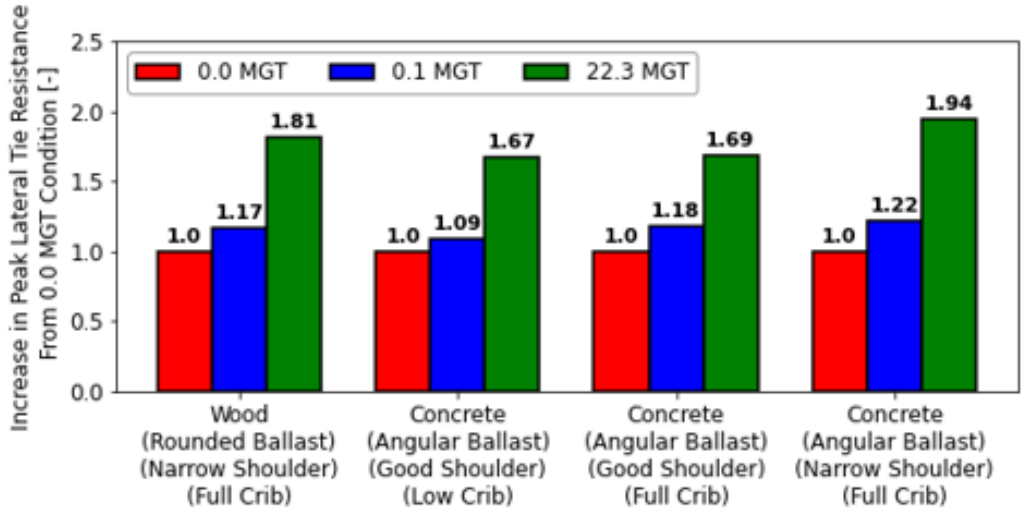

(c)

Figure 11: Peak Lateral Resistance Values at Each Tie (a), Median Values (b), and Increase (c) the 0.0 MGT Condition

A few observations can be made from the results, which:

1. All ties and tie categories showed increased resistance with MGT. This aligned with all previous studies [1] [2] [4] [53] [54]. In addition, the increase appeared proportional for all tie and ballast conditions. From 0 to 0.1 MGT, the lateral resistance increased about 10 to 20 percent (0.1 to 0.45 kips). From 0 to 22.3 MGT, the lateral resistance increased about 65 to 95 percent (0.55 to 1.35 kips).
2. The concrete tie section experienced significantly greater tie resistance values compared to the wood tie section (0.8 to 1.65 kips), even when accounting for the shoulder width. There are two explanations for the difference. One, concrete ties are expected to have higher lateral resistance values due to the heavier weight of these ties. Two, the more angular ballast and larger "resistance bulbs" in the concrete tie section likely contribute as well. The individual influence of the concrete and ballast is unclear since they cannot be separated from each other for this test.
3. The resistance values in the wood tie section were low when compared with previous tests and is presented in Section 2.5.1. The low values were likely due to a combination of factors, including a narrow shoulder, rounded ballast particles, and worn tie sides that did not allow for ballast indentation. The wood tie section was likely close to a lower bound for lateral resistance values.
4. The differences in resistance for each category in the concrete tie section (shown in Figure 11b) emphasized that both shoulder width and crib height affect the lateral resistance. These ballast condition factors will be analyzed in more detail in future sections.

2.3.4.1 Initial Lateral Tie Stiffness

Figure 12a shows the initial lateral tie stiffness at each tie at 0, 0.1, and 22.3 MGT and Figure 12b shows the median values for the wood and various ballast conditions in the concrete section.

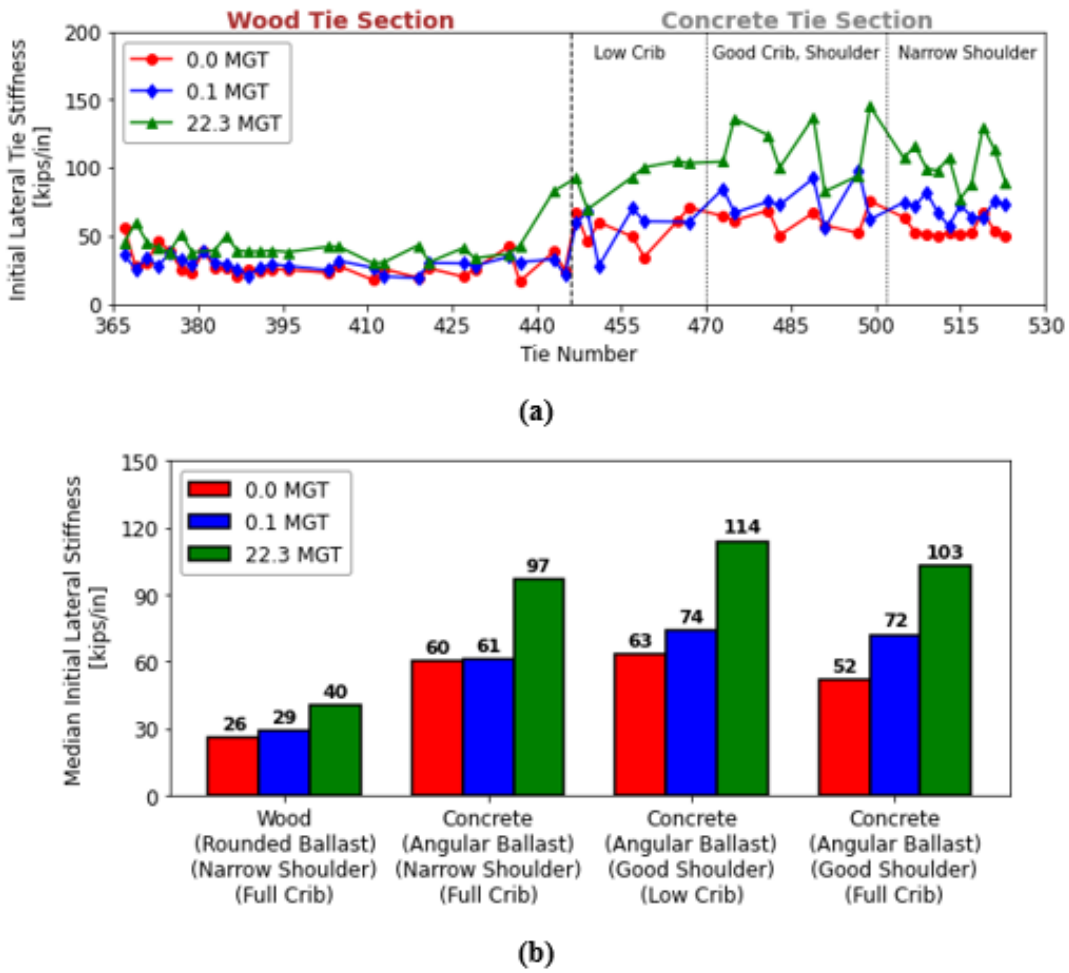

Figure 12: Initial Lateral Tie Stiffness Values at Each Tie (a) and Median Values (b)

For this particular test, the initial lateral tie stiffness showed very similar trends to the peak tie resistance and many of the same observations could be made.

2.3.4.2 Lateral Displacement

The lateral displacement at specific lateral force levels at each tie is displayed in Figure 13. Due to the large differences in peak resistance values, 0.5 kips was selected for the wood ties, and 1.25 kips was selected for the concrete ties.

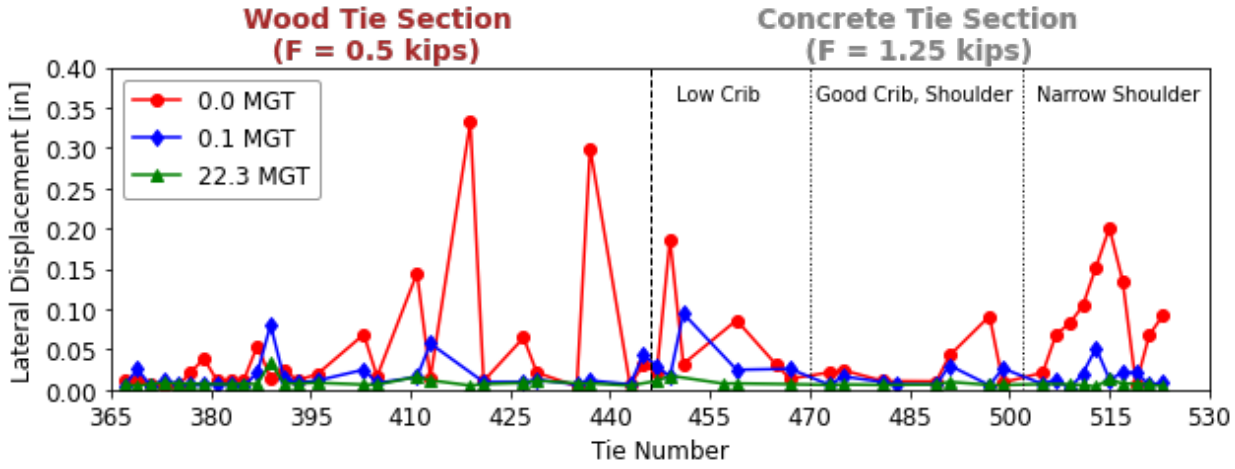

Figure 13: Lateral Displacement from Lateral Force at Each Tie

A large range of displacements were observed in the 0 MGT condition but that range decreased for 0.1 MGT and eventually all displacements were close to zero at 22.3 MGT. Section 2.3.6 provides a detailed analysis.

2.3.5 Tie Push Correlations

This section looks at the various relationships between the tie push outputs. The first comparison looks at how the initial 0 MGT resistance related to the change in lateral resistance from the 0 MGT value. Figure 14a shows the change to 0.1 MGT separated by tie and ballast condition, and Figure 14b shows the change to 22.3 MGT combined in a single case. The 0.1 MGT case was separated by the tie and ballast condition because the plot emphasized the influence of ballast density after tamping which required isolating the trend from the influences of tie type and ballast section. The 22.3 MGT case emphasized a very general trend that should hold true for all tie and ballast cases.

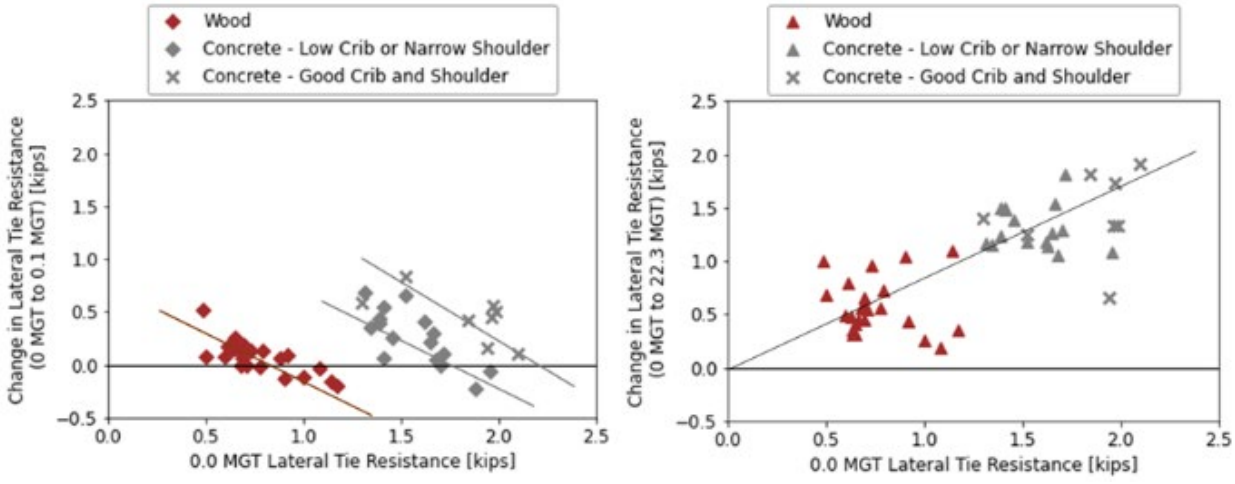

(a) **(b)**

Figure 14: 0 MGT Lateral Resistance vs. Change in Lateral Resistance from 0 MGT Condition at 0.1 MGT (a) and 22.3 MGT (b)

Two main observations can be made. First, an inverse relationship existed between the 0 MGT value and the change from 0 to 0.1 MGT (Figure 14a). An explanation for this behavior was that the ties with the lowest initial resistance were likely surrounded by the loosest ballast so the 0.1 MGT tonnage densified the ballast around those ties to a greater degree than denser ballast locations (higher 0 MGT lateral resistance values). The initial 0.1 MGT of tonnage likely had the largest influence on the loosest ballast regions and had the effect of evening out the ballast densities across the track.

The second observation was that if the wood and concrete ties were combined in a single dataset, a positive relationship existed between the initial resistance and the change in resistance to 22.3 MGT. As the ballast density from tonnage increased the ballast resistance, it may have had compounding effects on initially strong ballast sections. This compounding effect meant ties with initially high resistance because of angular ballast, good shoulders, and/or full cribs, would see the greatest lateral resistance increase. This observation agreed with the increase results in Figure 11c.

The results shown in Figure 14 suggested that increases in ballast density from tonnage had both a short- and long-term effect. In the short-term, tonnage would make the lateral resistance along the track more uniform by densifying the loosest ballast. In the long-term, the tonnage appears to have a proportional influence on lateral tie strength increase, meaning initially strong sections would have the greatest lateral strength increase because of the compounding influence of denser ballast with angular ballast, good shoulder widths, and/or full cribs.

The next comparison in Figure 15 shows a very strong relationship between peak lateral resistance and initial stiffness with an increase in 35 kips/in of stiffness for each kip increase in lateral resistance. This suggested that increases in large-displacement track buckling resistance were proportional to resistance to small-displacement tie movement.

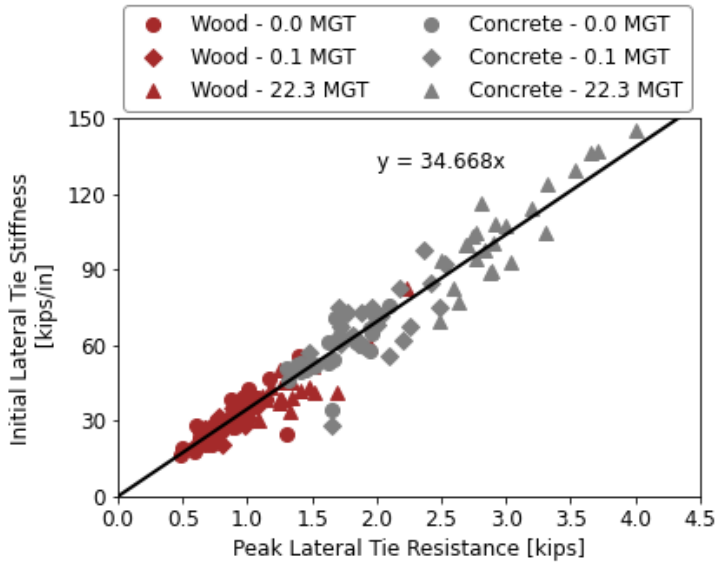

Figure 15: Relationship Between Peak Lateral Resistance and Initial Lateral Stiffness

The last comparison focused on the peak lateral resistance and displacement values at a given specified force and is shown in Figure 16a for the wood tie section and Figure 16b for the

concrete tie section. The results showed a non-linear relationship in which the closer the peak lateral resistance was to the specified force, the more likely it was to have a higher displacement.

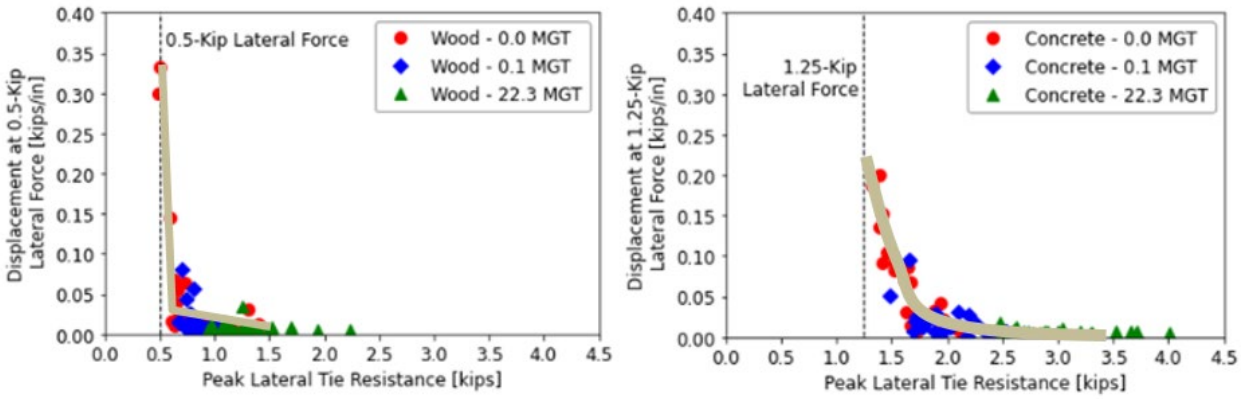

(a) **(b)**

Figure 16: Relationship Between Peak Lateral Resistance and Tie Displacement for Wood Tie Section (a) and Concrete Tie Section (b)

2.3.6 Statistical Analysis

This section aims to quantify the variation in tie push results for each scenario. This will emphasize that each condition had a range of values and not a single value.

2.3.6.1 Statistical Distributions

Figure 17a and Figure 17b shows the standard deviation and coefficient of variation (CV) of the lateral resistance values. The standard deviation represents the amount of variation in a dataset with higher values meaning more variation from the mean. The CV is the standard deviation divided by the mean and represents the variation that is normalized by the mean value.

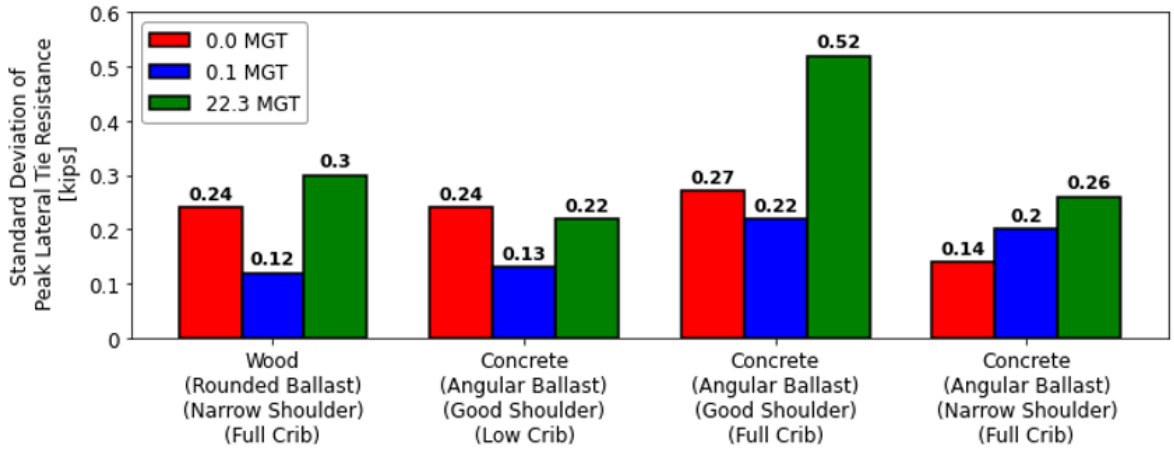

(a)

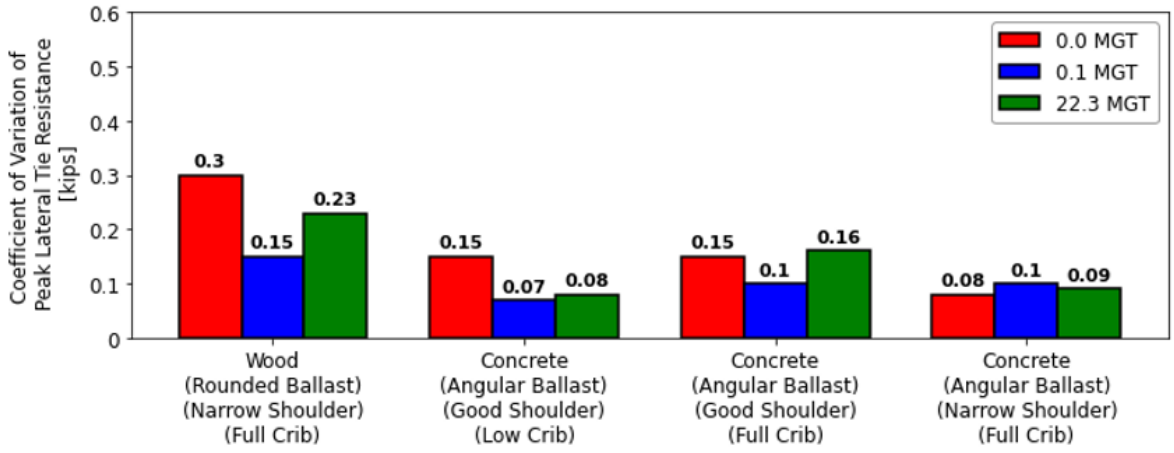

(b)

Figure 17: Lateral Tie Resistance Standard Deviation (a) and Coefficient of Variation (b)

The standard deviation results agreed with previous observations that the 0.1 MGT showed the lowest variation since ballast consolidation from the initial tonnage affected the loosest ballast regions the most. However, as tonnage continued to accumulate, the differences in ballast section (e.g., crib and shoulder) started to dominate.

In addition, the standard deviation appeared to be similar to most tie conditions and generally ranged from 0.2 to 0.3 kips with the exceptions of the 0.1 MGT run which showed values from 0.12 to 0.22 kips and a high value from the concrete tie section with a good shoulder and full crib at the 22.3 MGT push condition.

The CV showed the same general trend but emphasized that the variation was not particularly dependent on the mean value.

For visualization purposes, Figure 18 shows the box plots of the lateral resistance (a), initial lateral stiffness (b), and lateral displacements (c). The results agree with previous observations and emphasize the lowering of lateral displacements with tonnage.

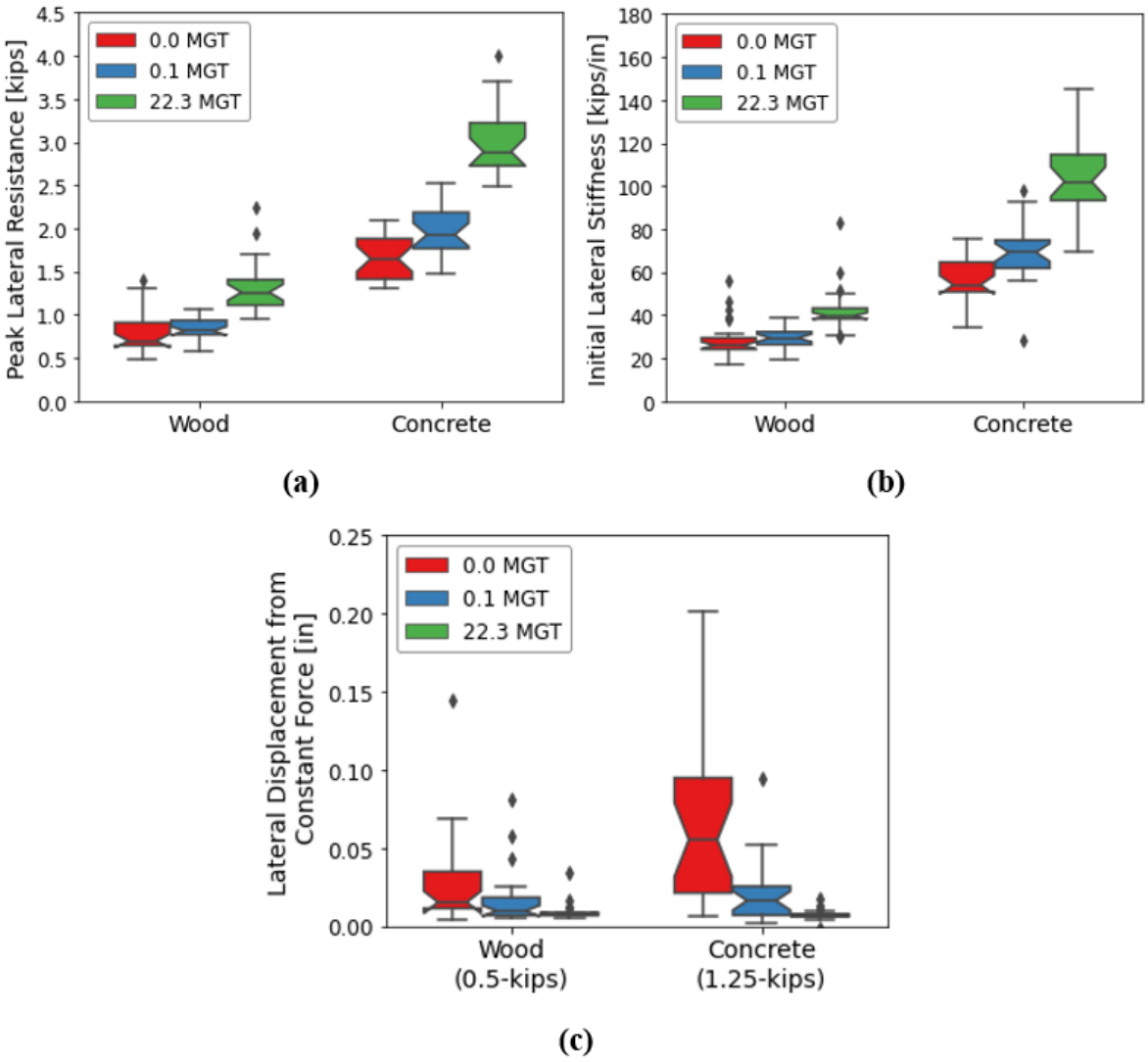

Figure 18: Box Plots of Lateral Resistance (a), Initial Stiffness (b), and Displacement (c)

Kernel Density Estimate (KDE) plots of the lateral resistance are displayed in Figure 19 with wood ties (a) and concrete ties (b). For the wood ties, the results generally had a single defined peak while the concrete ties often had a wider peak due to varying ballast conditions. Various statistical tests, such Anderson Darling and Ryan-Joiner, were used to check for normality but the results were unclear as some distributions checked for normality while others did not. It is unclear whether normal distributions or non-normal distributions could be assumed because of the influence of multiple conditions, low samples sizes (25 ties in each section) from a statistical perspective, and influence from outliers.

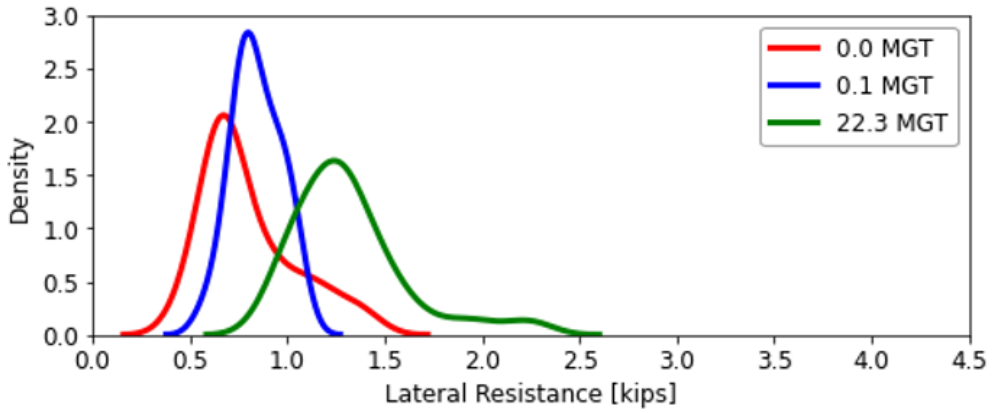

(a)

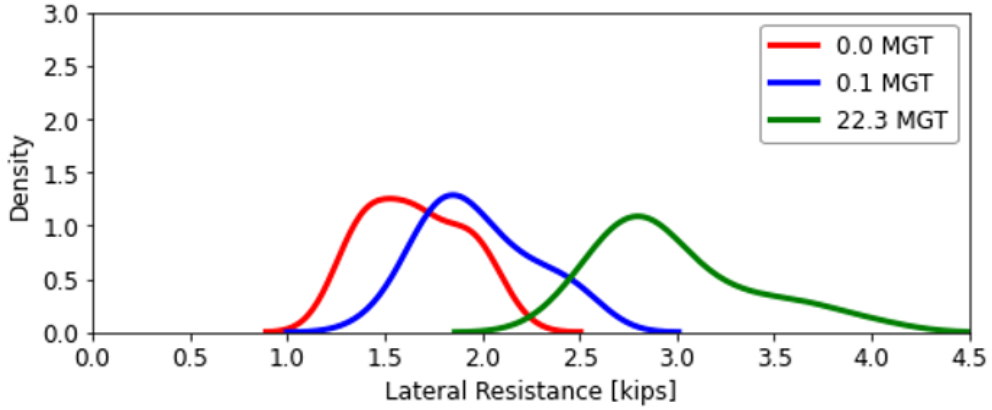

(b)

Figure 19: Distribution of Lateral Resistance Values for Wood Ties (a) and Concrete Ties (b)

2.3.6.2 Displacement with Force

This section reviews how the peak resistance is statically related to the lateral tie displacement. This relationship could be relevant for estimating tie displacement based on a known lateral force imparted on a tie.

Figure 20 shows the percentage of ties that displayed a tie displacement at or less than 0.02 inch for a range of lateral forces. The results showed the distributions for each condition were similar but offset from each other in a similar order to the peak lateral resistance. This was not surprising as the force-displacement curve had a similar shape for all tests.

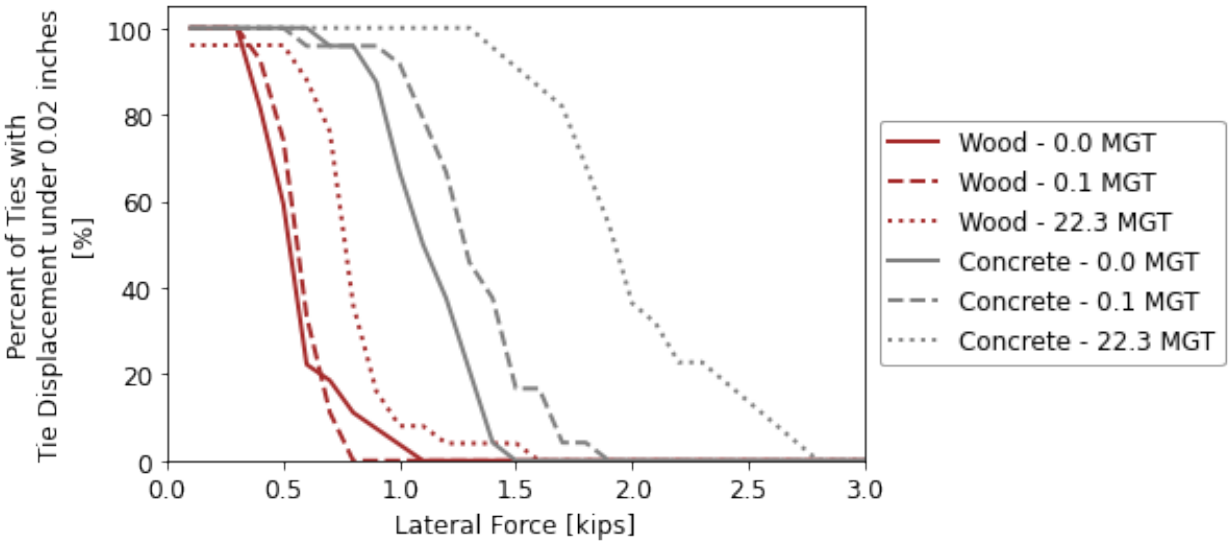

Figure 20: Percent of Ties Displacing Less Than 0.02 Inches

Figure 21 emphasizes the similar behavior when the lateral force was normalized by the median peak lateral resistance of each condition. The similar distributions occurred because of the similarities of the force-displacement curves. An idealized version of the curve suggested that about 50 percent of the ties displaced more than 0.02 inches at about 70 percent of the median peak lateral resistance.

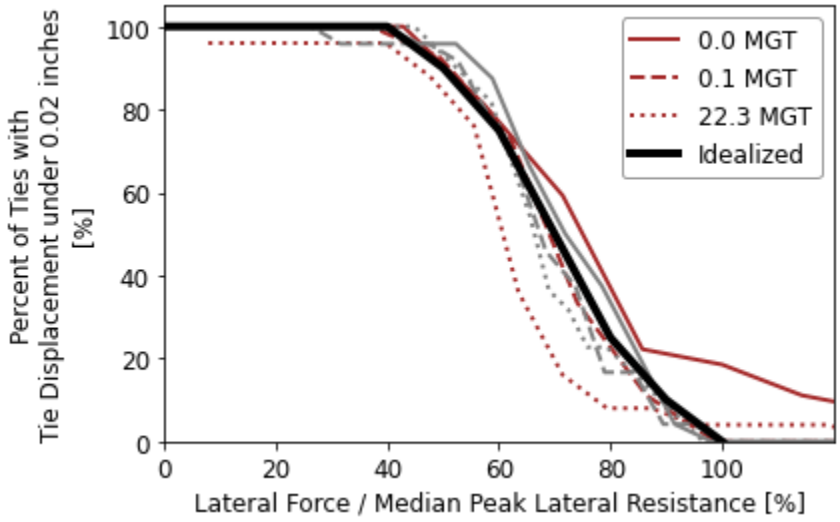

Figure 21: Percent of Ties Displacing Less Than 0.02 Inches Normalized by Peak Lateral Resistance

2.4 Settlement and Stiffness Measurements

Along with the tie pushes, multiple other measurements were taken including rail elevations and track modulus.

2.4.1 Rail Elevations

Rail elevations were collected along the test zone prior to tamping, post-tamping, and after 0.1 and 22.3 MGT of tonnage. From these measurements, the tamping lift height and track settlement could be calculated at each test tie.

Figure 22 shows the general results. The black line shows the tamping lift height (positive change in rail elevation) while the blue and green lines show the settlement (negative change in rail elevation). The tamping lift height ranged from about 0.5 to 1.0 inch with the largest lift (1.3 inches) near the transition between the wood and concrete ties. The average lift height in the wood tie section was 0.51 inch while the average lift height in the concrete tie section was 0.92 inch. The settlement at 0.1 MGT (blue line) and 22.3 MGT (green line) show a similar contour as the tamping lift height (black line) with greater settlement in the concrete region and with the greatest settlement occurring in the concrete transition region. This behavior agreed with previous knowledge that initial ballast settlement was a function of the tamping lift height.

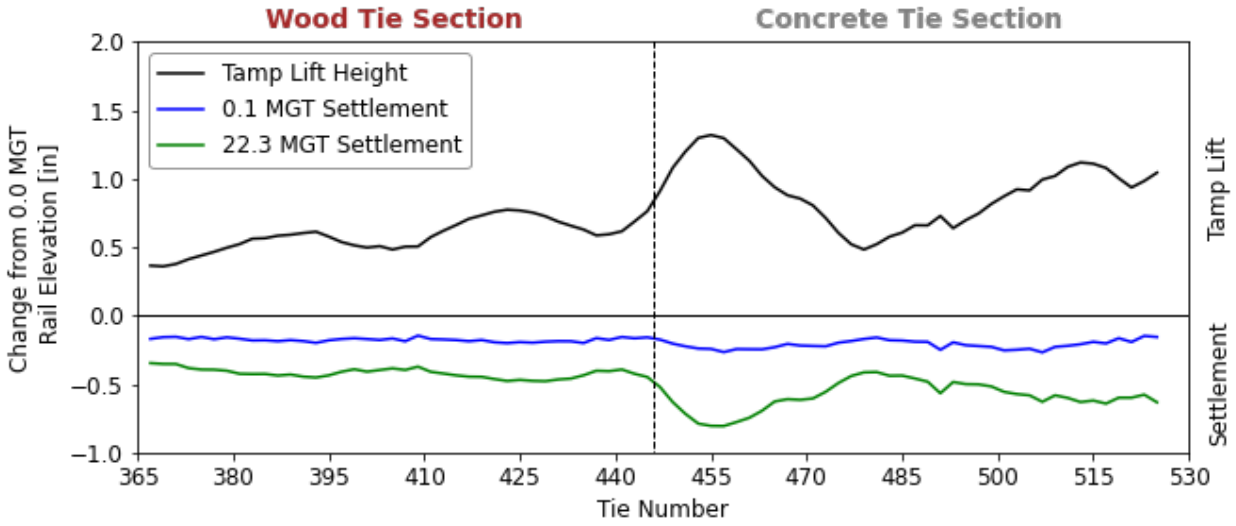

Figure 22: Change in Rail Elevation Emphasizing Tamping Lift Height and Settlement Along the Test Zone

Figure 23 emphasized the settlement at 0.1 and 22.3 MGT. A transition region between Ties 409 to 481 was defined and the behavior within this region was not considered representative because of the influence of the wood/concrete tie transition. Outside the transition region, the settlement in the wood tie section was fairly consistent while the settlement in the concrete section appeared to vary, especially at 22.3 MGT. However, this variation in settlement corresponded with the variation in the tamping lift height in that same area.

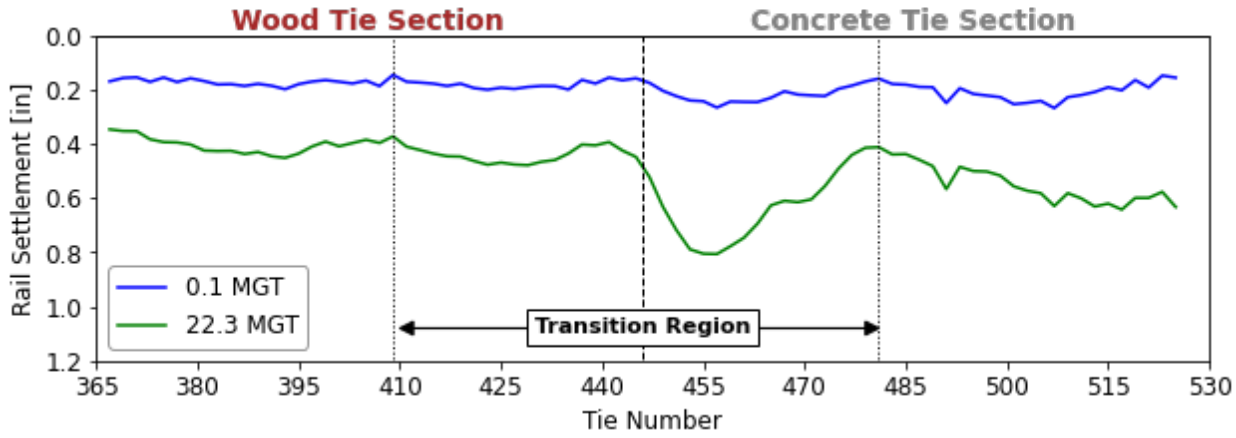

Figure 23: Rail Settlement at 0.1 and 22.3 MGT

Figure 24 shows the ratio between settlement and tamping lift height at 0.1 and 22.3 MGT. The results follow a similar contour as tamping lift height and settlement.

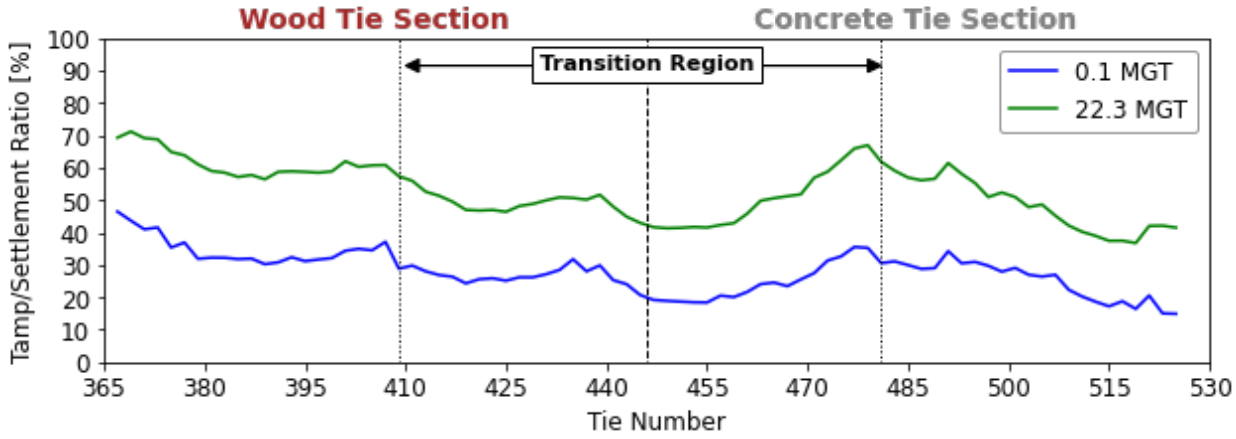

Figure 24: Tamp/Settlement Ratio at 0.1 and 22.3 MGT

Figure 25 further emphasizes the relationships between tamping lift height and ballast settlement. Figure 25a shows a near-linear relationship between tamping lift height and settlement. The trend was likely bounded by the 1:1 ratio line when tamping lift heights are low, meaning all the tamp lift was lost due to settlement. The results between tamping lift height and tamp/settlement ratio in Figure 25b show that the ratio decreases with increasing lift height. The wood and concrete ties appeared to behave similarly.

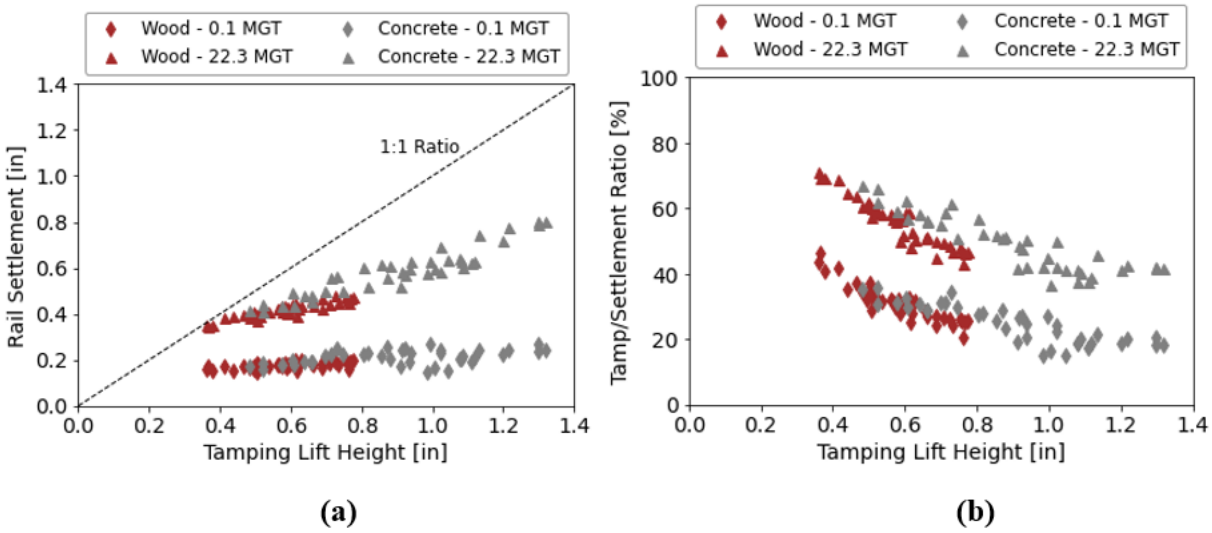

Figure 25: Relationship Between Tamp Lift Height and Settlement (a) and Tamp/Settlement Ratio (b) for Wood and Concrete Ties

The median tamping lift height, settlement, and tamp/settlement lift ratio outside the transition region (Ties 409 to 481) is summarized in Table 3 for reference purposes.

Table 3: Median Tamp Height, Settlement, and Tamp/Settlement Ratio Values for Wood and Concrete Ties Outside of Transition Region (Ties 409 to 481)

Tie Type	Tamp Lift Height (in.)	Rail Settlement (in.)		Tamp/Settlement Ratio (percent)	
		0.1 MGT	22.3 MGT	0.1 MGT	22.3 MGT
Wood	0.51	0.17	0.40	32 percent	60 percent
Concrete	0.92	0.21	0.58	27 percent	48 percent

2.4.2 Track Deflection, Vertical Track Stiffness, and Modulus

Track deflection, vertical track stiffness, and modulus can be calculated from the TLV results. These values give indication of hanging ties and increases in ballast stiffness with tonnage.

Figure 26 shows the rail deflections at 10- and 40-kip wheel loads at all three tonnage intervals. The results showed a clear increase in rail displacements in the wood tie section compared to the concrete tie section. In addition to and similar to settlement, the displacements outside the transition region appeared more consistent than those inside the transition region.

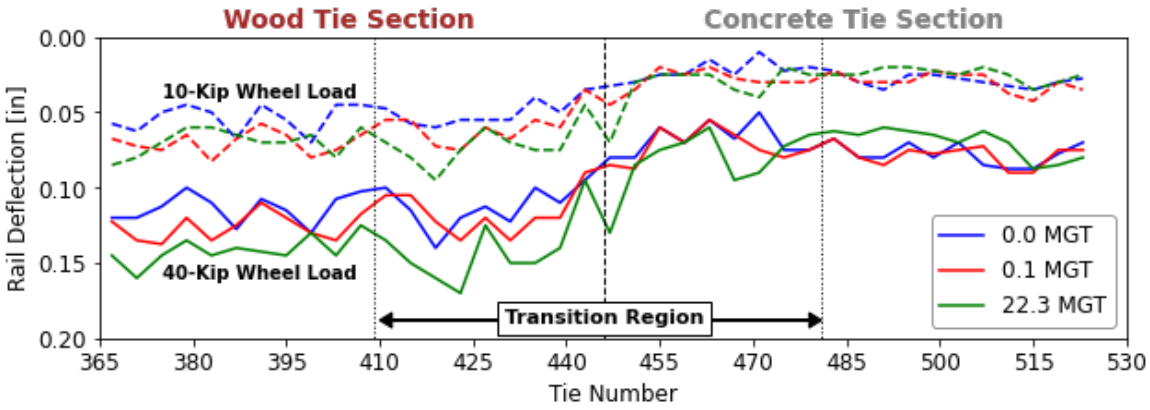

Figure 26: Tie Deflections at 10- and 40-kip Wheel Loads at 0, 0.1, and 22.3 MGT

Figure 27 shows the track stiffness (a) and track modulus (b) at all three tonnage intervals. The results showed higher track stiffness and modulus for the concrete tie section with more consistent results outside the transition region. As a note, track modulus values of 10,000 kip/in/in were considered very high, and this was likely due to a strong ballast section and very stable subgrade.

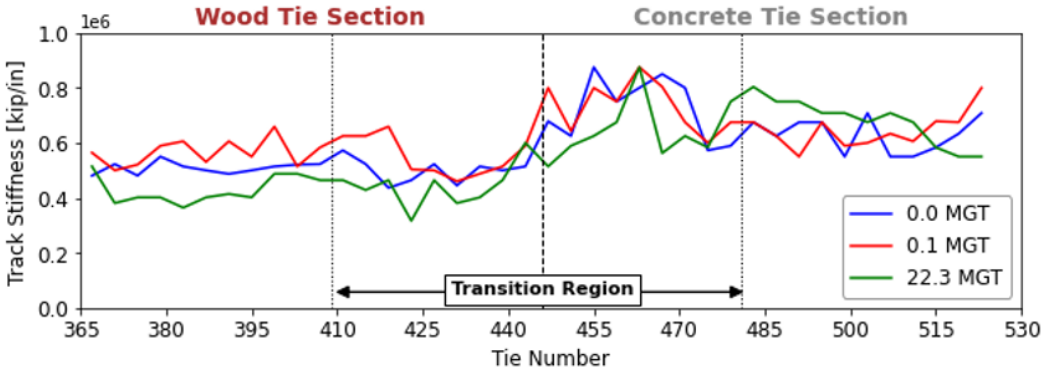

(a)

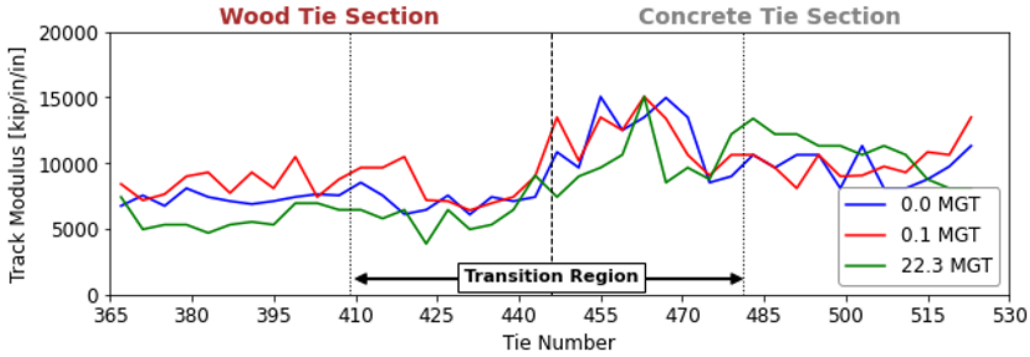

(b)

Figure 27: Track Stiffness (a) and Track Modulus (b) at 0, 0.1, and 22.3 MGT

Figure 28 and Table 4 summarize the median values outside the transition region for the wood and concrete tie sections at all tonnage intervals. The results showed different behavior for the wood and concrete ties. The wood ties show an increase in rail displacement with tonnage while the concrete ties show decreasing rail displacement. The concrete behavior was anticipated because displacements should decrease with increasing ballast density. The wood behavior was opposite of what was anticipated and was possibly due to deflections in the cut spike fastening system.

This displacement of both the wood and concrete tie sections were used to calculate track stiffness and modulus. The wood section showed an overall decrease while the concrete section showed the anticipated increase. This suggested that track modulus may not have been a good indicator of ballast density because track modulus measured the stiffness of the entire track system, and it may have been difficult to isolate ballast density from other variables such as subgrade and fastener behavior.

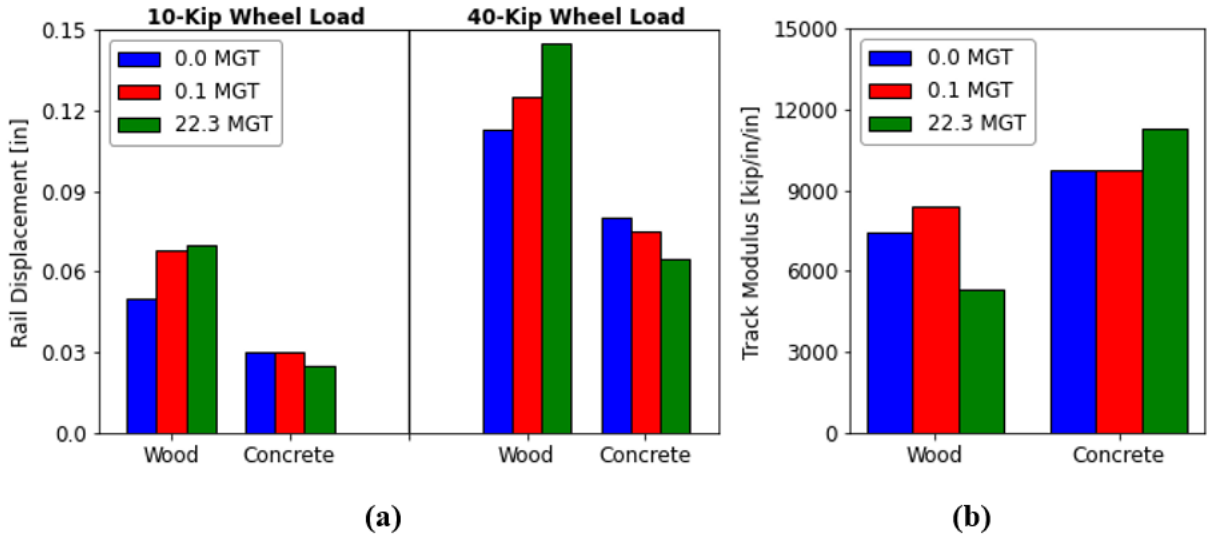

Figure 28: Median Rail Displacement (a) and Track Modulus (b) Values for the Wood and Concrete Tie Sections Outside the Transition Region at 0, 0.1, and 22.3 MGT

Table 4: Median Values of Rail Displacement, Track Stiffness, and Track Modulus for Wood and Concrete Tie Sections Outside the Transition Region at 0, 0.1, and 22.3 MGT

MGT	10-Kip Load [in]		40-Kip Load [in]		Track Stiffness [kip/in]		Track Modulus [kip/in/in]	
	Wood	Concrete	Wood	Concrete	Wood	Concrete	Wood	Concrete
0	0.050	0.030	0.113	0.080	514,000	633,000	7,430	9,750
0.1	0.068	0.030	0.125	0.075	564,000	633,000	8,410	9,750
22.3	0.070	0.025	0.145	0.065	402,000	708,000	5,320	11,320

2.4.3 SeiBIT

The SeiBIT measures a shear wave velocity which is related to the modulus of the material. Figure 29 shows the shear velocity profile with depth in the wood and concrete tie section. Much variation in the seismic response can be observed, and the system characterizes the substructure to much greater depth than the relevant ballast about 1 foot (0.3 m) below the track surface.

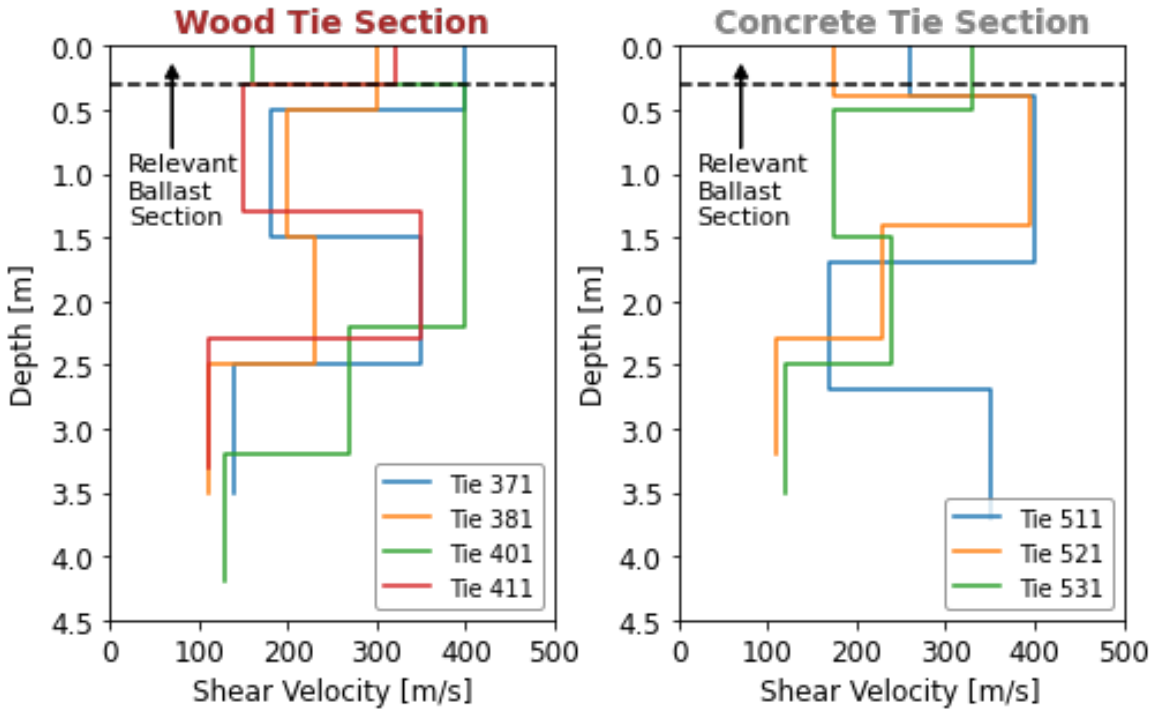

Figure 29: Seismic Shear Velocity with Depth in Wood (a) and Concrete (b) Tie Section

The shear velocity within the top 1 foot (0.3 m) for each tie is shown in Table 5. The results showed a wide range of behaviors from 160 to 400 m/s. The average for the wood (295 m/s) and concrete tie sections (255 m/s) were relatively similar considering the variations and low number of samples.

Table 5: Shear Velocity in Relevant Ballast Section

Wood Tie Number	Shear Velocity [m/s]	Concrete Tie Number	Shear Velocity [m/s]
Tie 371	400	**Tie 511**	260
Tie 381	300	**Tie 521**	175
Tie 401	160	**Tie 531**	330
Tie 411	320		
Average	295	**Average**	255

In summary, the SeiBIT is likely not an ideal system for measuring lateral track strength because it does not have the necessary resolution in the relevant ballast section. If the SeiBIT system could concentrate in the top 1-foot of the region and have a higher resolution, the SeiBIT might have be more useful for this particular application.

2.5 Relationships Between Parameters

This section investigates the relationships between the lateral resistance and various ballast and tie parameters from this current study along with historical tests. This investigation includes:

- Ballast Density: Ballast density is affected by surfacing events and tonnage. Surfacing typically disrupts and loosens the ballast, resulting in a lower ballast density while tonnage will increase ballast density. The initial 0.1 MGT, roughly equivalent to post-ballast maintenance slow orders, covers when the increase in ballast density from tonnage is the greatest.
- Tie Type: Heavier tie types can have a greater lateral resistance.
- Ballast Shape Characteristics: The shape characteristics, angularity, for example, of new ballast often depend on the quarry and rock type, and once installed, will degrade, round out, and smooth over time from tonnage. Ballast shape characteristics (i.e., angular or rounded ballast) may become important when making decisions of using reclaimed ballast after shoulder cleaning and during other similar maintenance activities.
- Ballast Section (shoulder width and crib height): The ballast section is recommended to have a 12-inch shoulder and full crib [7].
- Tie Interface: The tie interface can depend on the tie manufacturer for concrete and plastic ties and the age of tie and whether ballast can indent the wood tie.

Due to the strong relationships between the lateral resistance, initial stiffness, and displacement (reference Section 2.3.5), many of the same observations are true for all three outputs so only lateral resistance will be presented. In addition, all these relationships are only applicable for dry, clean ballast.

An additional note is that the comparisons will be made in kips and assume the change in lateral resistance of a single tie. This output is relevant for comparing the influence of ballast density and ballast section. However, track buckling results in a panel shift which combines the resistance of multiple ties, not a single tie. Since track buckling involves multiple ties, this presents an issue when comparing tie type because the tie spacing will be different. The spacing differences will be accounted for in those particular calculations, and the details are explained in those sections.

2.5.1 Historical Tests

Along with the current study, multiple historical STPT tests have investigated the influence of various parameters, namely ballast density through tonnage [1] [2] [4] [53] [54]. This section presents a summary of the results, and the actual studies can be referenced for additional detail.

The average peak lateral tie resistance 0 and 0.1 MGT, and consolidated (10+ MGT) conditions are shown for all the available tests in Figure 30. The bar color indicates the types of tie (brown=wood, gray=concrete, olive=plastic/EPC), and the slanted lines indicate whether the tie was textured or not. The bars used to indicate the ties for the current study are outlined in red.

In general, the results showed the concrete tie section matched the past studies better than the wood tie section did. The reasons for the lower values in the wood tie section were addressed

earlier and were likely due to the combination of narrow shoulders, rounded ballast particles, and worn tie sides that did not allow for ballast indentation.

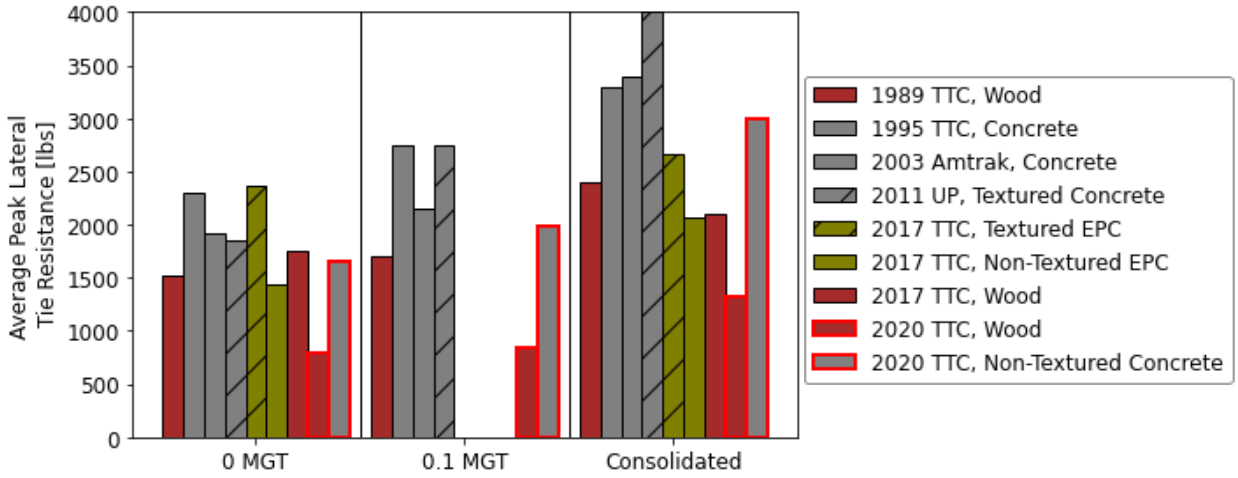

Figure 30: Average Lateral Tie Resistance of Current and Historical Tests

2.5.2 Influence of Ballast Density

One of primary recognized methods for increasing lateral tie strength after ballast maintenance is increasing the ballast density either through tonnage or dynamic stabilization. To investigate the effect of ballast density, four factors were compared: tamping lift height on 0 MGT lateral resistance, tonnage on the increase in lateral resistance, settlement on the increase in lateral resistance, and track modulus.

2.5.2.1 Tamp Lift Height and 0 MGT Lateral Resistance

It is well established that the ballast loosening and disruption from tamping reduces lateral strength but the amount of lateral strength loss by tamping lift height is not well defined. Figure 31 shows the influence of the tamp lift height on the 0 MGT lateral resistance. Note, that only data outside the transition region is used. The results showed a strong correlation between the tamp lift height and initial lateral tie resistance if the wood and concrete tie sections were separated. The regression fit has the wood ties losing about 1.9 kips of lateral resistance for every inch of tamping lift while the concrete ties showed 1.2 kips reduction per inch of lift. In theory, there should be a minimum threshold at which increasing the tamping lift height will not result in any further greater reduction of lateral resistance. However, this threshold cannot be confidently defined from this dataset.

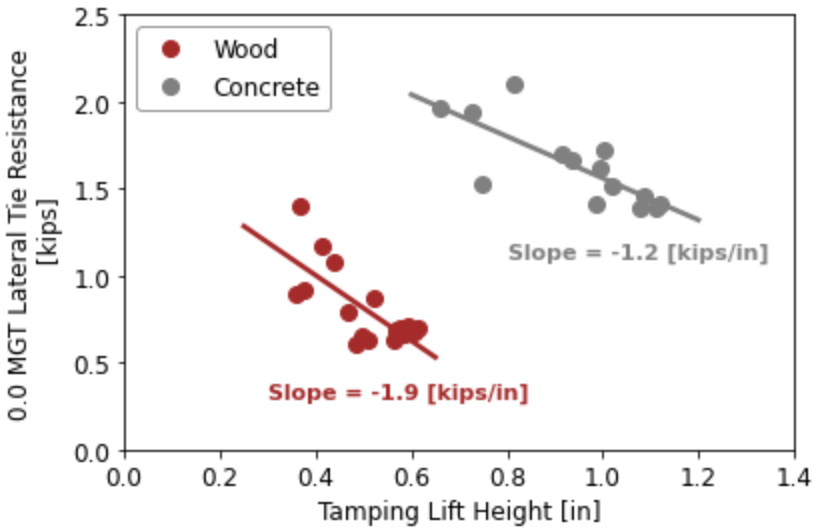

Figure 31: Relationship Between Tamping Lift Height and 0 MGT Lateral Resistance

One historical study compared the difference in a 0.4-inch lift and 2-inch lift for wood ties [2]. The difference at 0 MGT ranged from 0.1 to 0.15 kip. The influence of tamping lift height between this study and the historical study is significantly different, but it may be affected by other factors and methods of calculation.

2.5.2.2 Slow Order Tonnage and Increase in Lateral Resistance

In the current study, slow order tonnage, represented as 0.1 MGT in Figure 11, increased the lateral resistance, but the increase in lateral resistance varied based on the tie and ballast characteristics. The increase is about 10 to 20 percent and can range from 0.1 to 0.35 kip.

In historical studies, the increase from 0 to 0.1 MGT typically ranged from 5 to 20 percent (0.075 to 0.45 kip). This increase agrees with the current study.

2.5.2.3 Rail Settlement and Increase in Lateral Resistance

Slow order tonnage is effective at increasing the lateral resistance because the tonnage induces track settlement and causes the ballast to become denser. The density increase can be measured directly with rail settlement.

Ballast settlement from tonnage generally has been characterized as non-linear with initially high settlement rates as the ballast compacts and densifies, and then, as the ballast becomes denser, the influence of tonnage on settlement diminishes as the ballast approaches its maximum dense state. This concept is expanded in detail in Section 3.1. Figure 32 shows both the non-linear increase in lateral resistance and ballast settlement with MGT and similar behavior, further reinforcing the relationship between ballast density and lateral tie strength.

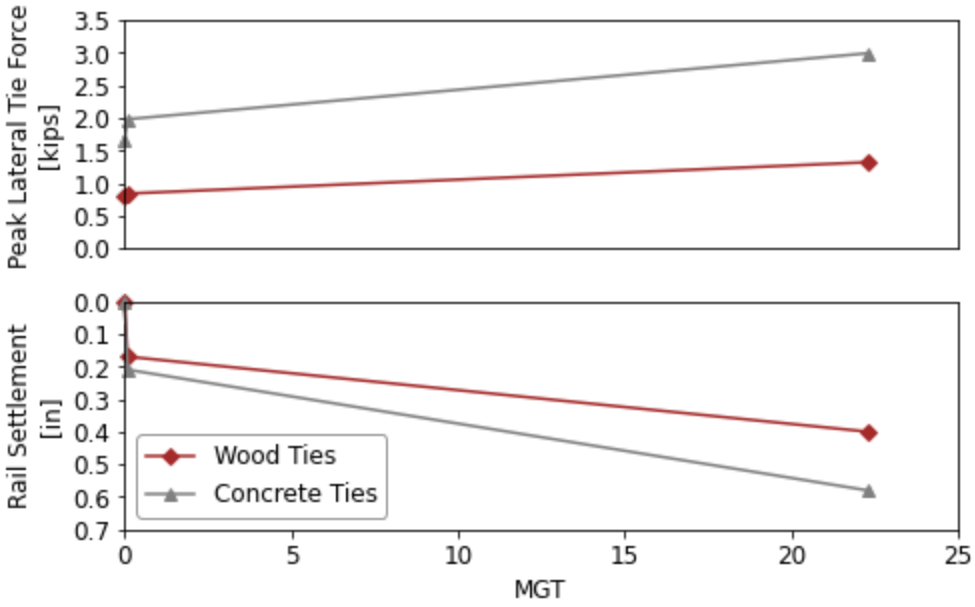

Figure 32: Non-Linear Increase in Peak Lateral Resistance and Rail Settlement with MGT

Figure 33 plots rail settlement and change in lateral resistance for each tie outside the transition region. When separating all the wood tie and concrete tie data, there are strong correlations which reinforce the relationship between ballast density and lateral tie strength.

Assuming a linear regression, the lateral resistance will increase by 0.12 kip for each 0.1 inch of rail settlement for wood ties and 0.23 kip for each 0.1 inch of rail settlement for concrete ties.

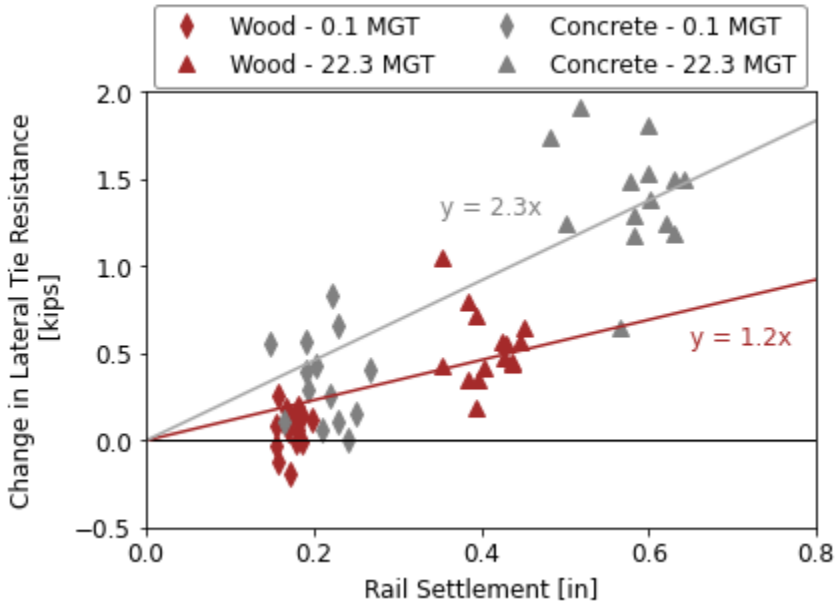

Figure 33: Relationship Between Rail Settlement and Change in Lateral Tie Resistance

2.5.2.4 Track Modulus and Change in Lateral Resistance

A fourth potential method of estimating ballast density is track modulus. Since track modulus incorporates the influence of ties, fastening systems, ballast, and subgrade, it may not always be well suited for estimated ballast density between sites with different track characteristics, but it may be helpful at a single location.

Figure 34 plots the change in track modulus and change in peak lateral resistance for the concrete tie section outside the transition region. There is not a clear relationship between the two parameters. It is likely that the ballast density near the surface was very small compared to the other characteristics of track modulus and would not have a significant influence.

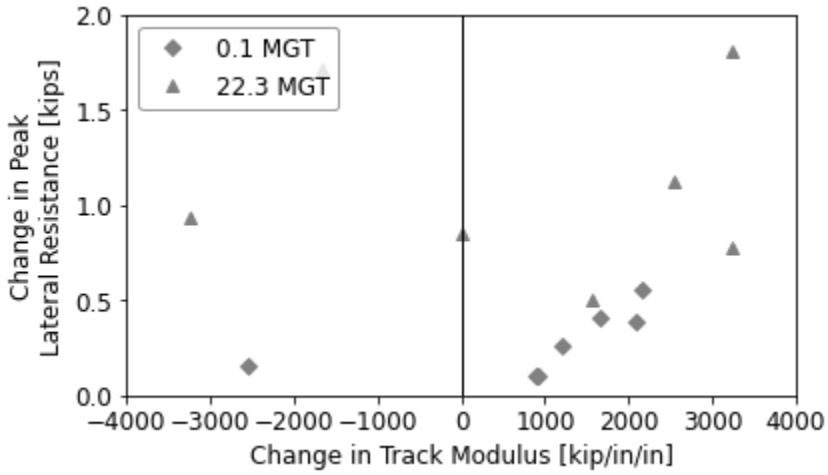

Figure 34: Relationship Between Track Modulus and Lateral Tie Resistance

2.5.3 Tie Type and Ballast Shape Characteristics

The original purpose of testing both the wood tie and concrete tie sections was to compare the influence of the tie types. However, with the noticeable differences in ballast shape characteristics between the two locations, it was difficult to separate the influence between the two tie types. One additional item for consideration was the spacing between the wood (19.5 inches) and concrete (24 inches) ties. The tie spacing would not affect the STPT output directly but spacing should be considered when comparing tie type with other parameters. When making comparisons regarding parameters, consider how the lateral resistance will apply to a multiple-tie panel shift that includes tie spacing, instead of a single-tie movement that does not.

When comparing the median results of the narrow shoulder region (columns 1 and 4 in Figure 11), the combination of tie type and ballast condition results in lateral tie resistance differences of 0.8 kip to about 1.6 kips. In terms of proportion, the concrete ties and angular ballast have higher lateral tie resistances of about 2.15 to 2.3 times the wood ties and rounded ballast. If adjusting for the larger concrete tie spacing, and therefore less ties in a panel shift, this involves multiplying the concrete tie values by 0.8. When adjusting for tie spacing, the difference in lateral tie resistance reduces to 0.5 to 1.08 kips.

Previous studies at the TTC comparing wood and concrete ties showed differences ranging from 0.68 to 1.15 kips, with concrete ties proportionally about 1.4 to 1.5 times higher than the wood ties [2] [53]. If adjusting for tie spacing, this difference becomes 0.25 to 0.55 kip.

One method of estimating the influence of ballast angularity would be to subtract the measured difference in tie type from the Kish et al. (1995) study from the difference between the concrete and wood tie section of the current study. This results in an influence of angularity of about 0.08 to 0.47 kip without adjustment and 0.25 to 0.55 kip with the tie spacing adjustment. For comparisons, the average adjusted value of 0.35 kip will be used but as reference the average non-adjusted value is 0.22 kip. This is not a high-confidence value because the ballast particles in the wood and concrete tie sections in the Kish et al. (1995) study may have not be the same, but this exercise should give insight into the rough order-of-magnitude influence of angularity.

2.5.4 Influence of Ballast Section Characteristics

This subsection investigates the influence of ballast section characteristics, namely ballast shoulder and ballast crib height, on the lateral tie strength.

2.5.4.1 Ballast Shoulder Width

For this study, the influence of ballast shoulder width can be compared using the concrete tie information in Figure 11, more specifically, the good 18-inch ballast shoulder results (column 3) and the narrow 8-inch ballast shoulder results (column 4), The 10-inch difference in ballast shoulder resulted in about 0.4 to 0.5 kip of lateral tie resistance difference. The 10-inch shoulder width difference can be converted to a change in lateral strength of 0.25 to 0.29 kip for a 6-inch change in shoulder width.

Past studies looked at shoulder width and found a range of 0.17 to 0.2 kip for a 6-inch change in shoulder width [53]. This reduction is slightly lower than the current study but generally agrees in rough order of magnitude.

2.5.4.2 Ballast Crib Height

The influence of ballast crib height from the current study can be compared using two methods. The first method is a comparison of the generalized categories in Figure 11 from the low crib (column 2) and the full crib (column 3) scenarios. The difference between the ballast crib height of about 3 inches ranges from 0.3 to 0.56 kip with a full crib proportionally increasing the lateral tie resistance from 1.2 to 1.3.

A second method is to develop a regression curve from the individual tests, which is shown in Figure 35 with only data points from the full shoulder concrete tie conditions at the 22.3 MGT scenario. The regression curve shows a slope of 0.225 kip per inch of ballast crib height. The roughly agrees with the 0.3- to 0.56-kip difference from the categorized full and low crib sections in Figure 11.

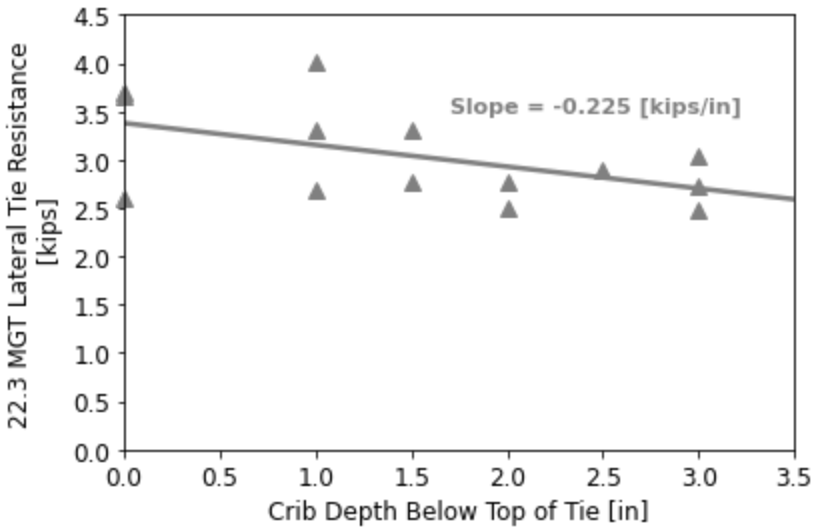

Figure 35: Relationship Between Lateral Tie Resistance and Ballast Crib Height for Concrete Ties at 22.3 MGT

In previous studies [53], the difference from a full crib and half crib resulted in a change of 0.3 to 0.5 kip which agrees with the current study.

2.5.5 Influence of Tie Interface

The current study did not allow for comparisons of tie interface differences which could include, but were not limited to, tie side texture and tie pads. Tie side texture included scalloped concrete ties, textured EPC ties, and the ability for ballast particles to indent wood ties. Tie pads included under-tie pads (UTPs) and their ability to be indented and interlock with the ballast particles. The variation from this parameter was anticipated to be large and difficult to characterize besides in general categories.

General observations were that textured concrete and EPC ties generally had higher lateral resistances than their smooth counterparts [4]. However, there has been limited side-to-side comparison, especially with concrete ties. In addition, there has been no formal study with UTPs, but previous tests by the TTC suggested that UTPs could increase the lateral resistance if the UTP allowed for ballast indentation (elasto-plastic pads), but further research is required.

2.5.6 Influence of Fines and Moisture

The previous tests have all assumed generally clean ballast with low levels of moisture. As with track settlement, the influence of fines and moisture was anticipated to be large and have a significant effect on the general lateral resistance behavior. The only known documented tests which compared a wood tie section in 4 different conditions were generally clean ballast, dry Selig's Fouling Index (FI) =40 ballast with no mud pumping and evenly distributed fines; dry FI = 40 ballast with previous mud pumping (allowed to dry for 1 week); and wet FI = 40 ballast with mud pumping. These were conducted at the Rainy Section, located in Section 36 of the TTC (i.e., a different location than the 2020 study).

Figure 36 shows the settlement (a) and lateral resistance (b) results. The settlement results showed very little change in settlement for the clean and dry conditions with significant increases

in wet mud pumped conditions. Regarding lateral resistance, the dry, fine-filled conditions resulted in the highest values, likely because of the very stiff shoulder that resulted from the suction (cohesive) forces in the fines. When wet, the lateral resistance was lowered significantly (water reduced or eliminated suction forces) and became similar to the lateral resistance from the clean ballast condition. As with settlement, it is likely that the specifics will depend heavily on the amount of fines, moisture, and fine type.

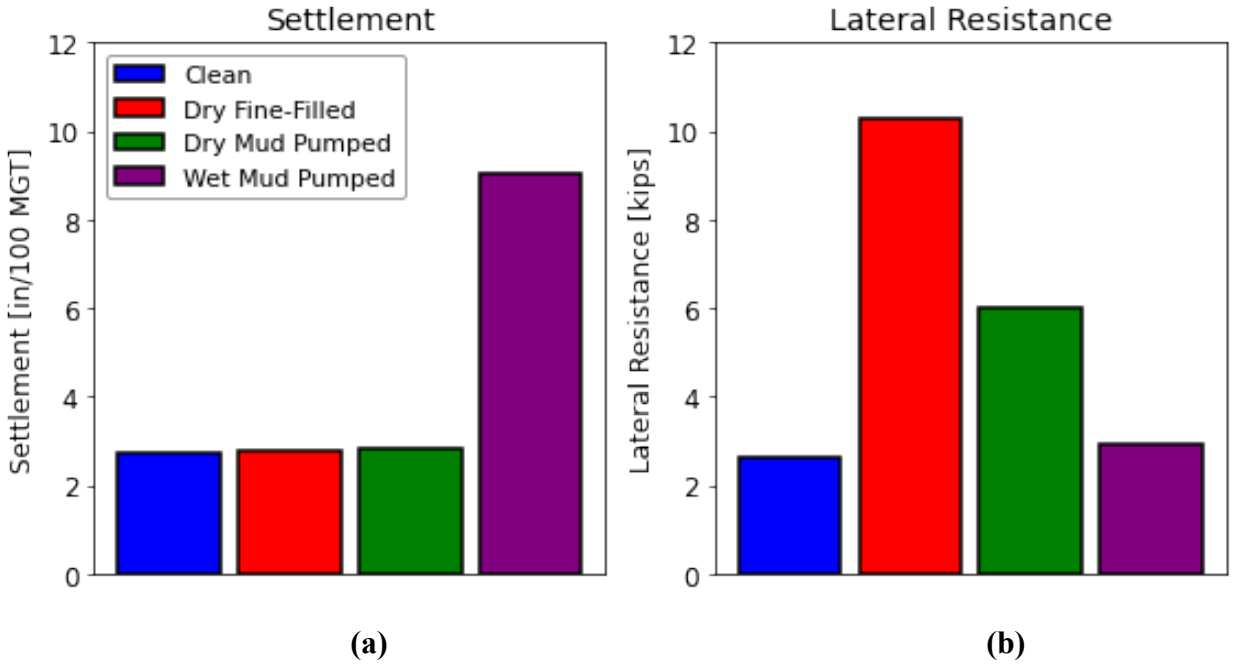

Figure 36: Behavior of Fine-Filled Ballast Regarding Settlement (a) and Lateral Resistance (b)

2.6 Summary of Parameters Influencing Lateral Tie Resistance

The current study and available historical tests allow for a fairly comprehensive view of the parameters that affect lateral tie resistance. Figure 37 defines the median influence of each variable for the current study and historical tests. Note that for each parameter, there is a range of potential values and these values often interact with each other. The range of values are shown in Figure 38. Therefore, Figure 37 and Figure 38 should be viewed as guides for the parameter influence and not the exact value.

The results showed that surfacing has had the greatest influence on lateral track strength and resulted in a significant reduction. The slow order tonnage (0.1 MGT) increased the lateral resistance by about 0.25 kip which may vary significantly depending on the situation. The results also suggested that other parameters regarding the ballast and ties (adjusted for tie spacing) had a similar influence on the lateral resistance.

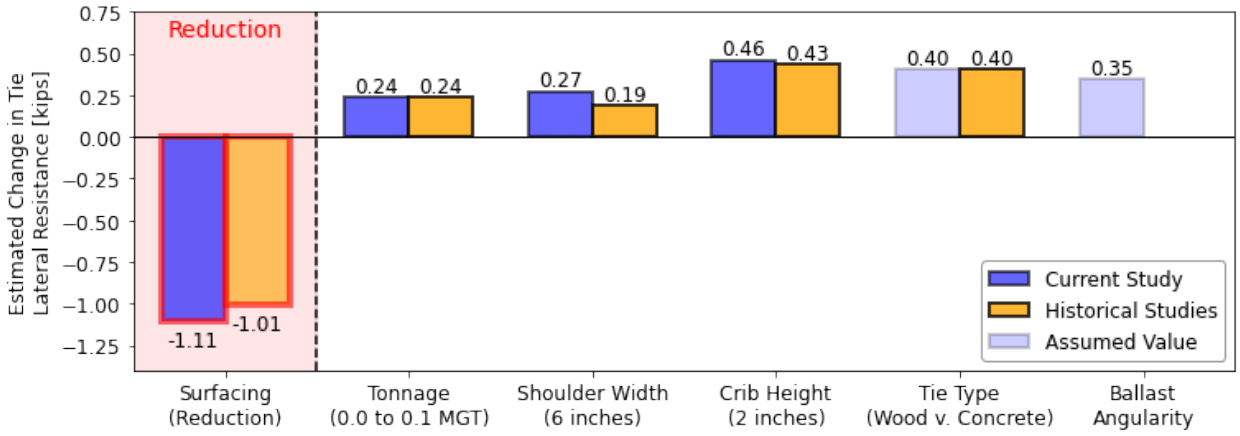

Figure 37: Median Influence of Each Parameter on Lateral Resistance

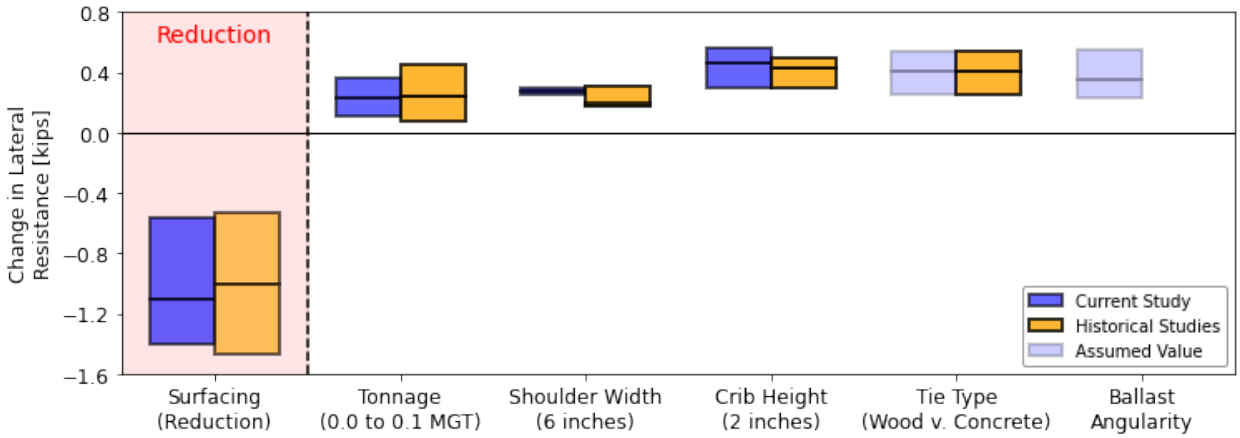

Figure 38: Maximum and Minimum of Each Parameter on Lateral Resistance

Based on these results and the parameters, lateral track resistance can be categorized in low- and high-risk scenarios. A simple, conceptual example is shown in Figure 39.

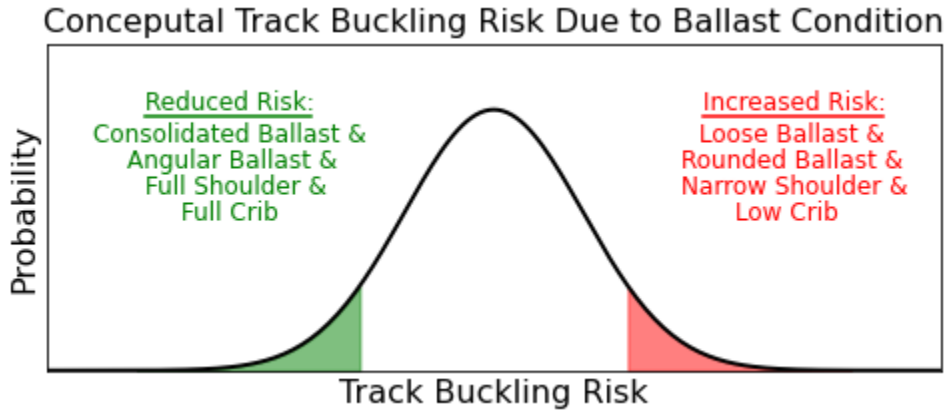

Figure 39: Conceptual Example of Buckling Risk Based on Ballast Conditions

2.7 Vertical vs. Lateral Ballast Behavior

This section compares observed vertical ballast behavior to lateral ballast behavior. While ballast particle orientation will change ballast behavior in both the vertical and lateral directions, additional key differences can give insight into important indicators that can be related to performance.

Figure 40 shows a diagram of a tie and ballast section and indicates the ballast locations that resisted the vertical and lateral movement of the ties. A few observations can be made. First, different areas of ballast are mobilized based on the direction of tie movement with the ballast below the tie mobilized in the vertical direction and ballast near the surface mobilized in the lateral direction. This shows that different ballast regions are important for resisting different directions of tie movement.

Second, despite the different regions, ballast density plays a similar role both in the vertical and lateral direction. While the ballast resisting the lateral movement is not directly compacted by the tie, as the ballast resisting vertical movement would be, the vibrations from train passage still compacts the ballast. This concept is supported by the observations in Figure 32 which showed similar trends of track settlement and the increase in lateral resistance with MGT even though the ballast affected by the two measurements was in different locations.

Third, the ballast resisting the vertical and lateral tie movements will likely experience different confining conditions. In the vertical direction, the ballast will be confined by the entire ballast section from the dead load and even residual stresses that are believed to occur after loading [8]. This means rounded ballast particles will be restricted from sliding off each other because of the confinement, causing the ballast particles to naturally interlock and reducing the influence of ballast shape. In the lateral direction, the top surface is unconfined so the ballast particles could move upwards during lateral tie movement, which was verified with the visual "resistance bulb" on the surface. This observation means that the ballast shape and its ability to interlock are likely more important in the lateral direction than the confined vertical condition.

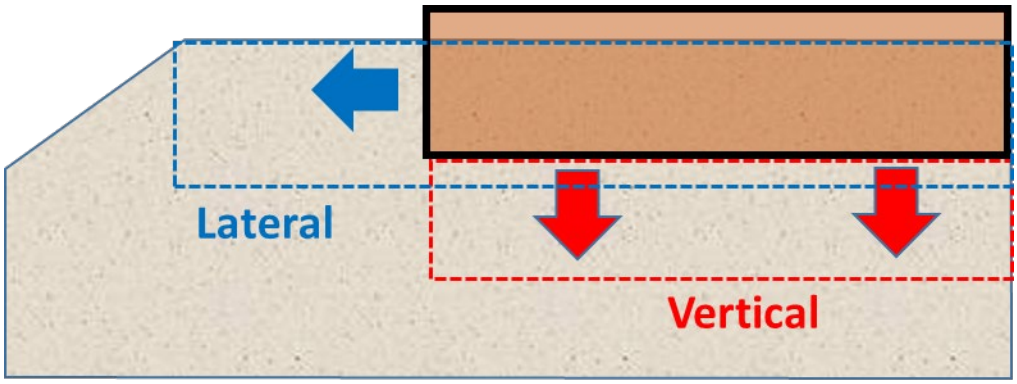

Figure 40: Diagram of Ballast Regions Resisting Vertical and Lateral Tie Movement

2.8 Ability of Inspection Methods to Characterize Important Parameters

Since the ballast resisting lateral tie movement was located near the surface of the track, track inspection devices (i.e., light detection and ranging [LiDAR] and machine vision) that measure the surface track condition could be used. LiDAR could identify the shoulder width while machine vision can identify tie type, crib height, and possibly even ballast shape characteristics.

2.9 Summary and Recommendations for Future Work

2.9.1 Summary

The lateral ballast behavior task investigated the ability of track inspection vehicles to estimate lateral tie strength using ballast condition outputs. Since the ballast section characteristics, such as shoulder width and crib height, and ballast condition could be controlled and quantifiably measured, an improved understanding of the ballast condition might reduce overall uncertainty in track buckling risk assessments and, in certain cases, provide potential fixes in higher buckle-risk situations.

The results showed that multiple parameters influenced the lateral tie strength of clean ballast including, but not necessarily limited to, ballast density, ballast shape characteristics, ballast shoulder width, ballast crib height, tie type, tie-ballast interface, and maintenance. Risk-based assessments can be made with general knowledge of the ballast parameters, but more work is required before forecasting models can be used with high confidence. There is potential for machine-vision- and LiDAR-based methods to characterize the important ballast parameters because the parameters of interest, such as ballast shoulder width, crib height, or tie type, can be visually identified from the track.

The list below summarizes the study's multiple observations and conclusions that:

- Multiple parameters including, but not necessarily limited to, ballast density, ballast shape characteristics, ballast shoulder width, ballast crib height, tie type, tie-ballast interface, and maintenance influenced the lateral tie strength of clean ballast.
    - Based on the current study and historical tests, a change in the 6-inch shoulder width, 1-inch crib height, heavier ties, and more angular ballast are roughly equivalent in their influence on lateral tie strength.
    - Ballast shape characteristics (angularity) were found to be a potential variable that could have significant effects on lateral tie strength because more angular ballast particles would engage the ballast to a greater degree than rounded ballast particles.

      In the long-term, the tonnage appears to have a proportional influence on lateral tie strength increase meaning initially strong sections would have the greatest lateral strength increase because of the compounding influence of denser ballast with angular ballast, good shoulder widths, and/or full cribs
    - Risk-based assessments can be made with general knowledge of the ballast parameters, but more work is required before forecasting models can be used with high confidence.
    - Slow order tonnage appeared to increase lateral resistance by 10 to 20 percent.
    - Higher tamp lift heights resulted in lower lateral resistance at 0 MGT.
- Small- and large-displacement lateral resistance metrics such as peak lateral resistance (large-displacement) and initial lateral stiffness (small-displacement) were strongly related, suggesting the shape of the pre-peak force-displacement curve remains similar but is scaled upwards depending on the peak resistance.

- Statistical distributions of the lateral resistance did not confirm normal distributions for all tests, and it was unclear if non-normal distributions could be used. The reasons for tests not conforming to normal distributions included non-normal distributions, significant influence of outliers due to low statistical sample size, and varying ballast conditions (e.g., not fully isolating a single condition within the sample size).
- Fine-filled ballast appeared to have a significant influence on the lateral resistance with dry fine-filled ballast producing very high resistance values, likely due to the suction pressures in the shoulders. The wet condition resulted in lateral resistance values much lower than the dry counterparts but not lower than clean ballast. These results were anticipated to vary significantly by location depending on the fines and ballast conditions.
- The ballast regions resisting vertical and lateral tie movement were different and should be reflected with different inspection technology strategies to address risk analysis.
    - The ballast resisting lateral tie movements were closer to the surface so surface inspection technologies such as LiDAR or machine vision may be used for site characterization. The relevant characteristics could include tie type, ballast shoulder width, and ballast crib height.
    - The surface ballast was less confined, so particle shape characteristics had a greater influence on the ability of ballast particles to interlock than the vertical direction counterparts.
    - The ballast section (shoulder width and crib height) was more influential for resisting lateral movement than vertical direction.

3. Background of Ballast Performance and Models

This section provides the background on topics for understanding the data analysis and forecasting models in later sections and includes three main parts. First, the background includes a full review of the parameters that affect ballast performance regarding settlement and track geometry and how these parameters can be characterized using track inspection methods or other informational sources. Second, multiple track geometry representations are introduced along with their potential data analysis applications. Third, a review of existing mechanistic and statistical models that forecast track geometry degradation based on ballast condition are included.

3.1 Background of Fundamental Ballast Behavior

Ballast is a key track component that is placed between the ties, subballast and natural subgrade. According to United States regulatory standards [9], ballast has a broad purpose, and it must:

(a) Transmit and distribute the load of the track and railroad rolling equipment to the subgrade

(b) Restrain the track laterally, longitudinally, and vertically under dynamic loads imposed by railroad rolling equipment and thermal stress exerted by the rails

(c) Provide adequate drainage for the track

(d) Maintain proper cross level, surface, and alinement

While the material type and quality are not specified in Federal regulations, typically, crushed angular rock particles are used as ballast material. Recommended practices, as specified by the American Railway Engineering and Maintenance-of-Way Association (AREMA) [7], include specific gradations, abrasion resistances, conductivity, and other material specifications that have been shown to improve ballast performance and lifespan.

The ballast section generally involves a ballast depth below the ties, a shoulder width, and ballast shoulder slope (Figure 41). While there is no specific design, a 12-inch ballast depth, 12-inch ballast shoulder, and 2:1 ballast shoulder slope is considered good practice [7]. In addition, the ballast should fill the crib until near the top of the tie. Field conditions, however, can significantly stray from this design.

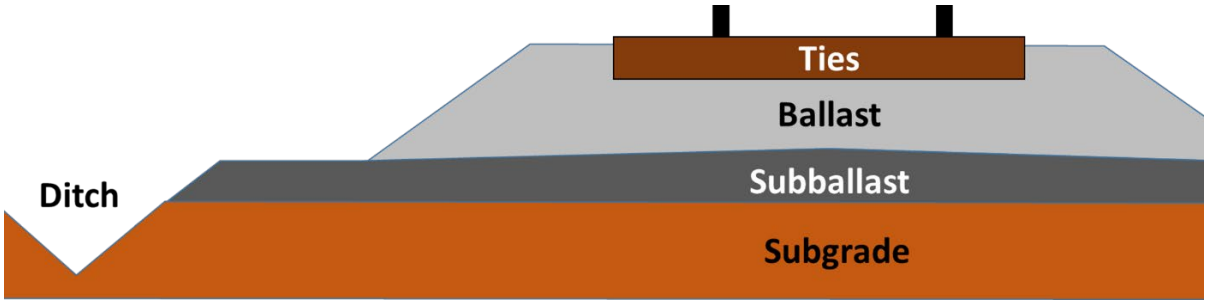

Figure 41: Typical Ballast Section

The current design has resulted primarily from decades of trial and error and has been adjusted over time to reduce the risks of derailment and to accommodate increased wheel loads and extended time between ballast maintenance. The purpose of the ballast depth is to ensure proper

load distribution to the subgrade and the ballast depth may need to be increased in the case of weak subgrade. The purpose of the shoulder and crib ballast is to restrain against lateral and longitudinal track movement which has become more important due to the lateral forces induced by larger trains and by thermal stresses in continuously welded rail (CWR). The ballast gradation and material quality specifications ensure adequate drainage and enough strength to maintain proper cross level, surface, and alignment.

Over time, the ballast section will deteriorate due to the natural breakdown of ballast material and infiltration from outside sources [10]. This often results in multiple trends, including the rounding and degradation of particles which reduces the ballast strength and changing gradation from the introduction of fine particles which inhibits drainage. This process is well known but difficult to quantify in a manner that reliability relates to the reduced performance of the ballast section.

3.1.1 Introduction to Ballast Behavior

During cyclic loading from train operations, the ballast has two responses: an elastic/recoverable deformation and an inelastic/permanent deformation. While the two responses are related, the scope of this project is to focus on the second response, inelastic/permanent deformation which will be referred to as ballast settlement. Ballast settlement occurs similarly to all granular materials through changes in gradation and deformation of the ballast matrix [11]. Specifically, ballast settlement can occur from particle rearrangement, lateral flow, and grinding or attrition of asperities (Type I damage), breakage of angular corners or projections (Type II damage) and splitting and crushing of particles (Type III damage) [12].

The parameters influencing ballast settlement are numerous and interconnected, and mathematically modeling ballast settlement is a difficult task for numerous reasons. First, since ballast characteristics are often dependent on the blasting or crushing techniques and rock types of locally available quarries, it can be difficult to isolate relevant parameters in the laboratory or field since each batch of ballast will have different characteristics that can significantly change the ballast response.

Second, ballast particle interaction is dictated on the particle scale, and, since characterizing and replicating each individual ballast particle is unreasonable, simple indices have been developed and used to capture relevant ballast matrix characteristics. While these indices are helpful, many other important ballast characteristics are currently difficult to measure on a large scale and the available indices can be imperfect when it comes to capturing ballast behavior.

Despite these challenges, there has been much effort to understand the various parameters influencing ballast settlement. While this has not led to perfect mathematical models, this work has significantly improved ballast performance through industry-agreed upon specifications as well as a conceptual understanding that led to improved decision-making capabilities for ballast maintenance [7]. The following sections provide a summary of the various parameters and their known influence on ballast settlement.

3.1.2 Clean Ballast Behavior

This section provides an overview of ballast behavior immediately after placement. This new ballast is often referred to as “clean” ballast behavior because of its lack of fine particles in the ballast matrix and will be close to the AREMA design specifications because it has not

experienced significant deterioration. The main factors attributed to clean ballast behavior are density (void ratio), gradation, material quality, and material angularity. Significant effort was put into testing and specifying clean ballast in the 1980s and 1990s, and these tests provided many of the ballast design specifications that are used today [7].

Ballast Density

Historically, ballast density has been known as a primary factor in ballast settlement [10] [13] [14] [15] [16]. Ballast is often in a loose state (high void ratio) after placement or tamping, and it experiences an initial rapid settlement as the ballast particles compact into a denser state. This rapid settlement is often referred to as the "Consolidation Phase." After this initial compaction, the settlement rate continues to decrease or reaches a linear trend. This is called the "Post-Consolidation Phase." Figure 42 displays a conceptual example of ballast settlement.

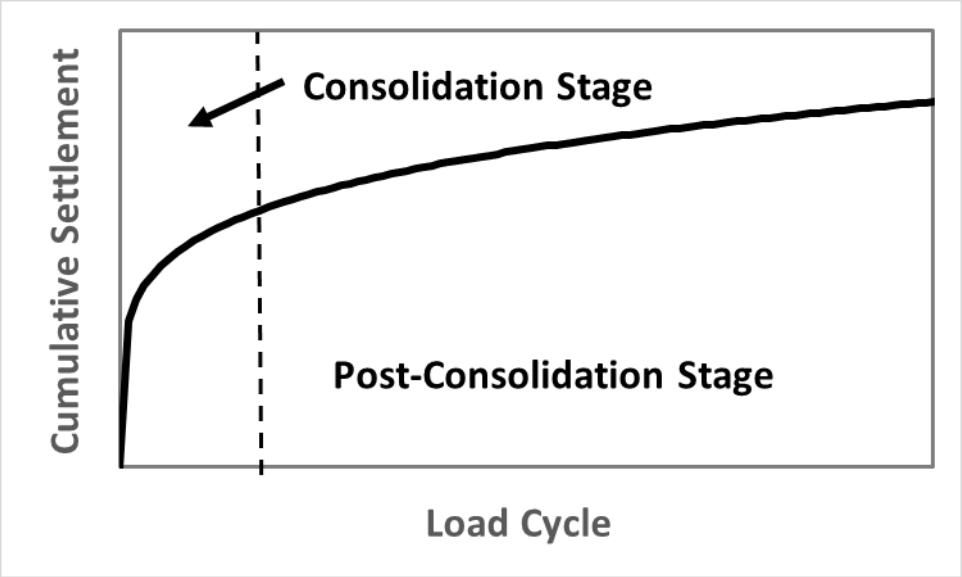

Figure 42: Conceptual Ballast Settlement Trends

Measuring or estimating ballast density can be done using one of four methods. The first method is to take physical measurements of the void ratio and the actual density. This is the most accurate characterization of ballast density, but it is exceptionally difficult to field measure due to the high level of physical effort and disruption of the ballast during sample collection.

A second method would be to measure the ballast modulus through seismic waves devices [17] or Falling Weight Deflectometers (FWDs) [18]. These devices are non-destructive and site specific but often require expert interpretation and still require wide-scale validation.

A third method would be to infer to the ballast density through track-based vertical stiffness measurements, such as track modulus [10]. Previous studies showed a relationship between track modulus and track performance in poor ballast and subgrade conditions but is not commonly measured outside research test sites [10]. Track modulus also includes other track characteristics such as fasteners, ties, and subgrade, so it can be difficult to isolate the ballast region.

A fourth method is to estimate the ballast density through tonnage after surfacing. This method calculates settlement curves as a function of the number of load cycles which can be estimated if the traffic characteristics such as annual tonnage and axles loads are known (see Figure 42). If

Wheel Impact Load Detector (WILD) sites are nearby [19], this method can become even more accurate. Currently, this method may be the most reliable indicator of ballast density on a large scale because it is the only method that can be applied over an entire track system. The second (seismic waves) and third method (track modulus) may be beneficial in site-specific cases that require more detailed information.

Ballast Gradation

Gradation is another factor that can affect the settlement of clean ballast. Typical ballast gradation ranges from AREMA specifications #3, #4, #4a, and #25 for main lines and can be referenced in AREMA Chapter 1 (Roadway and Ballast) and Chapter 2 (Ballast) [7]. These gradations involve large ballast particles that are usually of similar size, known as uniformly graded in geotechnical engineering. Laboratory studies suggest that more well graded samples reduce settlement but can inhibit drainage if too many degraded particles are present [10] [13].

Typically, the gradation of clean ballast is known because quarries provide it to a particular gradation, but the ballast will degrade over time and therefore, change its gradation. This degradation can be estimated using Selig's FI that is introduced in Section 3.1.3.

Material Quality

Material quality represents the rock material of the actual ballast particle and can also affect settlement of clean ballast. While ballast material quality affects the deterioration of ballast and its lifespan, material quality has also been found to affect the short-term track geometry performance. In general, railroads prefer premium rock types such as granite and traprock if that rock is available from a local quarry.

Multiple indices have been proposed to characterize material quality. Los Angles Abrasion (LA Abrasion), a test that replicates dry crushing resistance is commonly used and is often specified in AREMA and railroad standards, however, its ability to predict ballast performance is controversial [13]. Developed by Canadian Pacific Railway (CP), the Abrasion Number (AN) method combines the LA Abrasion and Modified Mill Abrasion (MAA), replicating both dry particle crushing and abrasion ballast degradation modes and considered more reliable than LA Abrasion [20] [21]. Lower ANs have been shown to result in lower settlement and ballast degradation over time [20] [21].

Particle Shape Characteristics

A fourth "group" of factors that can affect ballast performance is the ballast particle shape characteristics which can include the angularity of ballast particles with an angularity index (AI), flat and elongated ratio (F&E Ratio), and Surface Texture Index (STI) [22]. Ideal ballast particles should be angular and elongated with high surface texture so the particle edges can interlock with each other and create a strong resistance to impeding forces. Past studies show that higher angular particles generally perform better, but the combination of particle shape characteristics and performance can be complicated [13] [22].

The measurement of ballast particle shapes is historically a tedious task and would require measuring the individual ballast particles and counting number of ballast particle faces. Improvements in image detection software over the past decade now allow for ballast particle characteristics to be measured with photography methods. An example of this is the University

of Illinois Aggregate Image Analyzer (UIAIA) [22]. These photography methods are still required to bring samples to a laboratory, but these methods have the potential to become track-based and incorporated into machine vision techniques in the future.

3.1.3 Degraded Ballast Behavior

As the track experiences tonnage and climate conditions, the ballast particles will degrade over time. The ballast degradation mechanism can be from the multiple degradation modes mentioned previously, including abrasion, breakage, or crushing [11]. In addition, outside fine particles from multiple sources can infiltrate the ballast. These sources can include, but are not limited to, windblown particles from the surface or falling from passing trains, degraded tie particles, subballast particles, or particles pumped up from the subgrade. A study published in the early 1990s suggested that most ballast fines are from ballast degradation (73 percent), but the fine source can vary significantly from site to site [23].

Degraded ballast, referring to the degradation and rounding of the large ballast particles, and fine-filled ballast, referring to the change in gradation by the introduction of fines to the ballast matrix, reduce ballast performance through various means. First, the degradation of ballast particles will result in smaller, rounder ballast particles that have a reduced ability to interlock with each other and results in a weaker ballast matrix [24]. In addition, if the number of fines in the ballast matrix reaches a certain level, the interlocking will shift from particle or ballast-particle interlock to ballast-fine or fine-fine interlock. This means the strength of the ballast matrix will become dependent of the fine particles and the factors, such as moisture, which influence fine particles. The fine-fine interaction also tends to be weaker than the larger ballast particles and typically results in track that is more susceptible to settlement [10]. A third factor is that the smaller degraded ballast particles have smaller void openings for drainage and fines can block these drainage paths, resulting in excess water not being able to drain from the ballast section. This reduced drainage in the ballast section can cause water to be trapped within the track or ponded on the track surface which not only further deteriorates the ballast and ties but can also weaken the ballast section because the strength of fines is highly moisture-dependent [10] [25].

These factors are difficult to capture in detail, but multiple indices have been developed to characterize fine-filled ballast and relate it to performance. As with clean ballast, the fine-filled ballast parameters often interact in complicated ways making it difficult to isolate the exact influence of each parameter.

Fine Levels

Fine levels generally represent the amount of fine material that is present within the ballast matrix. Fines in North America are defined as particles passing through the No. 4 sieve (4.75 mm) but countries outside of North America have used different sieves as the cutoff.

Various indices have been developed to represent fine levels in track [26]. In the United States, mass-based measurements are used include percent passing and Selig's FI [10]. Percent passing regards the mass of material passing through the No. 4 sieve while Selig's FI takes the summation of material passing through the No. 4 sieve (P_4) with the material passing through the No. 200 sieve (0.075 mm) (P_{200}).

$$FI = P_4 + P_{200} \quad (3)$$

The purpose of doubling the influence of the materials that pass through the No. 200 sieve, which are typically silts and clays, is that these fine types resulted in reduced performance and inhibit drainage. FI is historically measured taking gradations but ground penetrating radar (GPR) has become more commonly used because it is track-based and therefore captures fine levels on a system-wide basis [26] [27] [28] [29] [30]. This report separates the gradation FI measurement (Selig's FI) with the GPR measurement ballast fouling index (BFI) because while similar, Selig's FI is a point measurement that physically measures mass while BFI is aggregated result based on radar reflections of a larger volume of track (e.g., 15 feet in length by 16 inches in depth).

Researchers in Australia and South Africa have developed volume-based indices to account for coal fines that have the specific gravity of about half that of typical geomaterials and may misrepresent FI measurements. The two volume-based indices are Percentage Void Contamination (PVC) and Void Contamination Index (VCI) [31] [32] [33]. These two indices essentially measure the amount of volume the fines fill in the void spaces. This measurement requires more specialized equipment than sieving, so it has not been adopted in North America.

Moisture

Moisture begins to have a significant influence on ballast settlement once fines start filling the ballast voids. That is because any excess moisture quickly drains in clean ballast, and water does not significantly reduce the particle-to-particle interlocking of the ballast. However, as commonly known in geotechnical engineering, moisture can significantly change the behavior of fine particles, especially very fine particles such as silt- or clay-sized particles [25].

Moisture is a difficult metric to measure on a large-scale. The moisture levels can be measured directly with sampling or through calibrated moisture sensors [30] [34]. Typically, these are only used at research test sites. GPR can be used to indicate moisture, and moisture often influences the FI measurement, but GPR's ability to directly measure moisture is still controversial and may depend on the analysis method. Moisture has been indirectly estimated based on climate and these moisture estimates can be useful for comparing different geographic regions but would not capture yearly or seasonal changes or specific rain events [20]. The climate-driven performance predictions could eventually be expanded to incorporate changes in climate.

Fine Type

Fine type is another potential influence on ballast settlement because different fines, such as sand, silt, or clay, tend to behave differently. For example, ballast filled with sand-sized particles are still likely to drain and will not be as affected by moisture as ballast fines filled with silt-sized or clay-sized particles. The silt- and clay-sized particles are typically highly impermeable and significantly influenced by moisture.

Fine type is a factor that is difficult to characterize and, while gradations can separate sand-size particles from silt- and clay-sized particles, hydrometer tests would be needed to separate silt-sized and clay-sized fines. In addition, minerology analyses are needed to identify the true source of the fine material.

Fine type can be estimated because most ballast fines occur from natural ballast degradation [23]. However, specific locations or track segments may be different due to other circumstances. Some examples are flooded cuts, which can pump up degraded shale, other fines in the ballast

[35], river flooding areas which can flood silt- and sand- particles, windblown sand areas, and coal lines and other commodities that can infiltrate the ballast.

Lab and Field Studies

The individual parameters affecting degraded fine-filled ballast settlement are not separated in this literature review because the three factors of fine levels, moisture, and fine type are highly interconnected, and previous studies were conducted differently, showing much variation in the results. Therefore, conclusions from the various past studies are better understood conceptually.

Large-scale cyclic triaxial tests have been performed on fine-filled ballast created by natural ballast degradation [24]. The test compared clean ballast, degraded ballast without fines, and degraded ballast with 40 percent fines, all in dry conditions. The degraded ballast without fines settled about 1.5 times more than the clean ballast because of the reduced frictional interlock from the breakdown of ballast shape characteristics. Even greater settlement was observed for the degraded ballast with fines (two times the clean ballast). Similar results were observed during other large-scale triaxial tests [36].

Cyclic ballast box tests were performed using a test matrix of various fine levels, moisture, and fine types [37]. The results emphasize the influence and interaction of fine levels, moisture, and fine type. In general, as the fine level increases, the influence of moisture and fine type become greater. For sand-sized particles, the influence of moisture is smaller; however, for clay-sized particles, moisture has a significant influence. For example, ballast with clay-sized fines showed almost no increase in settlement from clean ballast when dry but a 10 time increase in settlement when wet.

Full-scale tests at the TTC Rainy Section were performed on fine-filled ballast resulting from natural ballast degradation [34]. The test involved a track section with 40 percent fines from natural ballast degradation. The results showed that the dry section had similar settlement rates to those of the clean ballast condition; however, the settlement rates significantly increased when wetted. In addition, the wet tests caused the track section to mud pump and changed the distribution of fines on the surface track, further impeding drainage. The test results showed that moisture was the key factor influencing settlement and stiffness, while the distribution of fines (mud pumping near the ties) affected the ballast drainage ability.

Revenue service tests have compared FI from GPR and track geometry degradation at multiple site locations on both passenger and freight lines in the northeast United States [38]. The study implemented an exponential statistical fit to relate BFI and track geometry degradation.

3.1.4 External Conditions

In addition to the ballast condition, external conditions can play a significant role in ballast settlement. These include, but are not limited to, loading condition, tie and subgrade type, and maintenance.

Wheel Load

Historically, wheel load has been known as a main influencer of ballast settlement because it relates directly to the ballast stress imparted from the ties. Wheel load should have a proportional relationship to ballast stress at any individual location, but that relationship will vary from location to location because the vertical load distribution through the track structure depends on

rails, ties, ballast support, among others. Multiple laboratory tests have been conducted to investigate how increased vertical loading affects settlement and how wheel loads combinations can affect settlement [20].

Wheel load can be estimated from the train traffic characteristics or more accurately measured with WILD sites [19]. The distribution of load through the track system to the ballast is difficult to measure directly because of the extreme loading conditions between the tie and ballast. Therefore, the force and pressure values are often assumed through load distribution equations and/or modeling software. However, the actual conditions are likely to deviate from the idealized assumptions because the distribution of rail load to the ties and tie load to the ballast are highly dependent on the tie-ballast support conditions which are difficult to characterize without measuring the loaded track deflection. Modeling software is then required to back-calculate the load [11] [39].

Confinement

Confinement is another factor that will affect the settlement of geomaterials such as ballast. Ballast confinement occurs in the ballast section from the dead load of the track structure, train loading, and likely residual stress, from the interlocking of the ballast particles [25]. Confinement is a notoriously difficult metric to measure in the field or represent in the laboratory, but it has been shown to be an important factor (~4x influence) in laboratory testing [40] [41] [42]. Confinement is difficult to measure directly and would require lateral pressure cells but can be indirectly categorized with ballast shoulder and the existence of confining structures such as wing walls [43].

Loading Frequency

Loading frequency is influenced by vehicle speed and axle spacing. For the ballast, two axles will provide one load pulse [20], and the frequency of the pulse will be dependent on the vehicle speed. Multiple laboratory studies have investigated the influence of loading frequency and found an influence similar to confining pressure [42] [44] [45].

Tie Type

Tie type affects ballast settlement from different loading distributions due to changes in the vertical load distribution through the track, stiffness differences between the tie and ballast, and tie deterioration. Concrete ties generally produce a stiffer track than wood ties, and the stiffness difference between the concrete and ballast can result in a higher ballast pressure. This effect has been recognized [20], but other factors such as variability in settlement amongst a group of ties can play a role as well. In addition, the tie type can be determined from track charts or by inspecting the track location.

Subgrade

Subgrade affects ballast settlement by changing the stress and displacement of the ballast along with causing drainage and pumping issues. The subgrade stiffness affects how loads are distributed through the subgrade, and a soft subgrade will displace, causing movement of the ballast layer above it. A subgrade that settles will often cause drainage issues that result in standing water underneath the ballast which can result in increased ballast deterioration and pumping of subgrade fines into the ballast.

If the subgrade type is known and tested, the behavior can be modeled or conceptually understood. Determining the subgrade type is often not practical because it requires soil sampling and laboratory testing. The subgrade type may be estimated by using previous soil records from geological surveys or nearby highway projects, but these records may be incomplete or may not represent the soil underneath the track.

The subgrade behavior can be indirectly estimated using one of the three following methods. First, subgrade modulus has the greatest influence on track modulus [46], so a low track modulus may indicate a soft subgrade. Second, GPR can often determine the roughness of the ballast/subgrade interface with rougher areas representing a poorer subgrade performance. Third, GPR can also identify ballast pockets which are the direct result of subgrade settlement and can be another performance indicator [35].

Tie-Ballast Interface

The tie-ballast interface can affect ballast settlement because hanging ties (tie-ballast gap) will induce a different loading environment than a tie that has good contact because of the additional movement. This has not been well studied, but ballast box tests have shown that a tie-ballast gap increases ballast settlement rates up to 10 times and multiple studies on tie-ballast interaction have been conducted regarding bridge approach and the increased settlement rates experienced in those regions [11] [39] [47] [48].

A second aspect of the tie-ballast interface is the inclusion of under-tie pads (UTPs). These have been shown to reduce track geometry issues [49]. The reduction in track geometry issues is believed to occur because UTPs improve the load distribution along the track and the vertical load distribution amongst ties as well as providing a cushioning layer between the concrete ties and ballast.

The tie-ballast interface can be estimated from track deflections, especially in low load environments such as 10-kip wheel loads. Higher 10-kip rail deflections are often an indicator of hanging ties while higher 40-kip rail deflections could indicate both hanging ties but also soft ballast and/or subgrade. The inclusion of UTPs would need to be known from installation records.

3.1.5 Inspection Technologies and Performance Parameters

This section summarizes how various inspection technologies and other informational sources can measure important ballast parameters, which Table 6 lists the inspection method, the parameters it can measure, the rate of change of that parameter, and any additional comments. The goal of this exercise is not only to assess the ability of the inspection method to evaluate the parameter but also estimate what is available and how often that parameter is expected to change over the analysis period.

The review suggests that the current inspection technologies can estimate most of the important parameters, but the confidence in those estimations may not be very high. Most parameters (e.g., tie type, subgrade type, tonnage, etc.) will be relatively constant over a period of a few years, and therefore, can be documented after a single inspection. The factors that change continuously (e.g., BFI and moisture) have a greater influence on ballast performance.

Table 6: Inspection Methods and Performance Parameters

Inspection Method	Parameter	Change	Comments
GPR	Fine Levels	Continuous	
	Moisture	Continuous	Vendor dependent
	Subgrade	Constant	Roughness of ballast-subgrade interface
General Knowledge (Track Charts, etc.)	Axle Load	Constant Over Short Term	Supplement with WILD if needed
	Annual MGT	Constant Over Short Term	
	Tie Type	Constant Over Short Term	
	Subgrade	Constant	General estimates
	Ballast Type	Constant Over Short Term	
	Fine Type	Constant	
	Loading Frequency	Constant Over Short Term	
Machine Vision	Tie Type	Constant Over Short Term	
	Ballast Shape	Continuous	Depends on how surface ballast represents ballast below tie
LiDAR	Confinement	Constant Over Short Term	Shoulder width may represent confining conditions
Deflection Methods	Tie-Ballast Interface	Continuous	Labor intensive

3.1.6 Summary

Ballast behavior under cyclic loading is a complex process that involves many different parameters. Due to the difficulty characterizing each important parameter, the interaction between parameters, and differences between testing types, it is difficult to quantify the exact influence of each parameter.

The parameters with the greatest influence appear to be loading (wheel load) and tonnage, ballast density, ballast fouling, and moisture. These parameters can usually be measured or estimated using wayside equipment or track knowledge (loading), compaction estimations (density), and inspection methods (BFI and moisture). Moisture can potentially be measured using GPR, but this process is still in development.

3.2 Track Geometry Representation

The previous section shows how various aspects of the ballast and track system can affect track settlement and geometry behavior, but a third potential factor is how the ballast and track system varies along the track. It is possible that certain track geometry situations are indicative of potentially severe conditions. This section introduces topics that will be used later in Section 4.

3.2.1 Types of Track Geometry Representation

This report uses three different representations of track geometry: settlement, a 62-foot surface profile mid-chord offset (MCO), and a 200-foot running standard deviation (SD). Each of these representations are described below:

- Settlement (u): Settlement refers to the amount of permanent vertical displacement of a single-track location over time. Settlement can be measured using multiple methods, but it is typically measured with survey equipment or estimated from a track geometry space curve. Settlement is often used in wayside measurements and is most directly relatable to laboratory tests. In addition, settlement is not referenced in track safety standards. This makes settlement measurements valuable from a research standpoint but is often not used in practice. As a note, all the mechanistic models introduced in the next section use settlement as the main output.
- 62-foot surface profile MCO: The 62-foot surface profile refers to the vertical track geometry deviation over a 62-foot track segment. In this study, the absolute value is used to keep all values positive and is referenced as surface magnitude (SM). The 62-foot surface profile can be measured using stringlines or, more commonly, track geometry cars. While MCOs of different lengths exist, 62 feet-foot is the most commonly used and is used directly in track geometry intervention limits and track safety standards. Its common use with maintenance and regulatory limits makes SM valuable from a practice standpoint but is not often calculated in research projects.
- 200-foot running SD: SD refers to the track roughness over a 200-foot window. This track geometry representation can be calculated from elevation measurements or using MCO values from track geometry cars and has different variations. The window length can vary in different parts of the world (100 m often used in Europe). Researchers in the United States typically square the value, calling it a 200-foot Running Roughness (R^2). SD and R^2 representations are more suited for high-speed passenger lines, so they are rarely used in the United States except from a research standpoint.

In this study, the rate of change of the values u, SM, SD, R^2, referred to as the degradation rate, is of interest. To keep the values reasonable and applicable, the change in track geometry over 100 MGT is used unless noted otherwise. The notation for the change of these values over 100 MGT will be referenced in this report as dU, dSM, dSD, and dR^2.

3.2.2 Relationships Between Various Types of Track Geometry Representation

While each of the three representations provides insight into the vertical movement of the track, there are key differences between them. One of these differences is the track segment length. Due to this, using multiple representations may aid in the identification of different shapes of track geometry deviations.

There have been a few studies that have investigated the settlement-roughness (u and R^2) relationship, but these studies typically have not involved SM. This section will review previous work on the u and R^2 relationship and then conceptually explore the various relationships in detail.

Settlement (U) and Roughness (SD, R^2)

As mentioned, there have been a few previous studies that compared u to the 200-foot SD or 200-foot R^2. Studies summarized by Chrismer and Selig (1991) proposes a linear relationship between the two variables with a conversion factor (α) of 0.15 based on results that varied from 0.05 to 0.20. The equation is shown below where dSD is the change in 200-foot SD over 100 MGT and dU is the settlement rate per 100 MGT. Since the relationship is linear, any MGT value can be used if it is the same for dSD and dU.

$$dSD = 0.15\ dU \tag{4}$$

More recent studies compare the change in R^2 with change in settlement with a linear relationship [50]. The conversion factor between dR^2 and dU is estimated to be 0.018. If, however, the square root of the conversion factor is taken, the dSD and dU conversion is 0.17 which matches closely with the studies from Chrismer and Selig (1991). However, both studies assume linear relationships between dU and dSD and dR^2. Since R^2 is the square of SD, both relationships should not be linear, but no study has comprehensively looked at this topic.

While the past studies used dU, dSD, and dR^2. The assumed linearity generally allows for the assumption of the same relationship with u, SD, and R^2.

Sixty-two-foot Surface Profile (SM) and Roughness (SD, R2)

The authors are unaware of comparisons between the 62-foot SM and track roughness measurements (SD, R^2). However, the results of this study (data from Section 4) were used to explore this conversion.

Figure 43 shows the comparison between (a) SM and SD and (b) SM and R^2 for the entire dataset. The results suggest a linear relationship between SM and SD and non-linear relationship with SM and R^2.

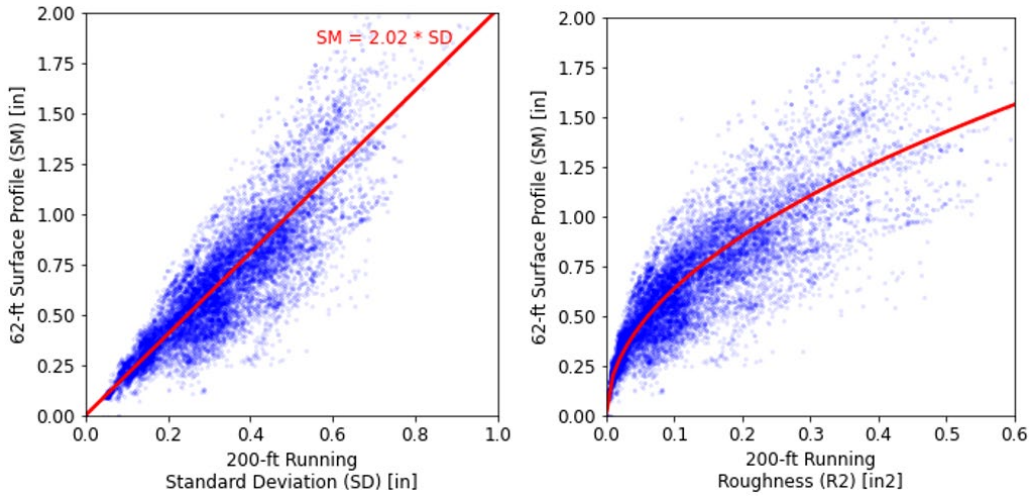

(a) **(b)**

Figure 43: Relationship Between the 62-foot Surface Profile (SM) and 200-foot Running SD (a) and R^2 (b)

The conversion factor between SM and SD is taken as the SM/SD ratio. The SM/SD values are plotted in Figure 44 against the SM values and a box plot of the distribution is also shown. The

results showed the median SM/SD value is 2.02 and ranges from about 0.8 to 3.2. The box plot shows that most data points are within 1.7 to 2.3, a fairly tight range. The scatter plot shows the SM/SD values are generally evenly distributed with SM, however, high SM values tends to additionally have high SM/SD value. This observation will be important in subsequent sections.

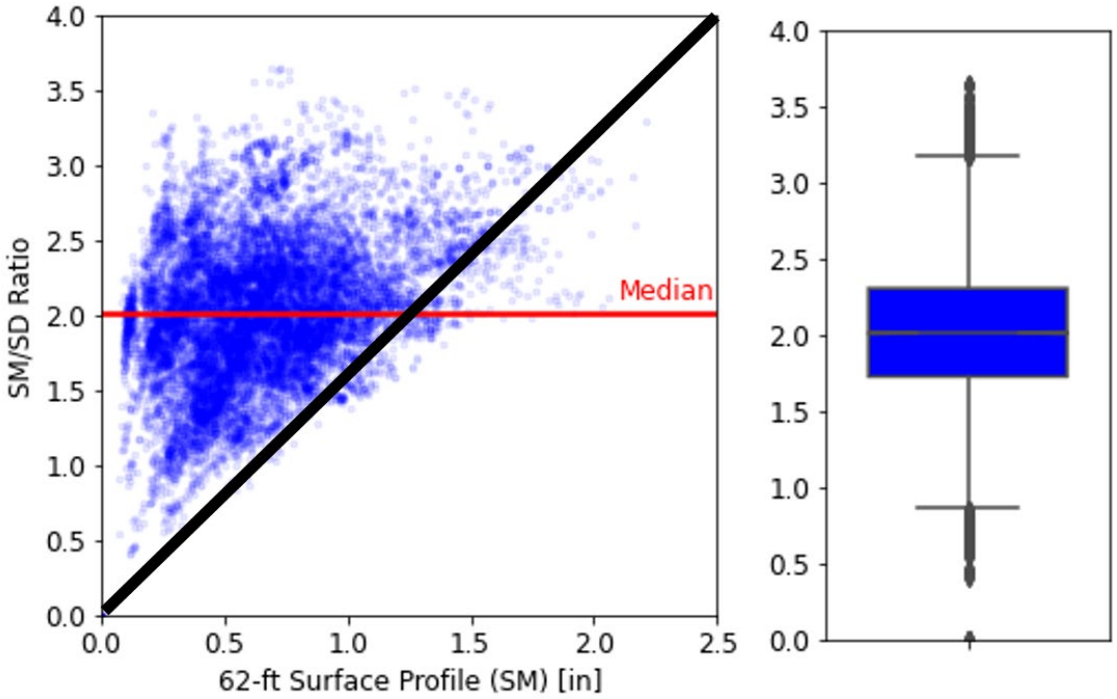

Figure 44: SM/SD Values Along with Box Plot of SM/SD Values

A simple conceptual example can be used to explain what causes this range in SM/SD values. Figure 45a shows two theoretical examples of a single deviation and a continuously rough track. These two situations are highly ideal but may give some indication of an "upper and lower bound" of SM/SD. By calculating the SM and SD from each example for a range of deviation magnitudes (1 inch is shown in Figure 45a), relationships can be established.

The results suggest that the SM/SD ratio is about 1.41 for a continuously rough track and 3.57 for a single deviation. This matches the data well for a simple conceptual example.

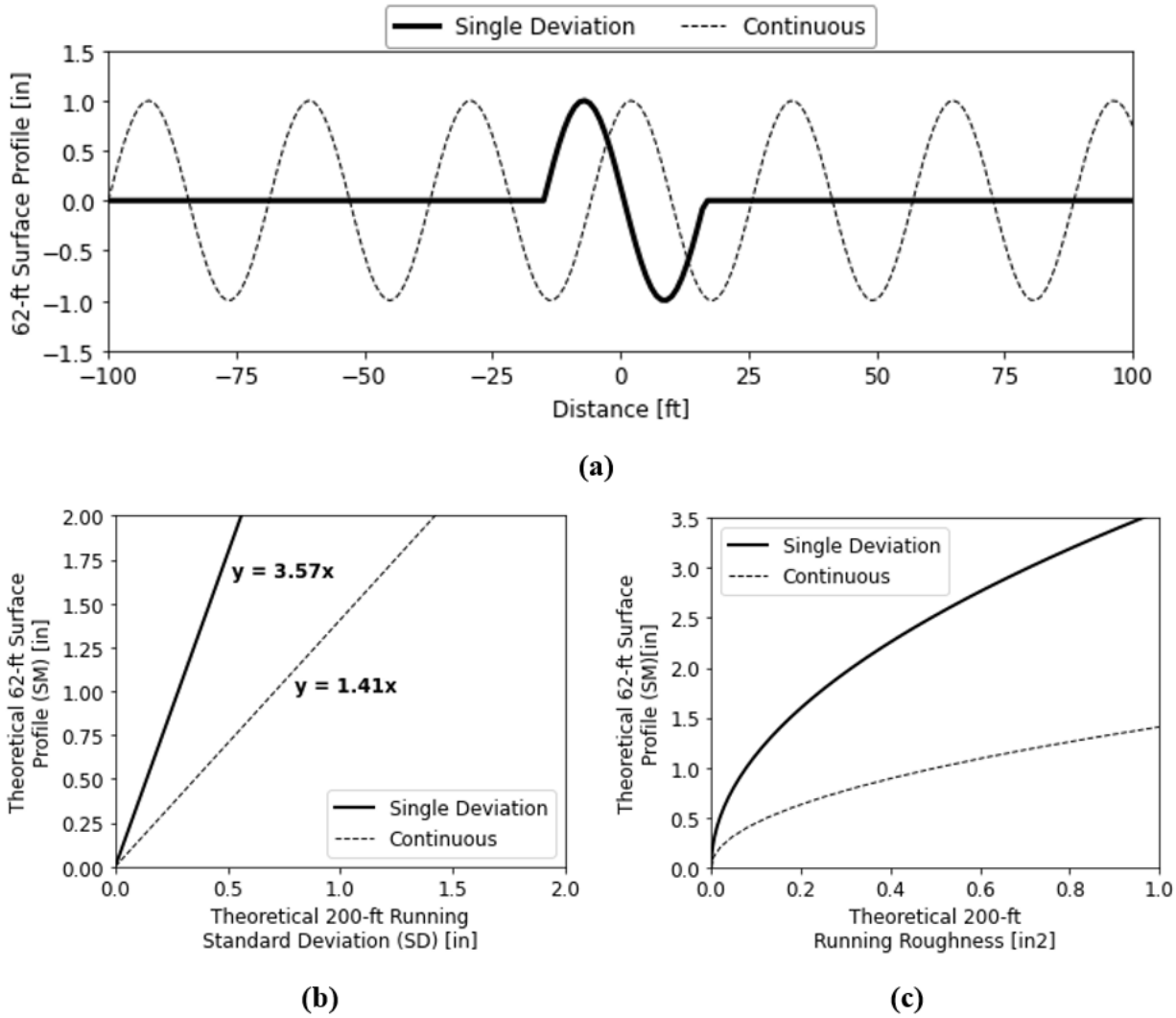

Figure 45: Conceptual Example Comparing Single Deviation vs. Continuous Roughness (a) and Effect on the SM/SD Relationship (b, c)

Two additional aspects that may affect the SM/SD value is the deviation wavelength and the window length of the running SD calculation. Figure 46a shows that shorter wavelength deviations produce higher SM/SD values than longer wavelength values. Continuously rough track will not be affected by the wavelength. Figure 46b includes the relationship with window length. This is not relevant for this study since the 200-foot window is used throughout but is included for theoretical comprehensiveness.

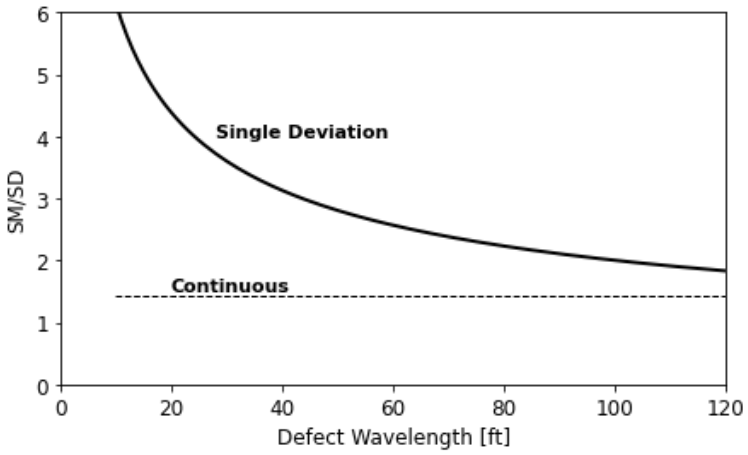

(a)

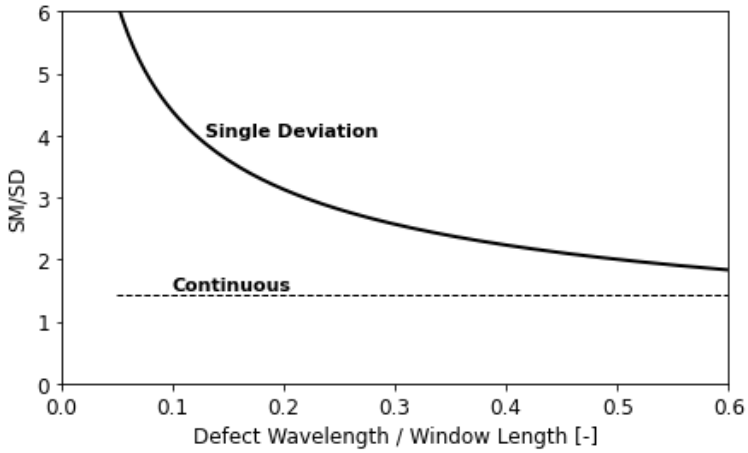

(b)

Figure 46: Plot of SM/SD Ratio for Single Deviation and Continuous Roughness with Defect Wavelength (a) and Normalized Defect Wavelength and Window Length (b)

In summary, the SM/SD relationship appears to indicate the shape of the deviation and whether the track geometry deviation is from a single location or a continuously rough track.

3.2.2.1 Settlement (u) and 62-foot Surface Profile (SM)

The authors are not aware of any study that investigated the relationship between settlement (u) and 62-foot surface profile (SM), but an estimate can be calculated by using the SD/u (α) and SM/SD relationships presented in the previous sections. The equation to relate u and SM is derived below:

$$SM = \left(\frac{SM}{SD}\ Ratio\right) * SD \tag{5}$$

$$SM = \left(\frac{SM}{SD}\ Ratio\right) * (\alpha * u) \tag{6}$$

$$SM = \left(\frac{SM}{u}\ Ratio\right) * u \tag{7}$$

Assuming α=0.15 and SM/SD=2, the SM/u Ratio will be 0.3. This ratio implies that a settlement of 1 inch will result in a SM of 0.33 inches. This SM/u Ratio assumption of 0.3 will be the assumption used in the remainder of the report. Using the high and low values, α ranging from 0.05 to 0.2 and SM/SD ranging from 0.8 to 3.2, the anticipated range of SM/u Ratio is 0.04 to 0.64. That means the SM/u Ratio is anticipated to vary significantly depending on the track condition.

3.2.3 SM/u Ratio in Different Simple Track Scenarios

This section expands on how various track scenarios may influence the SM/u Ratio and possible implications on track performance. These scenarios are considered simple but should at least help bound the range in possible conditions, explain outlier situations, and show the importance of the surrounding track for the behavior of a single location.

Scenario 1: Uniform Settlement (SM/u Ratio = 0)

The first scenario presented in Figure 47 shows the track response to uniform settlement where all track locations settle the same amount or at least at identical rates. The scenario shows that, in these cases, high settlement values at a single location do not necessarily produce an SM value. This situation may be relevant immediately after tamping. In this case, the SM/u Ratio would be 0.0.

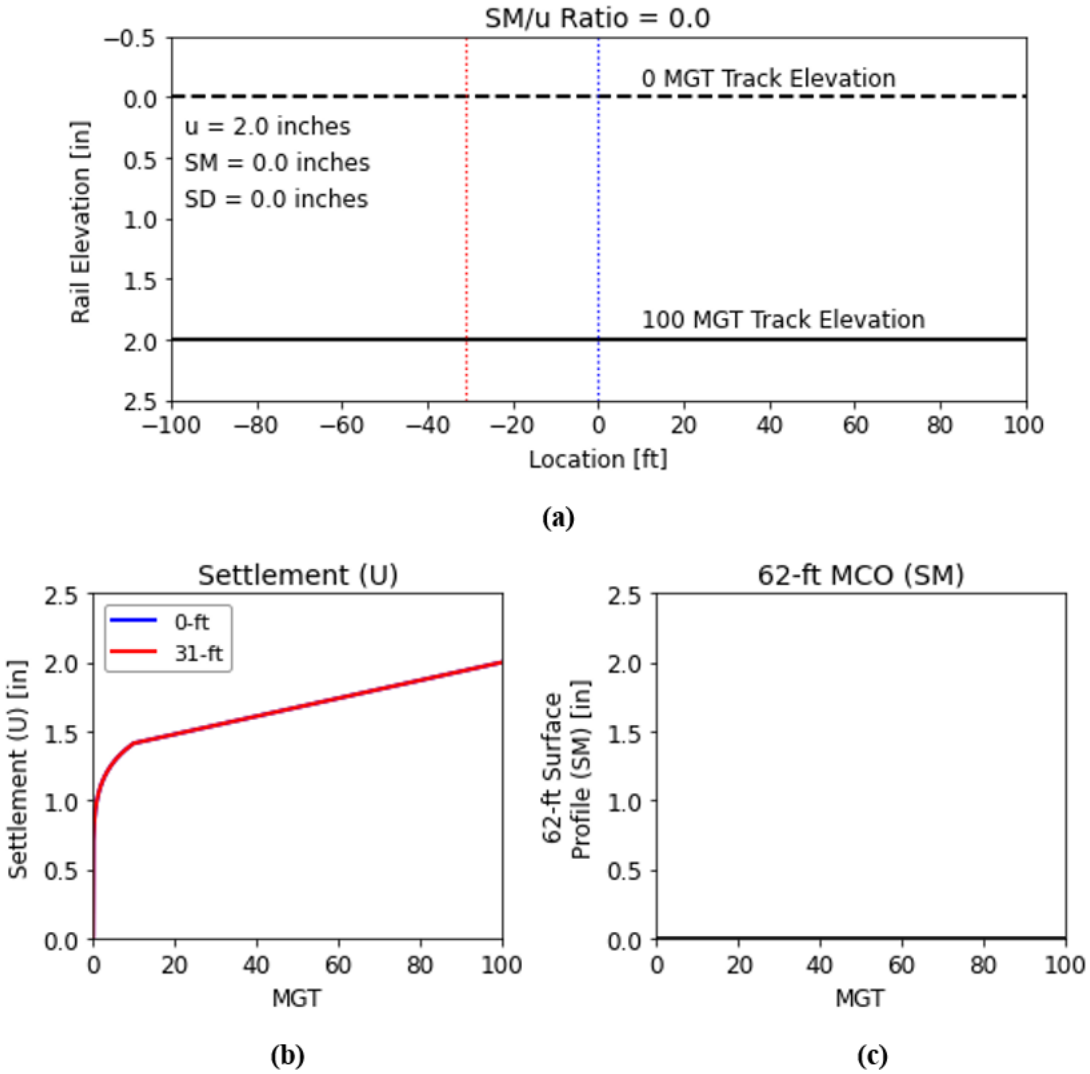

Figure 47: Simplistic Scenario Showing Uniform Settlement (a) and its 31 ft MCO Influence on Settlement (U) (b) and the 62-foot Surface Profile (SM) (c)

Scenario 2: Single Deviation (SM/u Ratio = 1.0)

The second scenario, presented in Figure 48, shows the opposite response where a single-track location settles, but the surrounding track does not. In this scenario, the SM/u Ratio is 1.0 with the settlement and SM value being equal. This scenario would also have a higher SM/SD ratio.

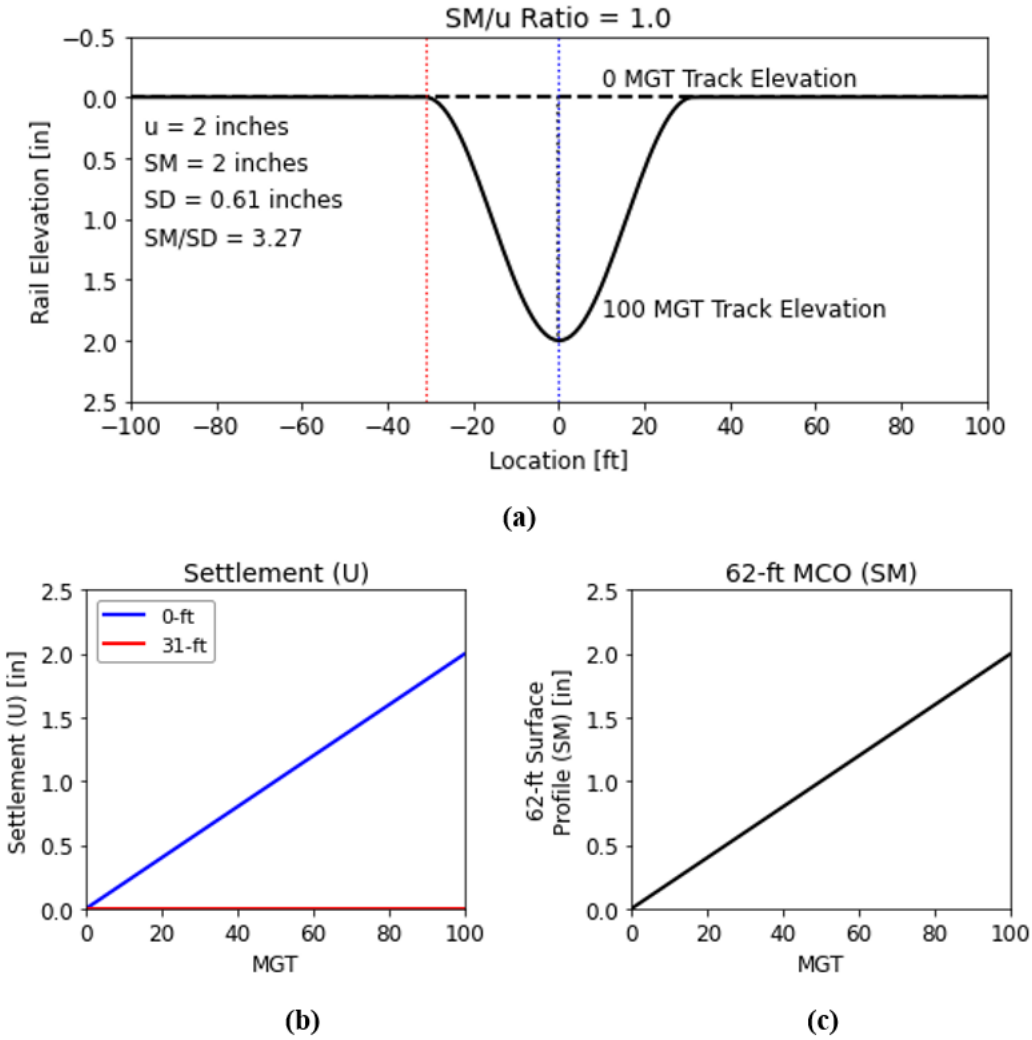

Figure 48: Simple Scenario Showing Single Deviation (a) and its Influence on Settlement (U) (b) and the 62-foot Surface Profile (SM) (c)

While the settlement and SM values are anticipated to be related, these scenarios show that while the ballast condition and track system may influence the settlement at a particular location, the behavior of the surrounding track is also important. It also appears that single deviations (high SM/SD value) pose a greater risk for high SM values than track that is degrading over long stretches of track (low SM/SD value). This is a potential explanation for the high SM/SD, high SM cluster in Figure 44.

3.2.4 Track Geometry Representation in Field Data

The previous sections present simple conceptual scenarios to explore how different track responses can affect the SM and SM/SD values. Field data is much more complex, but the concepts presented earlier can still be identified. The following two scenarios show how parameters indicate how the track is degrading use field data.

Scenario 1: Single Track Geometry Record

The first scenario compares two track geometry locations (~1,600 feet in blue and ~2,200 feet in red) with how the SM/SD ratio corresponds to the track geometry shape. Figure 49 shows this comparison. The ~1,600-foot location in blue is a typical situation where the track is rough with some noticeable deviations. This situation produces an SM/SD Ratio of 2.38 which would be within the range of most cases. The 2,200-foot location in red, however, has a clear single deviation and a corresponding SM/SD Ratio of 3.05, which would be considered high.

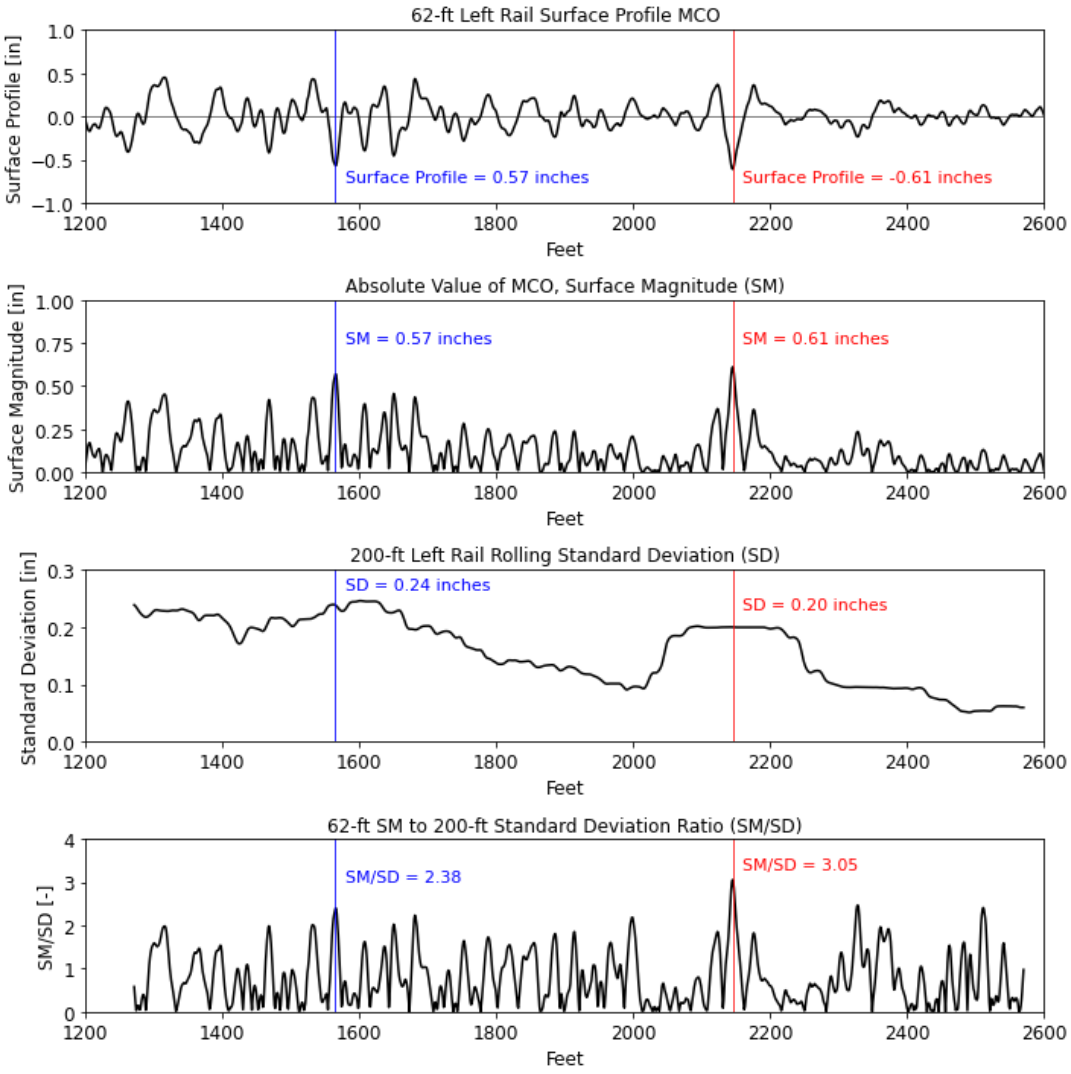

Figure 49: Example of the SM/SD Value from Field Data

Scenario 2: Track Degradation

The second scenario expands on how changes in the track geometry shape over time can also be characterized. A second parameter (dSM/dSD) is introduced. This parameter is the ratio between the SM and SD degradation rates (dSM and dSD). Essentially, a higher dSM/dSD value (>3) indicates that the location of the maximum surface profile is degrading at a quicker rate than the surrounding region. Lower dSM/dSD values (<1.5) indicate that regions around the location of

maximum surface profile are degrading at a quicker rate than the maximum location. The dSM/dSD parameter is likely not predictive but may be helpful in explaining track behavior.

Figure 50 shows a second track location that has two rough areas (4,000 to 4,300 ft and 4,500 to 4,800 ft). The first rough area is not ideal but would not appear to be high risk while the second area shows very high levels of degradation. This scenario is included to show how the SM/SD and dSM/dSD values correspond to these two locations. The first location shows moderate SM/SD (2.2 to 2.45), moderate dSM (0.75 in/100 MGT), and low dSD (0.19 in/100 MGT). This produces a higher dSM/dSD value (4.01), but this location would not be considered exceptionally bad by any means. The second location, however, has a very high dSM value (2.53 in/100 MGT) and a high dSD value (0.64 in/100 MGT). With the very high dSM value, the dSM/dSD is still considered high at 3.99. A second observation is that the SM/SD value increased from 2.49 to 3.0, with the second value considered high.

This scenario is included to show that track locations with high degradation rates tend also to display high SM/SD and dSM/dSD values. However, these parameters are complex and further understanding of the reasoning behind potential relationships needs to be explored in more detail.

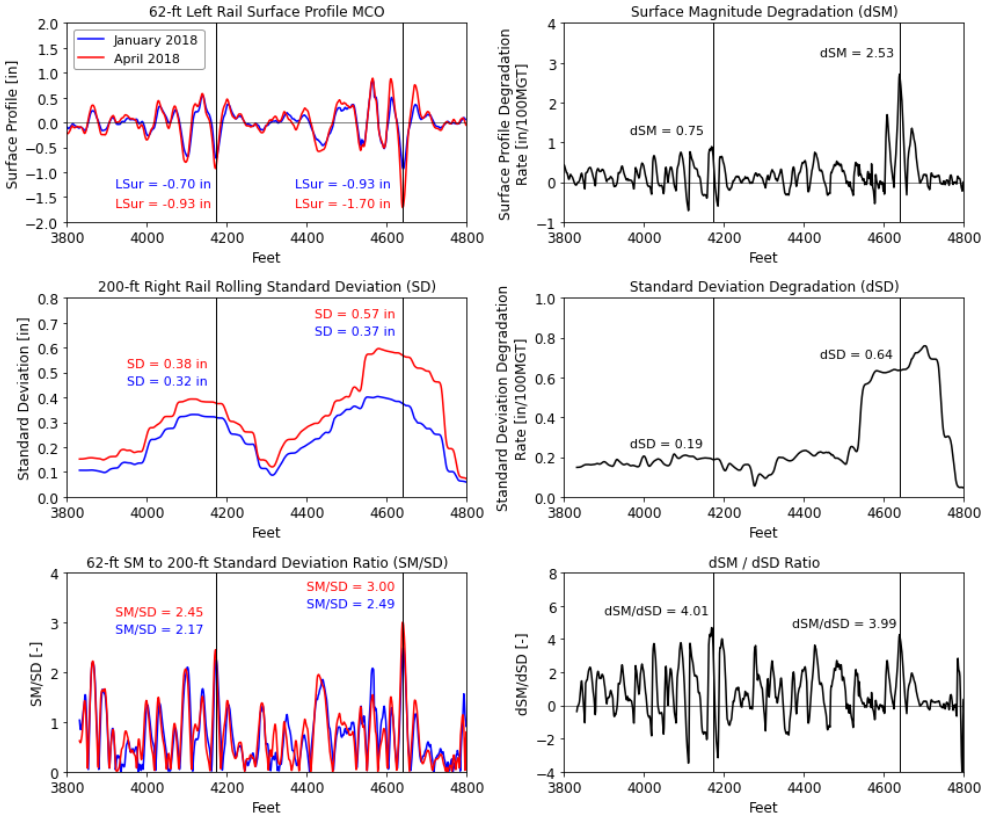

Figure 50: Example of SM/SD and dSM/dSD Values from Field Data

3.2.5 Implications of Track Geometry on Track Performance

In summary, the track geometry representations may provide additional useful information to explain the behavior of various track locations. Some general remarks:

- Two locations with identical settlement could have drastically different 62-foot SM values depending on the settlement of the surrounding track. This means even track with the same ballast conditions may end up producing different track geometry responses based on the behavior of the surrounding track.
- One potential method of characterizing the behavior of the surrounding track is with the SM/SD Ratio. Values on the higher end (2.5 or greater) potentially indicate track locations with a single deviation. These locations have a higher risk level of producing high SM values.
- A second parameter, dSM/dSD, helps indicate where the degradation is happening. Higher dSM/dSD values indicate the degradation is greatest at the location with the maximum surface profile while lower dSM/dSD values indicate the degradation is occurring at locations surrounding the maximum surface profile.
- While both these parameters may be indicators of high-risk locations, they do sometimes show similar values in lower-risk situations as well. Since the value itself does not always differentiate between high- and low-risk situations, these parameters may help explain outliers but may not be predictive.

3.3 Existing Track Geometry Deterioration Models

This section reviews existing track geometry deterioration models that can be useful for track geometry forecasting models. This report separates "mechanistic" models from "statistical" models. Mechanistic models are defined as track geometry deterioration models that can be used in situations where there are no historical track geometry records to reference. This means mechanistic models should be robust and incorporate the main factors that that affect performance. Statistical models are defined as track geometry deterioration models that were developed using historical track geometry records from a particular site. This means that performance predictions for a specific site will be based on the historical behavior of that site.

In this section, two mechanistic models, the Rainy Section and Railway Track Life-Cycle Model (RTLM) will be used along with one statistical model. The statistical model was developed by Kashani and Hyslip (2018) and will be referred to as "Kashani and Hyslip (K&H) model." More information on the statistical models will be provided in the following sections. Table 7 lists the three models and the parameters that are incorporated in each. The RTLM is the most robust and incorporates the largest range of conditions.

Table 7: Track Geometry Deterioration Models and Parameter Inputs

	Rainy	RTLM	K&H Model
BFI	✓	✓	✓
Moisture	Moisture	Climate	
Tonnage		✓	
Axle Loads		✓	
Track Structure		✓	
Track Modulus		✓	

The main output of all three models is settlement (u) and settlement (u) must be converted to 62-foot surface profile degradation (SM) to compare with track geometry measurements. The assumption used is SM/u Ratio is 0.30.

3.3.1 Clean Ballast Models

The first group of settlement models to be introduced are "clean ballast models." These are important for establishing ballast settlement trends but were not considered for the project because they do not incorporate BFI. The two clean ballast models are the Sato model [14] and Selig model [10]. Both models are similar at representing the initial non-linear consolidation phase of ballast settlement but differ at higher MGT with the Sato model continuing at a linear trend while the Selig model has a decreasing trend. The mathematical expression for the Sato model is below:

$$u = \gamma(1 - e^{-\alpha N}) + \beta * N \tag{8}$$

u = total settlement

α, β, γ = constants

N = Number of load cycles

The Selig model is represented below:

$$u = a * N^{b} \tag{9}$$

a,b = constants

Figure 51 shows how the two models predict ballast settlement in the short and long term. As can be observed, the short-term behavior (~3 MGT) of the two models is very similar with a high initial ballast settlement rate that starts to level off between 0.1 and 0.5 MGT. However, the long-term behavior shows significant differences with the Selig model continuously decreasing the settlement rate while the Sato model remains linear. This trend difference can result in significant differences in ballast settlement predictions after hundreds of MGT.

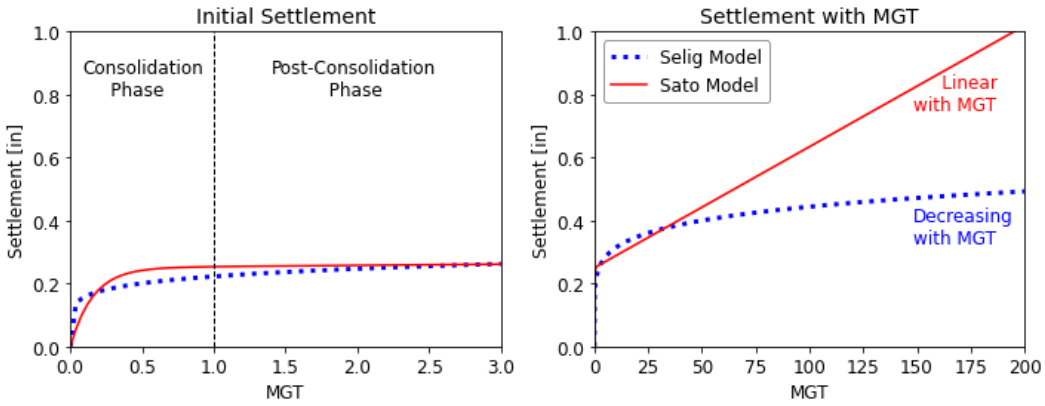

Figure 51: Comparison of Sato and Selig Clean Ballast Models

3.3.2 Rainy Section Model

The first mechanistic model is referred to as the "Rainy Section model." The Rainy Section model was developed in 2020 and is based on Rainy Section tests conducted at FAST at the TTC [34]. The testing involved a 20-foot section of FI = 40 ballast with fines deriving from natural ballast degradation, and a water system was able to simulate various rain events.

The model has two main parameters, BFI, and moisture content, both of which increase linearly. One of the objectives of the Rainy Section test was to determine the range of potential behavior from various moisture conditions, so the Rainy Section emphasizes the influence of moisture. One difficulty of the model is that the dry and saturated thresholds (10 and 15 percent moisture in the Rainy Section model) will depend on the gradation and fine type, so the model should be considered site specific.

Equations 10 and 11 show the model below.

$$du_{Rainy} = 0.001 + \frac{BFI}{40} * [0.1 + 0.38 * -(w-10)] \quad (10)$$

$$dSM_{Rainy} = du_{Rainy} * \frac{SM}{u} Ratio * \left(\frac{1}{100} MGT\right) \quad (11)$$

du_{Rainy} = settlement rate per MGT [in/MGT]

dSM_{Rainy} = SM degradation rate per 100 MGT [in/100 MGT]

w = moisture content [percentage]

$SM/u\ Ratio$ = Conversion from settlement (u) to SM (assumed as 0.3)

The main components of the model are listed below:

- The 0.001 represents the base settlement rate assuming a FI = 0.
- The settlement rate increases linearly with BFI.
- Increasing moisture levels increase the sensitivity of the model to BFI. Essentially, the high settlement rates occur from the combination of BFI and moisture.

Figure 52 shows the model response at different moisture levels with an output of settlement (a) and track geometry degradation (b).

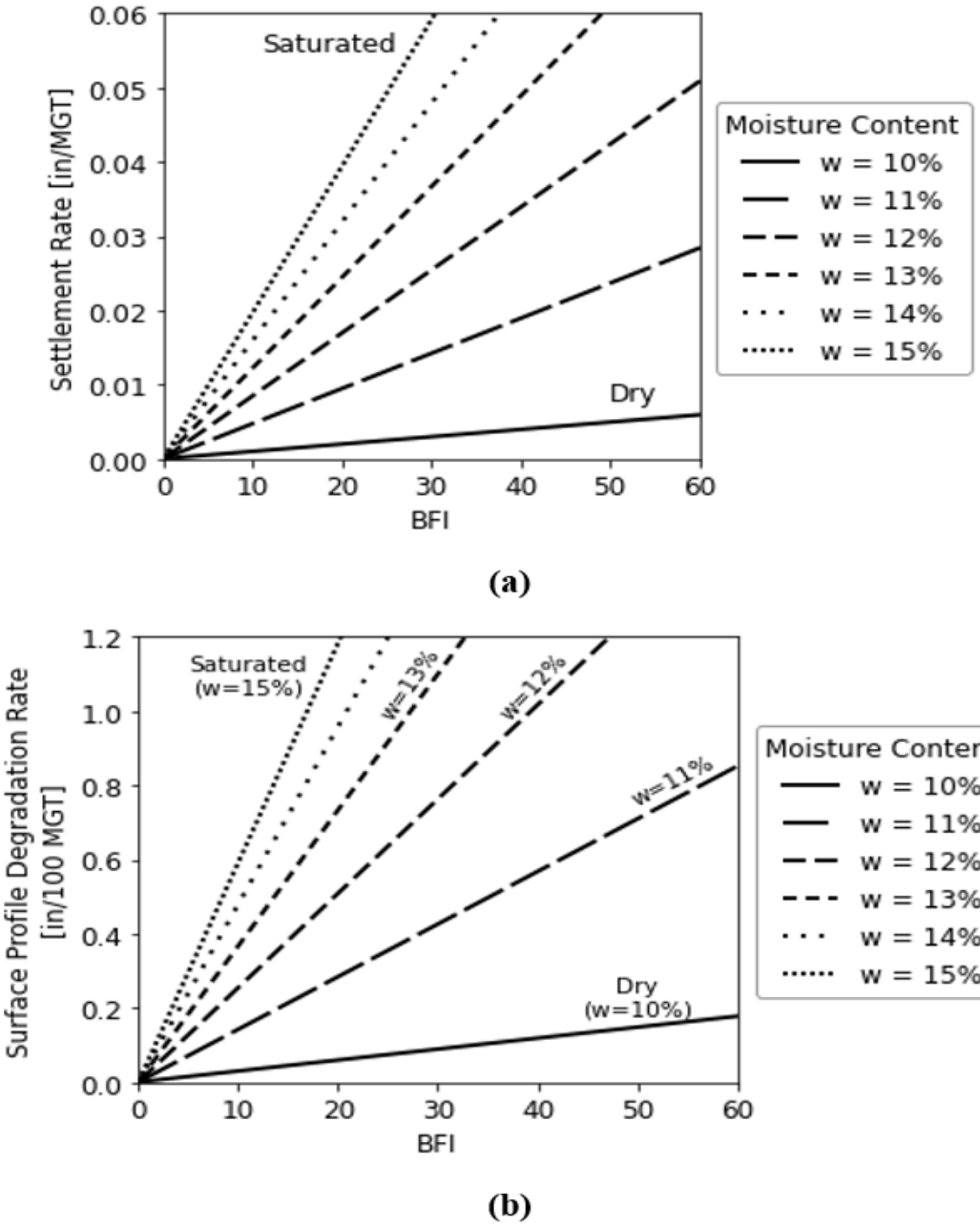

Figure 52: Rainy Section Model Outputting Settlement (a) and Track Geometry (b)

3.3.3 Railway Track Life-Cycle Model (RTLM)

The RTLM was developed in the 1990s and is based on tests from laboratory, the TTC, and revenue service testing. The model was generated to be robust and applicable to a variety of North American freight railroads by incorporating many of the important parameters that affect ballast and track performance. These parameters include wheel load, ballast AN, FI, and climate, track structure, and track modulus.

The settlement output from the model is shown in Equations 12 and 13 with various correction factors:

$$du_{RTLM} = h_b * (\varepsilon_{1(NOM)} k_W k_{An} k_{FI} k_\sigma ku) * N_b \quad (12)$$

$$dSM_{RTLM} = du_{RTLM} * \frac{SMRatio}{u} * \left(\frac{1}{100} MGT\right) \quad (13)$$

h_b = Ballast Height [inches]

$\varepsilon_{1(NOM)}$ = Base 1st Cycle Strain (assume 0.0022)

κ_W = Wheel load Correction Factor

κ_{An} = Abrasion Number Correction Factor

κ_{FI} = Fouling Index Correction Factor

κ_σ = Track Structure Correction Factor

κ_u = Track Modulus Correction Factor

N = Number of Load Cycles

b = exponential factor (assume 0.15)

The wheel load correction factor is a linear relation with 33 kips assumed to be the base value. Equation 14 shows W representing wheel load.

$$k_W = \frac{W}{33} \quad (14)$$

The Abrasion Number correction factor will not be addressed in this report because it is rarely tested and uncommonly known. The base value of 1.0 will be assumed.

The Fouling Index correction factor has equations depending on four different climate regions. The relation until FI = 30 is linear and a non-linear relation exists for FI>30. Equations 15 through 20 are listed below:

Arid Climate (<10 inches/year):

$$K_{FI} = 1.0 + 0.01 * FI \quad (FI \leq 30) \quad (15)$$

$$K_{FI} = 1.0 + 0.01 * FI\ (FI \leq 30) \quad (FI \geq 30) \quad (16)$$

Semi-Arid Climate (10–25 inches/year):

$$K_{FI} = 1.1 + 0.02 * FI \quad (FI \leq 30) \quad (17)$$

$$K_{FI} = 1.1 + 0.02 * FI + 0.1 * (FI - 30)^{1.2} \quad (FI \geq 30) \quad (18)$$

Wet Climate (25–50 inches/year):

$$K_{FI} = 1.2 + 0.03 * FI \quad (FI \leq 30) \quad (19)$$

$$K_{FI} = 1.2 + 0.03 * FI + 0.1 * (FI - 30)^{1.4} \quad (FI \geq 30) \quad (20)$$

Very Wet Climate (>50 inches/year):

$$K_{FI} = 1.3 + 0.04 * FI \quad (FI \leq 30) \quad (21)$$

$$K_{FI} = 1.3 + 0.04 * FI + 0.1 * (FI - 30)^{1.6} \quad (FI \leq 30) \quad (22)$$

The track structure correction factor depends on the tie type and subgrade. The RTLM has the numbers as functions of ballast depth as well but a ballast depth of 12 inches is assumed due to its minimal influence. The correction factors are listed in Table 8.

Table 8: RTLM Track Structure Correction Factors

	Clay		Sand	
	Good	**Poor**	**Good**	**Poor**
Wood	0.86	0.88	0.86	0.97
Concrete	1.70	1.73	1.30	1.28

The track modulus correction factor is a linear relation with track modulus where u is track modulus in kip/in/in. Note that track modulus indirectly incorporates almost all the other factors including track structure and FI/moisture [10]. The base value is 5 kip/in/in.

$$K_u = 1.75 - 0.15 * u \tag{23}$$

The various correction factors affect the settlement and track geometry degradation rate. Figure 53 shows the general behavior of the RTLM and the influence of various factors.

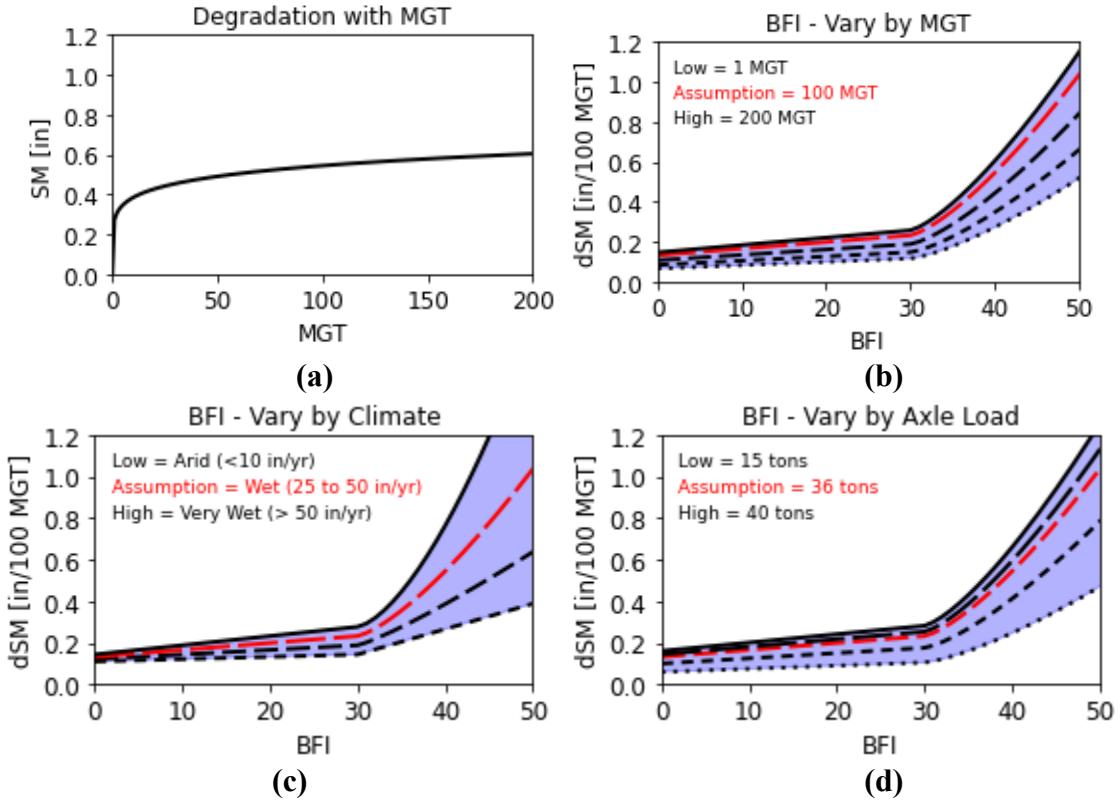

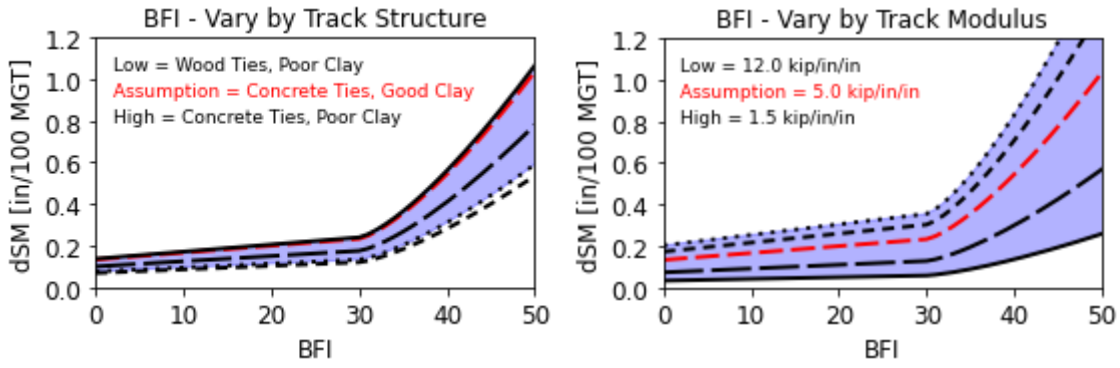

(e) **(f)**

Figure 53: RTLM Behavior with MGT (a) and Range of Behavior from Various Track Parameters (b–f)

Some general observations are the following:

- The settlement/track geometry degrades in a non-linear fashion (Selig model) with most of the settlement occurring in the first few MGT and the degradation rate decreasing with MGT.
- The BFI relation is non-linear for FI>30.
- The largest influences appear to be BFI, climate, and track modulus.

3.3.4 K&H Statistical Model

Kashani and Hyslip (2018) developed the K&H statistical model which is based on passenger, freight, and laboratory ballast box data in the northeastern United States. The model involves a statistical power fit that relates BFI to track geometry degradation. One additional note from this model is that the ballast in this study was near the end of its life meaning the recommended maintenance would be renewal.

The power fit Equations 24 and 25 is shown below:

$$du_{K\&H} = a * BFI^{b} \quad (24)$$

$$\boldsymbol{dSM_{K\&H} = du_{Kashani} * \frac{U\_SM}{100}} \quad (25)$$

a,b = constants
a = 8.2738E-7
b = 3.1767

3.3.5 Model Comparison

This subsection compares the three models with BFI and MGT to emphasize similarities and differences between the track geometry deterioration models. Figure 54 shows how the K&H statistical models compare to the various moisture assumptions for the Rainy Section model and RTLM. The results showed that the K&H model is within the anticipated moisture range for the Rainy Section model, but the BFI relation tends to deviate from the RTLM assumptions because

the RTLM assumes poor performance from BFI begins around FI = 30, when it is assumed that all the voids within the ballast are filled.

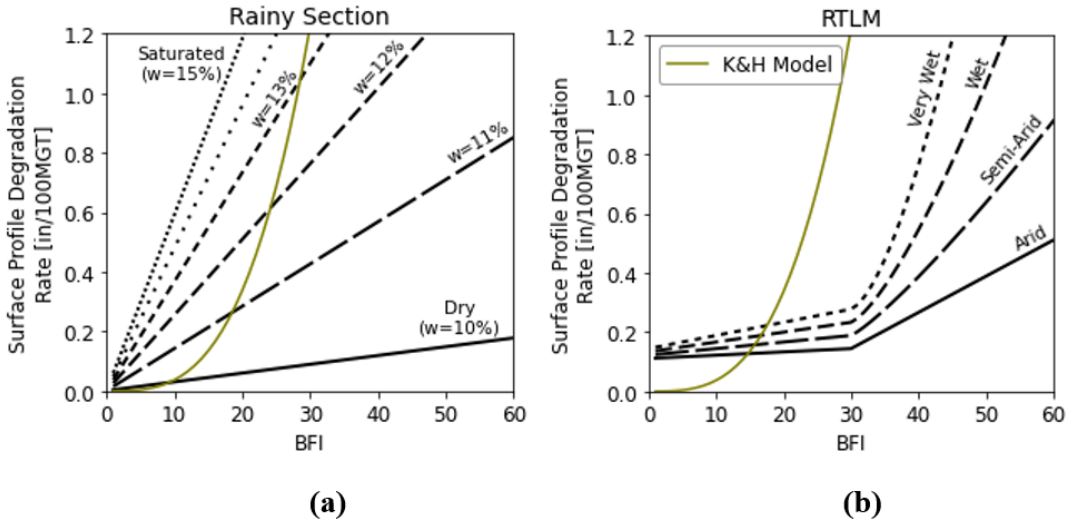

(a) **(b)**

Figure 54: Comparison of BFI Relations with Rainy Section Model (a) and RTLM (b)

Figure 55 compares the performance with MGT for a BFI = 3 (a) and BFI = 38 (b). The Rainy Section model is assumed to have a moisture level of 11 percent and the RTLM assumes a wet climate. The model starts with a surface profile MCO of 0.2 inch and the RTLM has two versions, one starting at 0.0 inch and one starting at 0.2 inch since the model theoretically incorporates the initial settlement after tamping.

The results showed similar behavior for the models at BFI = 3.0 but divergent behavior at BFI = 38, shown in Figure 55. From the BFI-relation in Figure 54, the higher track geometry degradation rate from the K&H statistical model is unsurprising. The RTLM response is also unique because of its non-linearity with MGT. Note that this response is due to the RTLM being based on settlement data, settlement, and a 62-foot surface profile that may not have similar behavior.

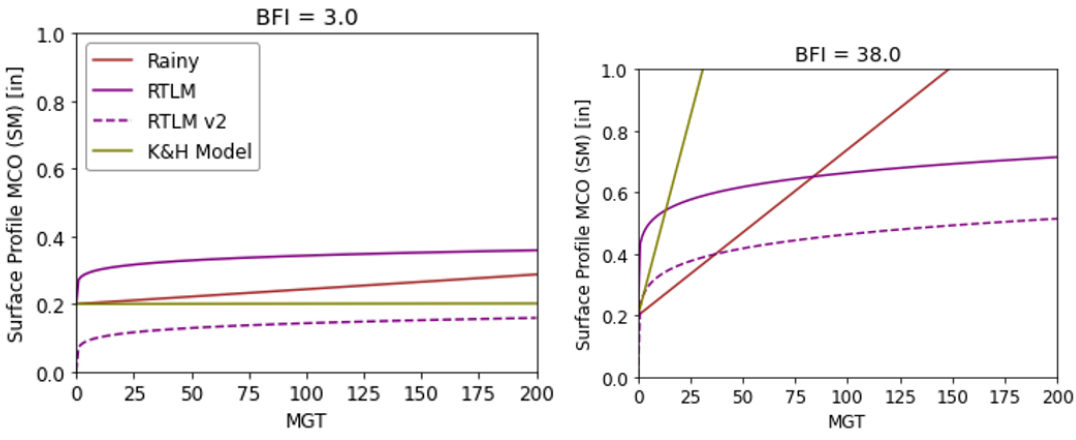

(a) **(b)**

Figure 55: Comparison of Multiple Models with MGT assuming BFI = 3 (a) and BFI = 38 (b)

3.3.6 Summary

Three track geometry deterioration models, which include BFI as an explicit input parameter, are introduced to project future track geometry degradation or at least explain ranges in behavior due to other parameters that are often not directly characterized.

- The Rainy Section model is a simple, site-specific mechanistic track geometry deterioration model that emphasizes a wide range of track settlement depending on the moisture levels.
- The RTLM is a robust mechanistic track geometry deterioration model that incorporates multiple parameters and degradation rates that are affected by BFI, climate, track structure, wheel load, and track modulus.
- The K&H model is a site-specific statistical track geometry deterioration model that has a power law relationship between settlement and BFI.
- Each of these models has a similar trend in which settlement is low for low BFI levels and then increases with BFI. If moisture or climate is included, the wetter regions have a greater increase in settlement.
    - While the models share similar general trends, the behavior of these models becomes significantly divergent at BFI levels above 20. This is likely because the models were based on different track locations that displayed different behaviors.
- The RTLM has a highly non-linear behavior with MGT so this is another cause of divergent results for high BFI levels.

4. Field Data Analysis

This section presents the analysis results of FRA-provided data from track-based track geometry and GPR systems. The results of this section are considered preliminary and will be updated in the final report. The goals of this analysis were to understand key parameters that affect track geometry degradation, develop relationships for future projections, and assess parameters and trends that could be incorporated into a forecasting model.

4.1 Data Organization

Bruzek et al. (2022) conducted a ballast waiver that occurred between 2017 and 2019 on a western Class 1 track, mostly in Missouri. During the study, 405 locations were identified for analysis. At each location, FRA, in coordination with ENSCO, collected track geometry data for a 1,500-foot section of track at least once a week until the location was maintained or repaired [51]. The track geometry data at these locations were then aligned by ENSCO. GPR data was sporadically collected.

At the time of this report, research team requested that ENSCO provide the aligned track geometry records from 43 sites within the St. Joseph subdivision, resulting in a total of 236 calculated surfacing cycles. These 236 surfacing cycles included multiple surfacing cycles at any of the selected locations along with other locations within the 1,500-foot range. Out of the 236 surfacing cycles, 127 of those cycles could be matched with BFI from GPR data. At these locations, additional data such as tie type, curvature, and other factors were provided.

4.2 Data Processing

The data was processed by finding the maximum track geometry and BFI values within a "window" typically of about 200 feet. This "window" method was selected over more continuous analyses because the window method is more manageable with the initial data sets, more closely represents the outputs from the mechanistic and statistical track geometry degradation models, and can account of unscheduled maintenance, which is difficult in a continuous analysis.

The processing of the track geometry and GPR data involved multiple steps. This included: 1) converting the data to different track geometry representations; 2) aligning and representing data; 3) selecting the window and location, 4) calculating track geometry degradation rates, 5) calculating BFI; and 6) aligning track geometry with additional parameters. Each of these steps will be discussed in the subsequent subsections.

4.2.1 Data Processing

The first data processing step involved converting the track geometry measurements into different track geometry representations. The representations used for this analysis included left and right 62-foot surface profile MCO, an absolute value of 62-foot surface profile MCO (SM), and the 200-foot running SD of the 62-foot surface profile MCO (SD). The concepts were introduced in Section 3.2.

4.2.2 Aligning and Representing Data

The second step involved aligning and representing the data. The provided track geometry records were already aligned, so only the GPR data had to be aligned with the track geometry records. The GPS coordinates from the GPR and track geometry data were used to get a close possible match.

With the data aligned, the data from each ballast waiver location (1,500-foot record) could be visualized. Figure 56 shows an example (BW# 145) of this visualization by plotting BFI, the 62-foot surface profiles, and a heatmap of the absolute value of the 62-foot surface profile. As a note, BW# 145 references the numbering system used in the ballast waiver study. Some general observations are that BFI (bottom plot) and surface profile (middle plot) generally trend together. From the heatmap, at least two surfacing events can be identified around October 2017 and July 2018 along with a smaller surfacing event around June 2017. The colored windows represent windows that will be discussed in the subsequent section.

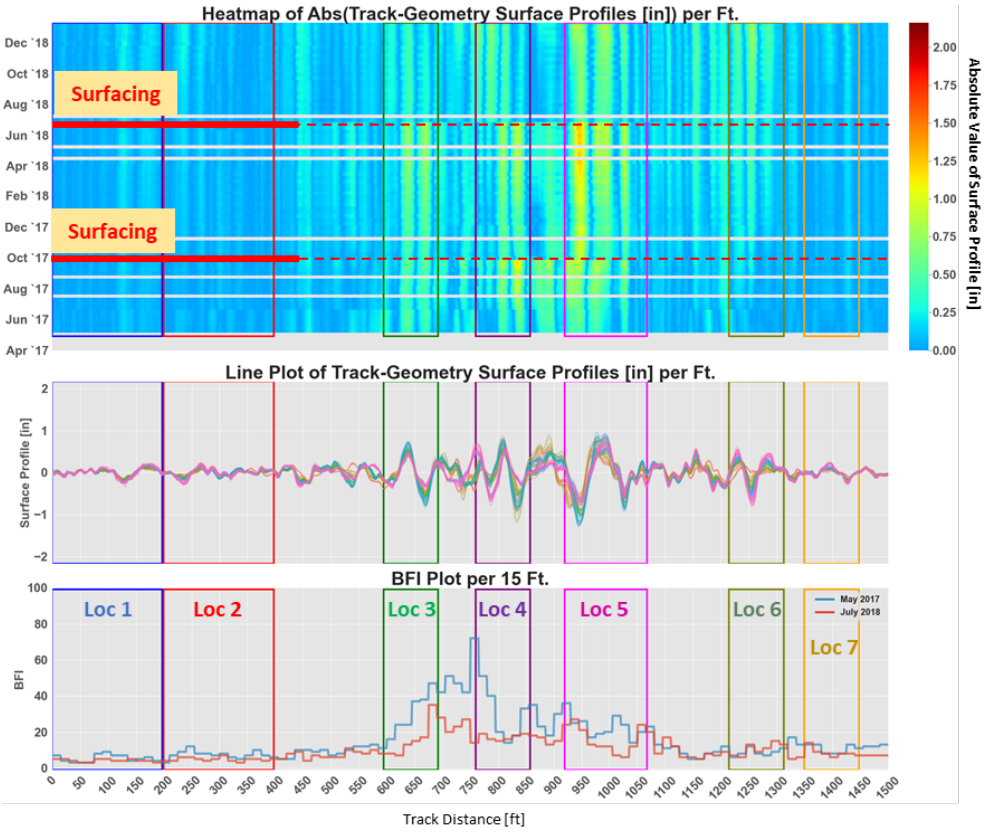

Figure 56: Visualization of BW# 145 by Showing BFI, Surface Profile, and a Heatmap of the Absolute Value of the Surface Profile

4.2.3 Window and Location Selection

The third step is to select windows for each 1,500-foot location. The windows were selected manually to emphasize locations of high track geometry deviation magnitude or degradation. Some non-problematic regions were also included to balance the dataset. The size of the windows was typically 200-foot so the entire track geometry deviation could be incorporated, but the window size did vary based on the shape and size of the particular track geometry deviation

or whether the location of the deviation moved over the course of the monitoring. Figure 56 shows BW# 145 with seven window locations, each represented by a different color.

4.2.4 Maintenance Identification and Track Geometry Rate Calculation

The last step was calculating the track geometry degradation rates. At each window, the maximum SM value (absolute value of the 62-foot surface profile) for each track geometry record was plotted with time (or MGT). Based on these plots, surfacing events could be identified along with the surfacing cycle. Within each surfacing cycle, the track geometry degradation rate was calculated by assuming a linear trend. While not all locations displayed linear behavior, this approximation made analysis easier for a given amount of tonnage (e.g., 100 MGT).

Figure 57 shows BW# 121 with the top plot visualizing the change in track geometry and BFI along the track with time and the bottom plot showing the change in track geometry degradation with time. Focusing on Location #2, represented in red, at least three surfacing events and four clear surfacing cycles can be identified. The surface degradation rate (dSM) is calculated by taking the linear slope between the first and last data points within each surfacing cycle and is represented by a dotted red line. The dSM values are labeled and were generally consistent throughout the four surfacing cycles. The BFI levels showed no major changes from 2017 to 2018, suggesting that no major ballast maintenance occurred at this location during the study.

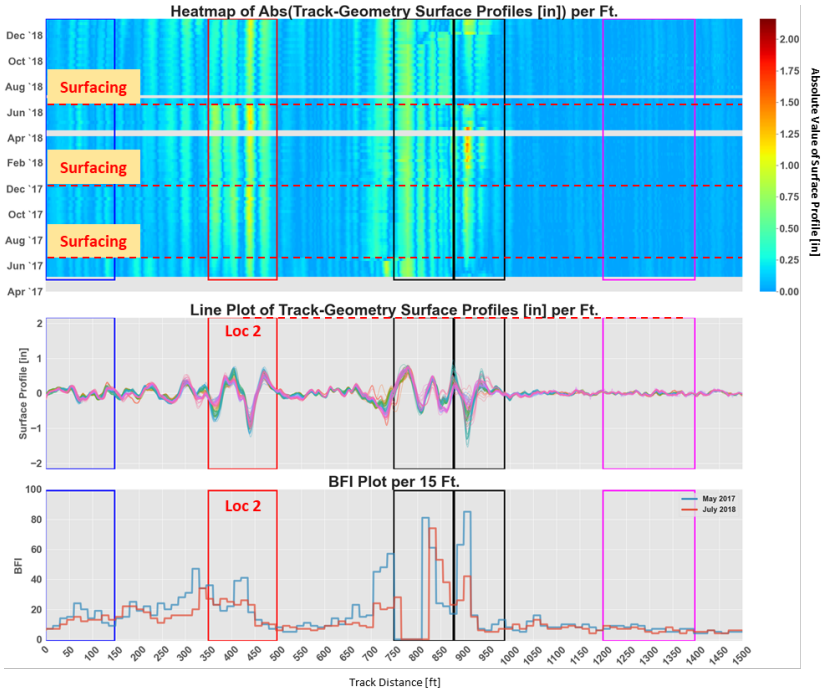

(a)

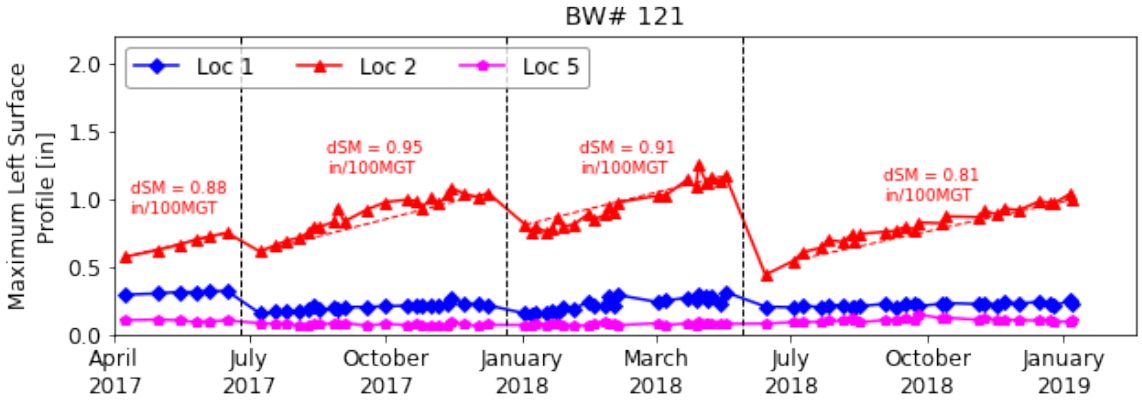

(b)

Figure 57: BW #121 Visualizations Showing Heatmap (a), Surface Profile, BFI, and Surface Degradation (b)

In addition to dSM for the left and right rail, the track geometry degradation using the 200-foot running SD was also calculated for each location using the same process.

4.2.5 BFI Calculation

At each selected window location, the maximum center BFI and left and right shoulder BFIs were identified to compare against track geometry degradation rates (dSM). Since the track geometry measurement intervals were much greater than the GPR measurement intervals (1 week versus 1 year), not every track geometry surfacing cycle had a GPR measurement within its cycle. Those surfacing cycles without GPR measurements were not assigned BFI values because the authors felt interpolating or assuming the GPR value could not be justified due to the

high levels of maintenance that occurred over the course of the monitoring. Therefore, only surfacing cycles with a GPR measurement within that surfacing cycle had both a track geometry degradation rate and BFI value.

Figure 58 shows BW# 121 which includes the BFI values from the two GPR runs together with the surface degradation from these runs. As can be seen, the GPR runs only matched with the first and fourth surfacing cycles (shaded blue and orange) so only those locations have both dSM and BFI values. The second and third surfacing cycles have a dSM value, but no BFI value.

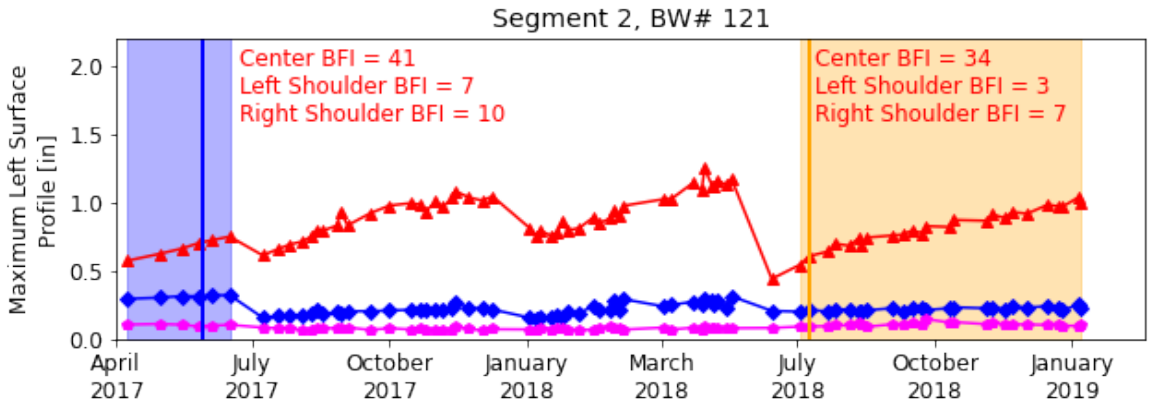

Figure 58: BFI Values for Location #2 at BW# 121

4.2.6 Additional Parameters

At the ballast waiver locations (one location per 1,500-foot record), additional information, such as tie type and curvatures, was provided by ENSCO. While transition locations could not be verified, suspected locations near fixed assets such as bridges, roadway crossing, and turnouts were identified as "suspected transition" locations. These locations were generally identified when the BFI recorded no value or went to an unreasonably high number (BFI = 200), since this high number likely indicated open-deck bridges, roadway crossings, or turnouts. The general criteria for a "suspected transition" could be any window within 200 feet of these suspected fixed assets but could vary if the authors felt it was appropriate.

Figure 57 shows two "suspected transition" locations that are represented with black boxes. At about 800 feet into the record, the BFI had no output. The BFI is seen to be very high for the next 100 feet or so, and therefore, the adjacent window is also considered a "suspected transition" location.

Additional parameters such as the ratio between SM and SD (SM/SD) and the ratio between the degradation rates of SM and SD (dSM/dSD) are also calculated and aligned. Section 3 introduced these concepts.

4.3 Data Analysis – General Trends

The first step of the analysis involved reviewing general trends of the entire dataset. This section presents those very high-level trends and includes track geometry degradation rates and BFI.

Figure 59 shows box plots representing the absolute value of the track surface degradation (dSM) for the left and right rails and BFI on both shoulders and center track. The dSM results are presented in a log scale to emphasize the wide range of values. The dSM values range from 0.01

in/100 MGT or lower to over 10 in/100 MGT. The median value for the left and right rails are 0.277 in/100 MGT and the 25th and 75th percentile values are 0.113 inch/100 MGT and 0.725 in/100 MGT.

The BFI values are plotted in linear scale, and the center BFI is clearly higher than the left and right shoulder values, agreeing with maintenance records that these track sections were often shoulder cleaned. The median center BFI is 33 and median shoulder BFI is 6, with the 25th and 75th percentile of the center BFI being 20 and 47. The center BFI values are considered higher, likely resulting from the monitoring locations focusing on high BFI locations, so the data may not be fully representative of typical track.

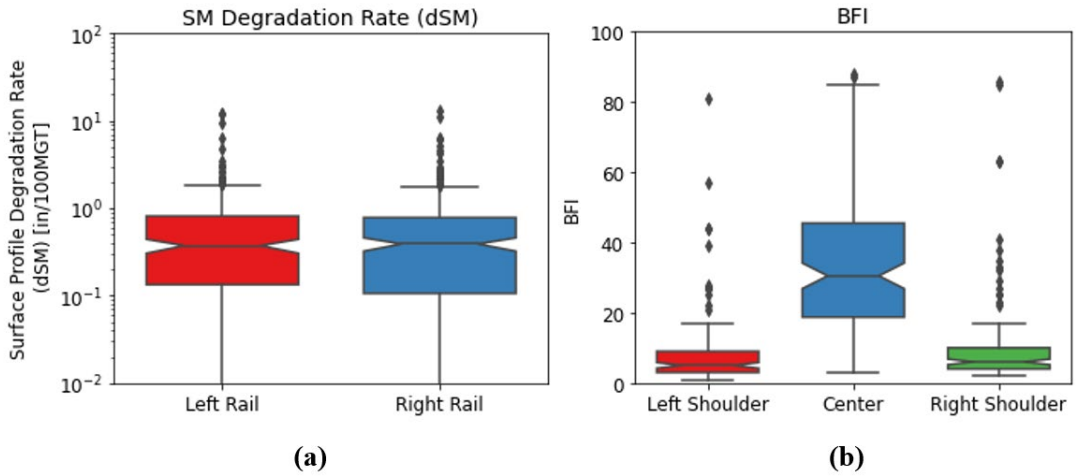

Figure 59: Box Plots of (a) Track Geometry Degradation (SM) and (b) BFI

4.4 Data Analysis – BFI-dSM Relationships

The primary parameter compared with track geometry degradation (dSM) for this analysis is BFI. There were multiple reasons behind the decision to use BFI. First, BFI is historically known as one of, if not the main, contributor to substructure-induced track geometry degradation, and second, the data is more available compared to other potential parameters. To check these assumptions, Pearson's Correlations between track geometry degradation and all the parameters were calculated. For Pearson's Correlations, a result of 1.0 represents a perfect positive correlation while -1.0 represents a perfect negative correlation, and a value of 0.0 represents no correlation between the two compared values.

For all the values compared with dSM, BFI had the strongest correlation and a value of 0.38. This low value is relatively unsurprising considering the complexity and number of factors influencing track geometry degradation. As a note, the limited dataset did not allow for a valid sample of many other parameters (e.g., tie type) so those additional parameters should be investigated once larger datasets are available.

4.4.1 Fitting Equation Procedures

The author manually performed the fitting equations to relate BFI and dSM because automated best-fit methods did not fit the data well regarding the entire range of values. The less-than-ideal fit from the automated methods is likely due to the relatively small dataset and as larger datasets

are collected, best-fits may eventually perform better. The fitting procedure involved the following steps:

1. Putting the data in log-log scale by calculating the natural log of the track geometry degradation (dSM) and BFI values. Any negative degradation values had to be discarded.
2. Constructing a linear fit line in log-log scale
3. Converting the linear fit line in log-log scale to an exponential fit curve in linear-linear scale

The fitting equations are defined below where track geometry degradation (dSM) is in in/100 MGT:

$$\ln(dSM) = a * \ln(BFI) + b \tag{26}$$

$$dSM = e^{b} * BFI^{a} \tag{27}$$

An example of this fitting procedure for the entire dataset is shown in Figure 60, with both the linear-linear and log-log plots shown. Data from a previous analysis of the same location was also included [52]. The fitting equations are also included.

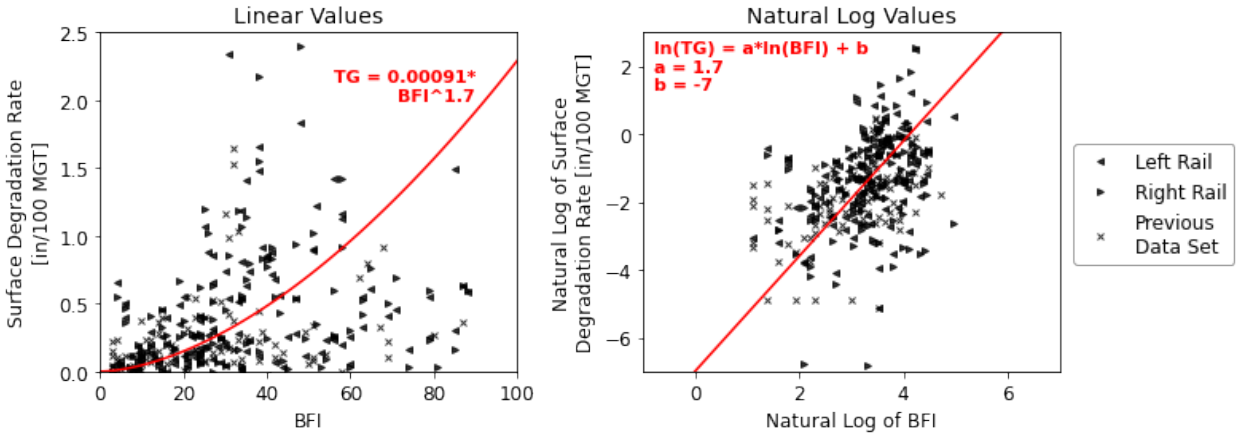

Figure 60: BFI-dSM Fitting Equations for Entire Data Set in Linear and Log Scale

4.4.2 Track Section Breakdown

One of the observations made during the analysis was that the BFI-dSM relationship had a lot of scatter and different track segments often had different trends. Therefore, the data was broken down into multiple groups:

- Suspected Transition Regions
- Non-Transition Regions
  - Segment 1 (MP 75 to 90), Track #0
  - Segment 2 (MP 190 to 205), Track #0
  - Segment 2 (MP 190 to 205), Track #2

By breaking down the data in track segments, it became clear that the BFI-dSM relationship was different for different track segments. Figure 61 compares the breakdown between the suspected

transition and non-transition regions while Figure 62 compares the breakdown between the three track segments, which are all non-transition locations. Separating the "Suspected Transition" and "Non-Transition" locations showed two different trends. The "Suspected Transition" locations showed a very weak correlation between BFI and dSM and BFI levels generally above 20. The "Non-Transition" locations showed a stronger correlation between BFI and dSM but still included large amounts of scatter.

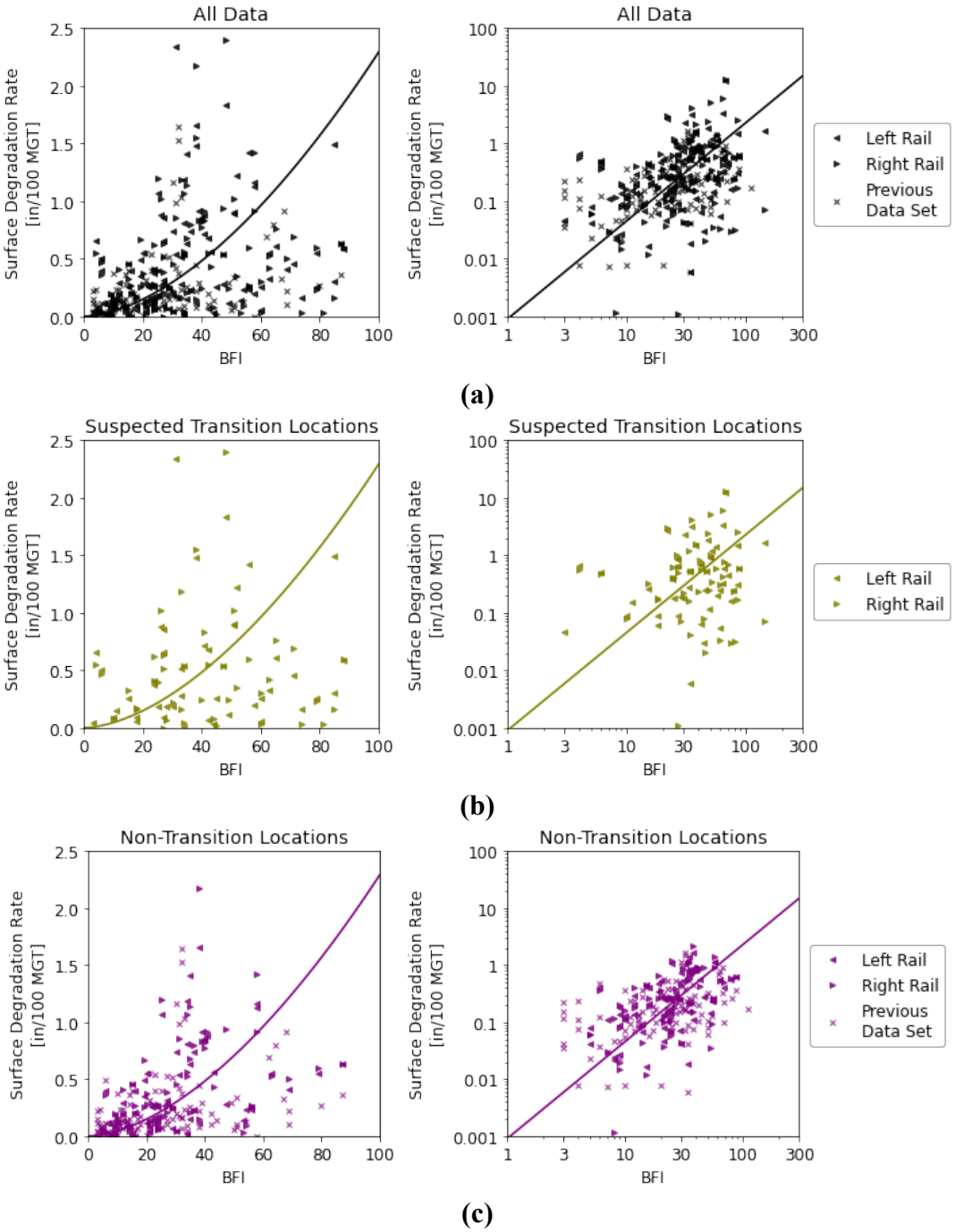

Figure 61: BFI-dSM Trends for Entire Dataset (a), Non-Transition Locations (b), and Suspected Transition Locations (c)

A more detailed breakdown of the Non-Transition locations is presented in Figure 62 and shows much stronger relationships between BFI and dSM, which is more strongly emphasized in the log-log scale plots. It appears that Section #1, Track #0 (blue, Figure 62a) and Section #2, Track #0 (red, Figure 62b) have less scatter than Section #2, Track #2 (green, Figure 62c).

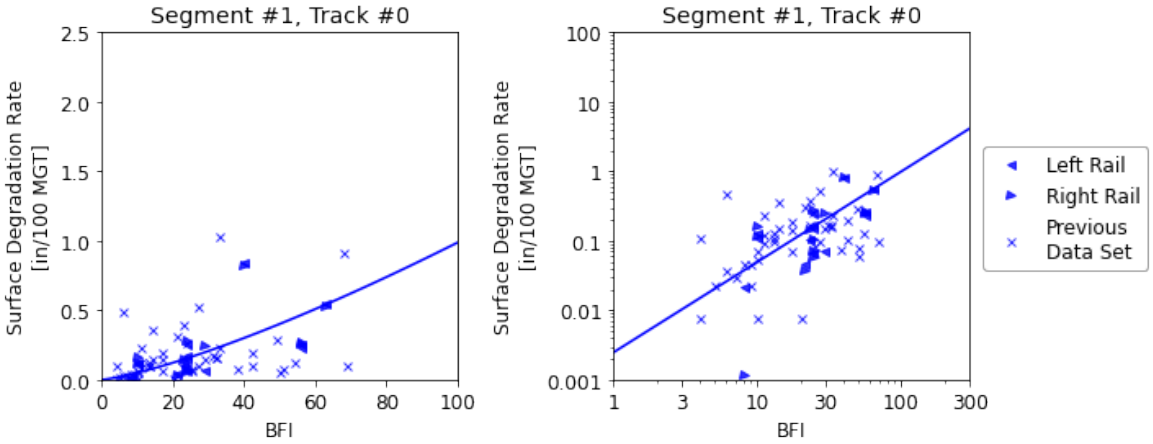

(a)

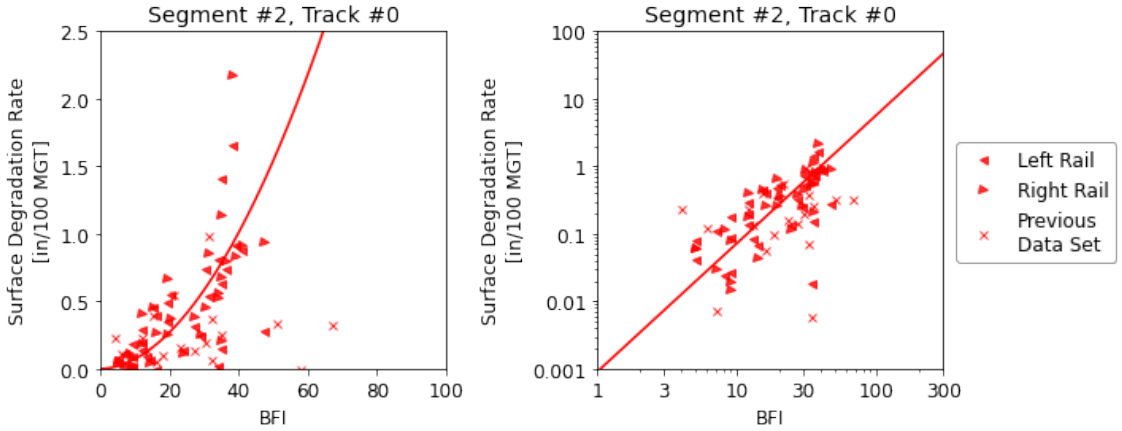

(b)

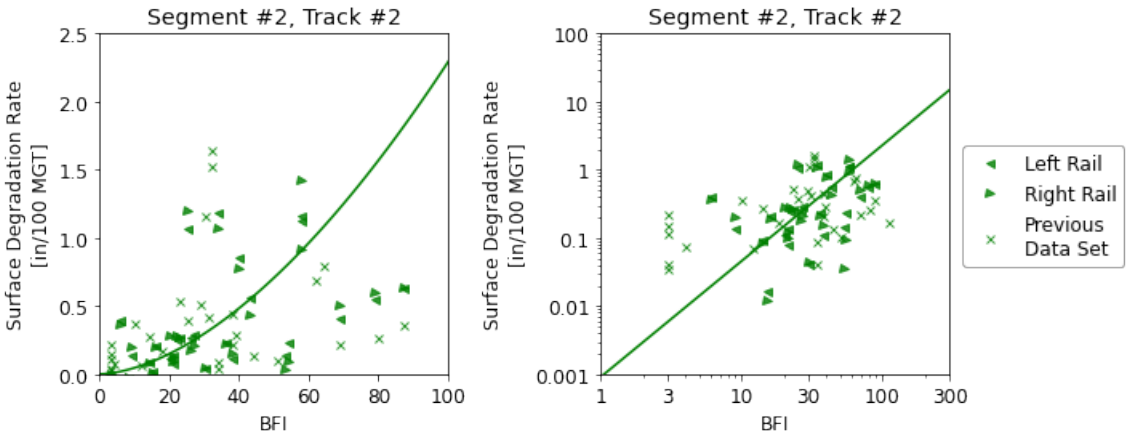

(c)

Figure 62: BFI-dSM Trends Broken Up By Track Segment for Segment #1, Track #0 (a), Segment #2, Track #0 (b), and Segment #2, Track #2 (c)

Table 9 documents, for each group, the a- and b- values along with the Pearson's Correlation between BFI and dSM in the natural log forms. The left and right rail values are averaged together. As can be observed, the Pearson's Correlation generally becomes stronger by breaking the data up into individual track sections, and non-transition locations have stronger correlations than suspected transition locations.

Table 9: Fitting Constants and the Pearson's Correlation

Location	a-constant	b-constant	Pearson's Correlation
All Data	1.7	-7	0.38
Suspected Transitions	1.7	-7	0.15
Non-Transitions	1.7	-7	0.54
Segment #1, Track #0	1.3	-6	0.68
Segment #2, Track #0	1.9	-7	0.75
Segment #2, Track #2	1.7	-7	0.39

The different BFI-dSM trends at different track sections, even in the same subdivision, suggest that historical ballast maintenance and possibly localized variations in drainage, subgrade, and tie type may play a role on track geometry degradation. A comparison of the three trends is shown in Figure 63. For example, Segment #1 was undercut 2 years prior to the study and shows the shallowest BFI-dSM curve. The most recent undercutting of Segment #2 is unknown, but it has been longer than 5 years prior to the study. This observation also has implications for future analysis and forecasting, but those will be expanded on later in the report.

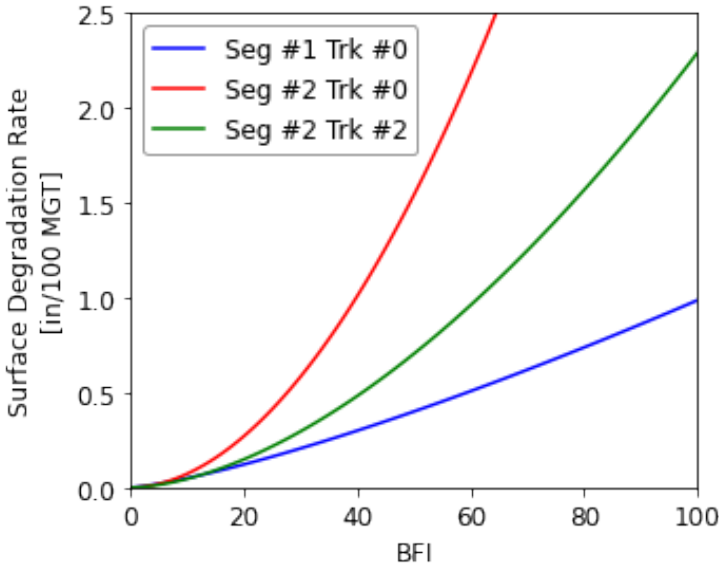

Figure 63: Comparison of the BFI-dSM Trend for Each Track Segment

4.4.3 Accuracy Measurements

The accuracy of the fitting equations can be assessed in multiple ways and each possible method would emphasize different aspects of the "accuracy" of the fitting equations. While subjective, the authors determined that a good fit should have the following two characteristics: 1) fit the

data over a wide range of both TG degradation (dSM) and BFI values and 2) emphasize the median and not be greatly influenced by outliers. For this reason, the selected accuracy measurement is the percentage of projected degradation rates that are within a 2:1 ratio of the actual degradation rate. The projected degradation rates are calculated by taking the center BFI at each location and calculating the dSM based on the best-fit equations presented earlier.

Figure 64 visualizes which locations fall within the 2:1 ratio, represented by the gray shaded area. The left plot shows the BFI-dSM curve, and the right plot compares the projected versus actual surface profile degradation rates in a log-log scale.

One observation from the plots is that many low degradation rate locations fall outside the 2:1 ratio, but practically, this lack of accuracy is not an issue from a safety standpoint. This is one reason the interpretation of "accuracy" is still important and why the authors generally prefer to avoid simple accuracy metrics.

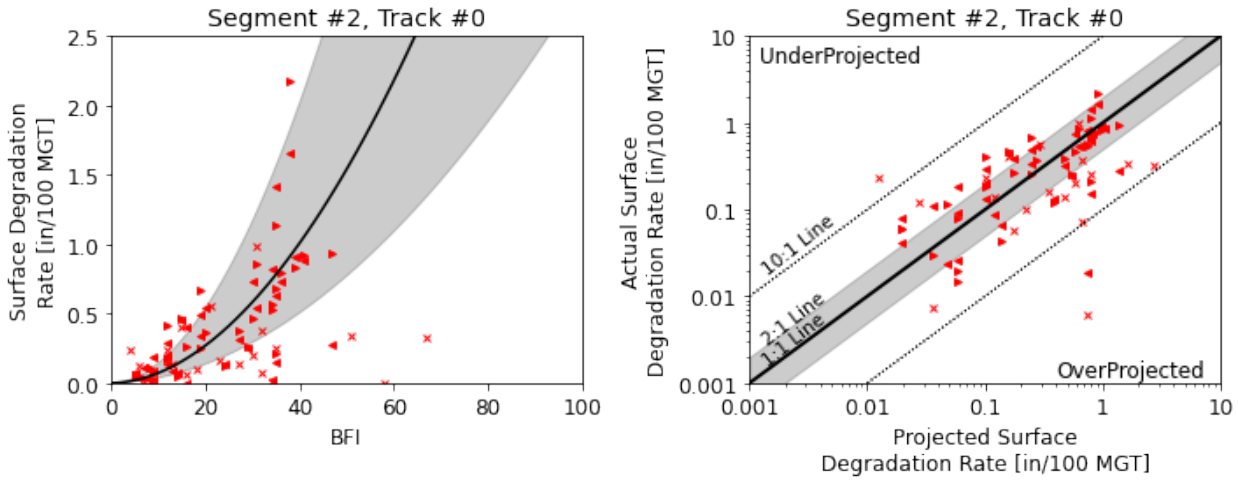

Figure 64: Visualization of 2:1 Accuracy for Segment #2, Track #0

Figure 65 plots the projected versus actual dSM for all the various groups. This plot again shows how the transition region displays higher levels of inaccuracy and that breaking up the data by track sections improves the accuracy.

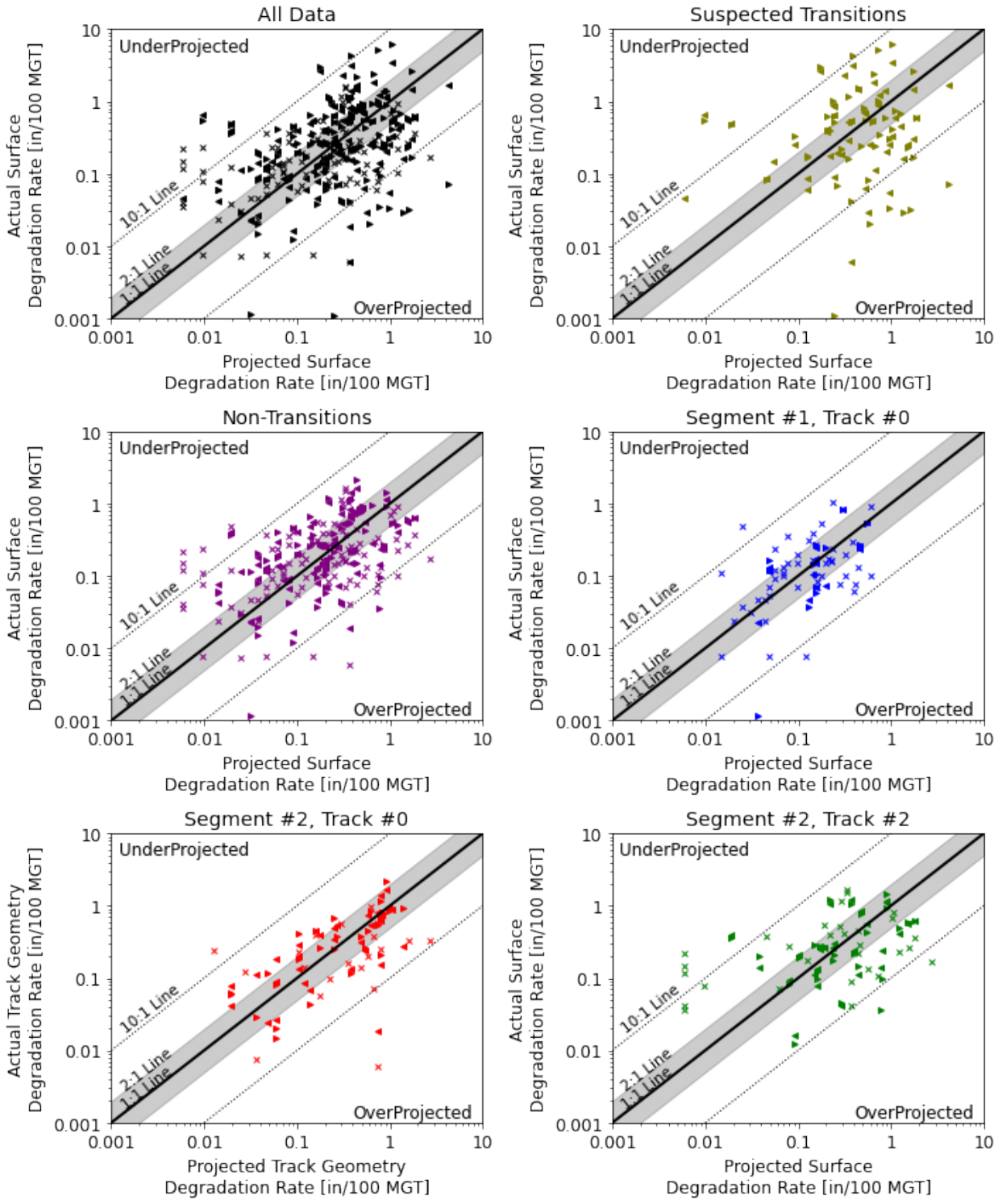

Figure 65: Projected vs. Actual Surface Profile Degradation Rates (dSM) for All Data Groups

While the authors believe that what is shown in Figure 65 is currently the best approach, Figure 66 and Table 10 present some commonly used accuracy metrics for context. Figure 66 calculates the percentage of projections within a specified normalized percent error (NPE). The NPE is

similar to the typical percent error calculation and is calculated by subtracting the actual degradation rate from the projection and then dividing that number by the actual degradation rate. However, for negative values (actual > projection, underprojection), the equation is flipped so the projection is subtracted from the actual and then that percent error is multiplied by -1 to get the value. Equations 28 and 29 are shown below:

$$NPE\ (OverProjected) = \frac{Projected - Actual}{Actual}\ if\ Projected > Actual \quad (28)$$

$$NPE\ (UnderProjected) = -1.0 * \frac{Actual - Projected}{Actual}\ if\ Projected < Actual \quad (29)$$

As opposed to a typical percent error calculation, this method avoids singularities and means that a projection that falls on the 2:1 line would be 100 percent while a projection that falls on the 1:2 line would be -100 percent. For a typical percent error calculation, the 2:1 would still be 100 percent but the 1:2 example would be calculated as -50 percent. As a second example, using the NPE method, a projection on the 10:1 line would be 900 percent and a projection on the 1:10 line would be -900 percent. For a typical percent error calculation, this would result in a range from 900 percent to -90 percent. By using the NPE, the errors are symmetric for both overprojections and underprojections, and this symmetry will be important for future sections

Figure 66 plots the percentage of projections that fall within a specified NPE. The absolute value of the NPE is used so overprojections (positive NPE) and underprojections (negative NPE) of the same value are considered equal. In other words, the y-value at the 2:1 Ratio line (100 percent NPE) represents the percentage of projections within the gray shaded region of the previous figures.

The results again agree that transitions have the lowest accuracy, and that breaking up the data into track sections, each with its own unique curve, can increase the accuracy. In addition, both Segment #1 and Segment #2, Track #0 have the highest accuracy, and this agrees with the BFI-dSM plots.

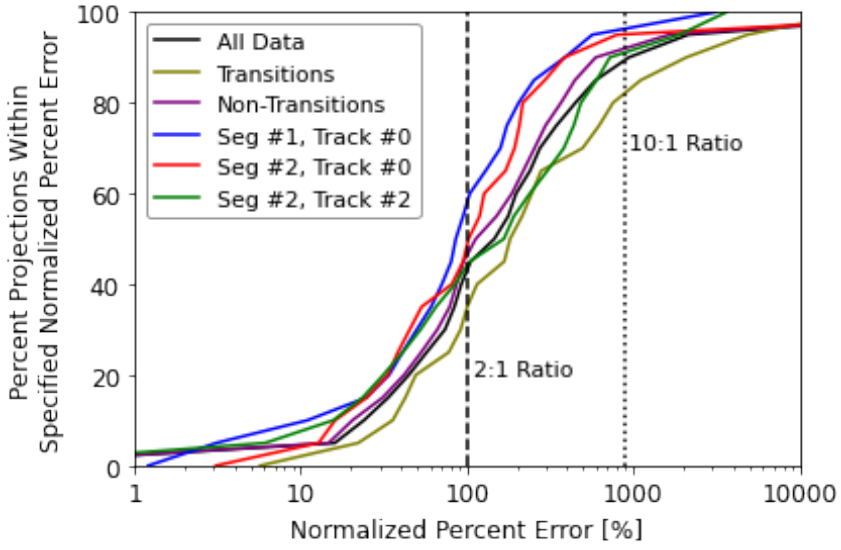

Figure 66: Percent of Projections with a Range of Normalized Percent Error

Table 10 presents the percent of projections within a 2:1 and 10:1 ratio along with root mean error (RME) and root mean square error (RMSE). For the most part, these values agree with previous observations, but they do show some differences because of the different measurement methods.

Table 10: Accuracy Metrics for Each Data Group

Location	Percent Within 2:1 Ratio	Percent Within 10:1 Ratio	Root Mean Error (RME)	Root Mean Square Error (RMSE)
All Data	42 percent	90 percent	1.35	1.83
Suspected Transitions	35 percent	82 percent	1.98	3.96
Non-Transitions	45 percent	92 percent	0.55	0.31
Segment #1, Track #0	58 percent	96 percent	0.20	0.04
Segment #2, Track #0	45 percent	95 percent	0.51	0.26
Segment #2, Track #2	44 percent	91 percent	0.46	0.46

4.5 Correlation with Other Parameters

The previous section showed that breaking up the dataset by track segment and fitting a unique BFI-dSM curve for each track section improves the accuracy and reduces scatter. However, scatter does still exist, and the background (Section 3) emphasized that many other parameters besides BFI influence the track behavior. This section compares additional parameters with the NPE from Section 4.4 with the goal of determining whether other parameters can explain why some locations are consistently overprojected or underprojected based on BFI.

Due to the trends being split by track segment, many of the parameters that would typically be compared cannot be analyzed because certain track characteristics, e.g., tie type, are often consistent throughout an entire track segment. For example, tie type cannot be used to explain scatter because all the ties within each of the three track sections are of the same type. Comparing between track segments will introduce other variables, such as ballast maintenance history, so the track characteristics, cannot be isolated in this dataset. However, these parameters are included in the report for completeness and can still serve as a template for future analyses.

The analyzed parameters are split up into three groups: track structure parameters (Section 4.5.1), track tonnage and collection date parameters (Section 4.5.2), additional BFI parameters (Section 4.5.3), and roughness parameters (Section 4.5.4). The selected parameters were chosen because the parameter is believed to possibly have an influence, and the parameter was available from the data. This means that there are likely additional parameters (e.g., moisture) that could explain the scatter, but these could not be included in this analysis due to unavailable data.

4.5.1 Track Structure Parameters

Two track structure parameters, tie type and curvature, were selected. Past research suggests that tie type can have an influence on track geometry degradation, and tie type was included as a relevant parameter in the RTLM. Curvature was included because curved sections of track sometimes behave differently than tangents.

Tie Type:

The available data did not allow for any analysis on tie type. Segment #1 had only one available data point, and it was a single concrete tie. Segment #2, Track #0 was mostly concrete with 10 concrete tie locations and only one wood tie location. Segment #2 Track #2 was mostly wood track with eight wood tie locations and one concrete tie location.

It is possible that tie type is a contributor in helping explain the difference between the Segment #2, Track #0 and Track #2 BFI-dSM curves, but the influence of tie type cannot be isolated from other potential factors such as ballast maintenance history, ballast condition, subgrade, and drainage. Therefore, the available data does not allow for any conclusions.

Track Curvature:

All non-transition locations were tangents so no analysis could be performed.

4.5.2 Track Tonnage and Collection Date Parameters

Two track tonnage and collection data parameters, single or double track and GPR collection date, were selected. Whether the line was single and double track could have an influence because while Track #2 typically carried loaded cars and should have an MGT close to single track (Track #0), the actual tonnage of Track #2 will be slightly lower. The GPR collection date is important because the GPR collection and analysis process can sometimes change from year to year. Changes in the GPR antenna locations are believed to have occurred between 2017 and 2018 which increased the overall accuracy of the GPR, but this means the same FI (physical gradation) may have had a different BFI (GPR interpreted gradation) based on the collection year.

Single or Double Track:

It would be anticipated that single track (Track #0) would have a higher BFI-dSM curve than the double track (Track #2) that mostly runs loaded cars because the single track should have a slightly higher MGT. However, since the sections are split up by track turnouts, this factor cannot be analyzed.

GPR Collection Year:

There were changes in the GPR collection techniques between 2017 and 2018, but since most of the GPR values used in this study are from the 2018 run, there is not enough data to determine and/or verify any effect on a large-scale basis.

4.5.3 Additional BFI Parameters

Two additional BFI parameters were the ratio of the maximum and average center BFI over a particular window and the maximum shoulder BFI at each location. The subsequent subsections go into detail about both parameters, but Figure 67 shows the Pearson's Correlation values for each data group.

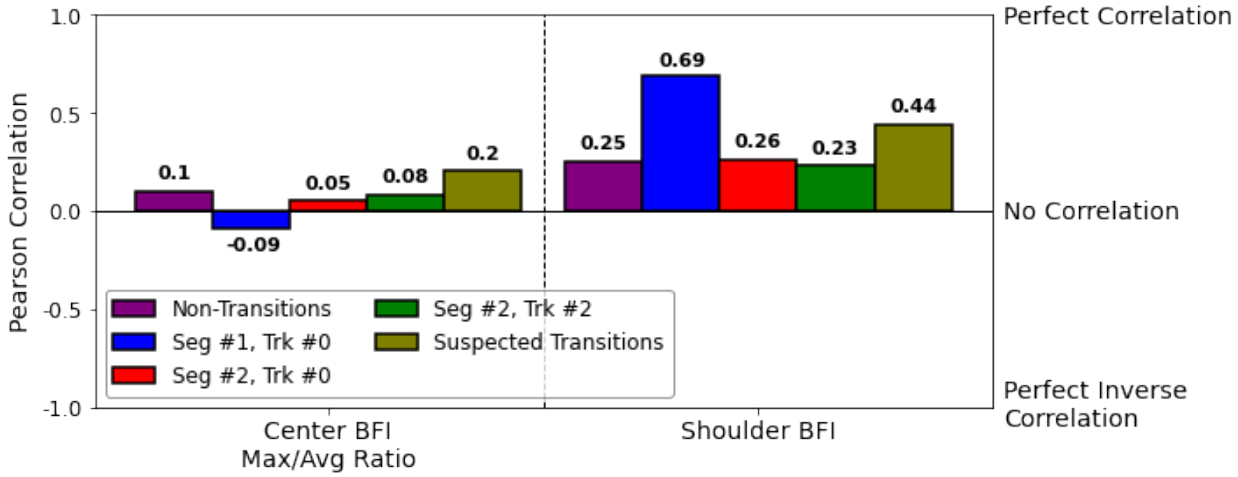

Figure 67: Pearson's Correlation Values for Additional BFI Parameters

Center BFI Max/Avg Ratio:

The ratio between the center BFI maximum and average over the selected window was chosen as a parameter because there may be different behaviors between an isolated mud spot (high ratio value) and a region where the entire section is fine filled (low ratio value). Figure 68 plots the ratio against the NPE for the non-transition data, and it shows no discernable relationship between the BFI ratio and NPR. The low Pearson's Correlation value of 0.10 agrees with this observation.

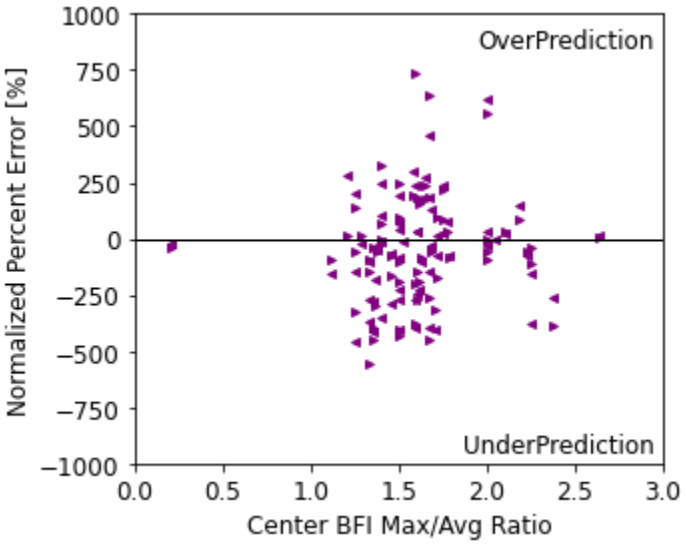

Figure 68: Center BFI Max/Avg Ratio Against Normalized Percent Error for all Non-Transition Data

Shoulder BFI:

The shoulder BFI value was another selected parameter because the shoulder BFI may influence the drainage ability of the track section. Figure 69 shows three graphs for each data group. The left graph plots the left shoulder BFI versus the NPE. The center and right graphs are both the typical BFI-dSM plots, but with the center graph having data from the first three quartiles of left

shoulder BFI and the right graph only showing the fourth quartile of left shoulder BFI data. This means the center graph shows the data with the lowest 75 percent of left shoulder BFI while the right graph shows the data with the highest 25 percent of left shoulder BFI.

The left graph shows that most locations have low shoulder BFI values (<10). This again agrees with the maintenance records that these locations are often shoulder cleaned. However, for Segment 2, Track #2 (Figure 69d) and the transition locations (Figure 67), there are few higher shoulder BFI values. When isolating those higher shoulder BFI locations by taking the fourth quartile, many of these locations also have high center BFI values and low track geometry degradation (overprojected).

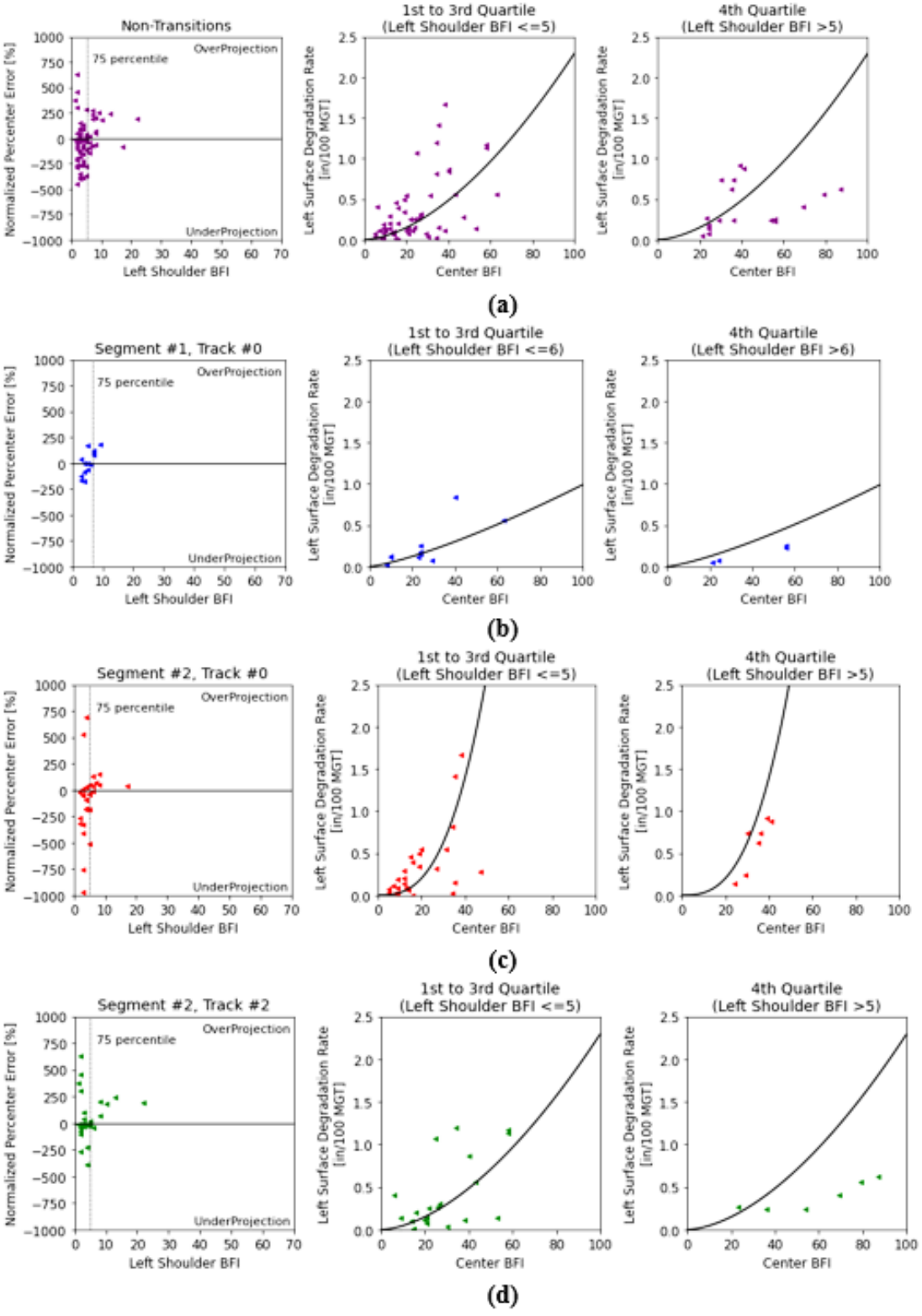

Figure 69: Relationships Between Left Shoulder BFI and Normalized Percent Error from BFI Projections for Non-Transitions (a), Segment #1 Track #0 (b) Segment #2 Track #0 (c), and Segment #2 Track #2 (d)

If no shoulder cleaning occurred, this behavior would be opposite of what was expected because locations with higher shoulder BFI values are anticipated to have poor drainage, and therefore, higher track geometry degradation rates. However, the high levels of shoulder cleaning likely do not allow for enough fine buildup to block shoulder drainage.

The reason for the higher shoulder BFI data point, which is relativity high for this particular dataset, is unclear and could have multiple possible explanations. One potential explanation is that these regions were shoulder cleaned, but the depth of the shoulder cleaning did not reach the depth that was analyzed by the GPR. That means the top ballast section may be clean (FI<5), but the bottom section could still be filled with fines or be the actual subgrade (FI>100). This would cause the BFI, which was analyzed to a depth of 16 inches, to be higher than the top ballast section gradation would suggest. Additional parameters, such as the Free Draining Layer (FDL), which was not available for this study, could help better explain these situations if included in future studies.

4.5.4 Roughness Parameters

Two track roughness parameters were analyzed because they could give some indication of the shape and roughness of the track geometry deviation. A conceptual view (Section 3.2) showed that single deviation locations may be at higher risk of higher dSM values than more continuously rough track, even with identical track settlement rates. This is largely due to how the shape of the track geometry deviation was measured by the 62-foot chord. These parameters should be studied further as they may serve as additional indicators of high or low track geometry degradation locations.

Figure 70 shows the Pearson's Correlation of all six locations for SM/SD and dSM/dSD. The results showed that correlation values were not particularly high besides for Segment #2, Track #2 which shows a relatively strong inverse correlation. As a note, that location had much greater scatter than Segment #1 or Segment #2, Track #0.

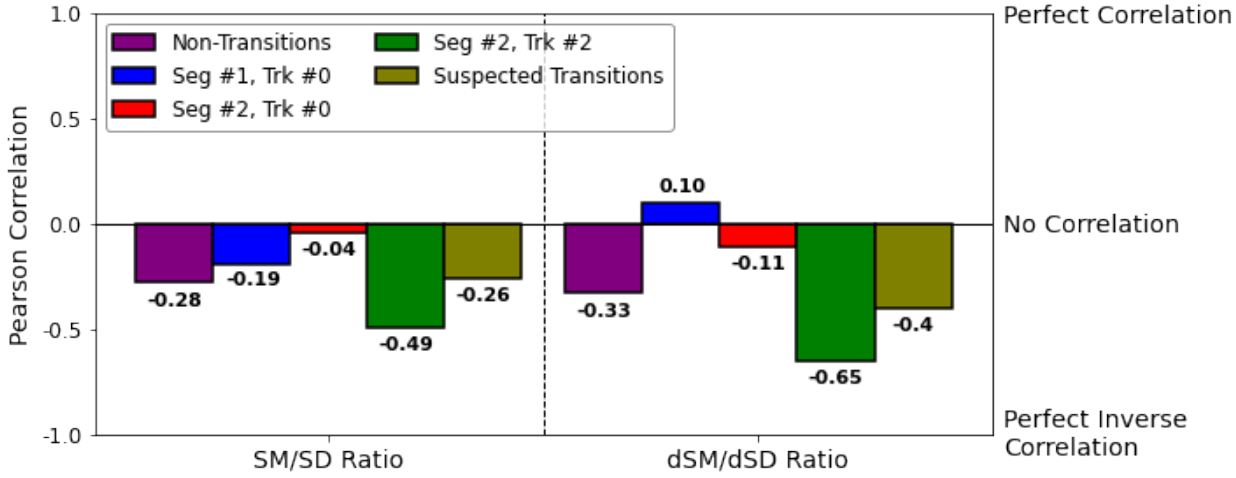

Figure 70: Pearson's Correlation Values for Roughness Parameters

SM/SD:

The first roughness parameter to be looked at is the SM/SD ratio. Section 3.2.4 introduces this parameter essentially by showing that the SM/SD ratio gave an indication of the track geometry

deviation shape. High SM/SD values are indicative of single deviation locations while low SM/SD locations are indicative of more continuously rough track. Brief conceptual examples showed that single deviations were more at risk of having high dSM values due to how the shape of a single deviation was measured by the 62-foot chord.

If this parameter is influential, an inverse correlation with the NPE is anticipated. High SM/SD values should produce greater dSM values than anticipated, and therefore, the BFI projections would underproject the actual dSM value (negative NPE). Low SM/SD values should produce lower dSM values than anticipated, and therefore, the BFI projections would overproject the actual dSM value (positive NPE).

Figure 71 presents multiple aspects of the SM/SD ratio. Figure 71a shows a box plot of the non-transition, all three sections, and the suspected transition locations. The results showed generally similar values, and it is not apparent that one track section has consistently higher values than another. The suspected transitions do show the lowest value.

Figure 71b–f plots the SM/SD Ratio against the NPE for the various track sections. Segment #2, Track #2 (Figure 71e in green) shows the strongest relationship. While there is scatter, it is apparent that the highest SM/SD values generally show an underprojection (higher dSM than anticipated based on the BFI) while the lowest SM/SD values generally show an overprojection (lower dSM than anticipated based on the BFI). This trend, observed in Segment #2, Track #2, agrees with the conceptual exercise, first introduced in Section 3.2.3, that showed that isolated track geometry deviations (high SM/SD values) may produce higher surface profile values than more continuously rough track (low SM/SD values) even when experiencing identical settlements.

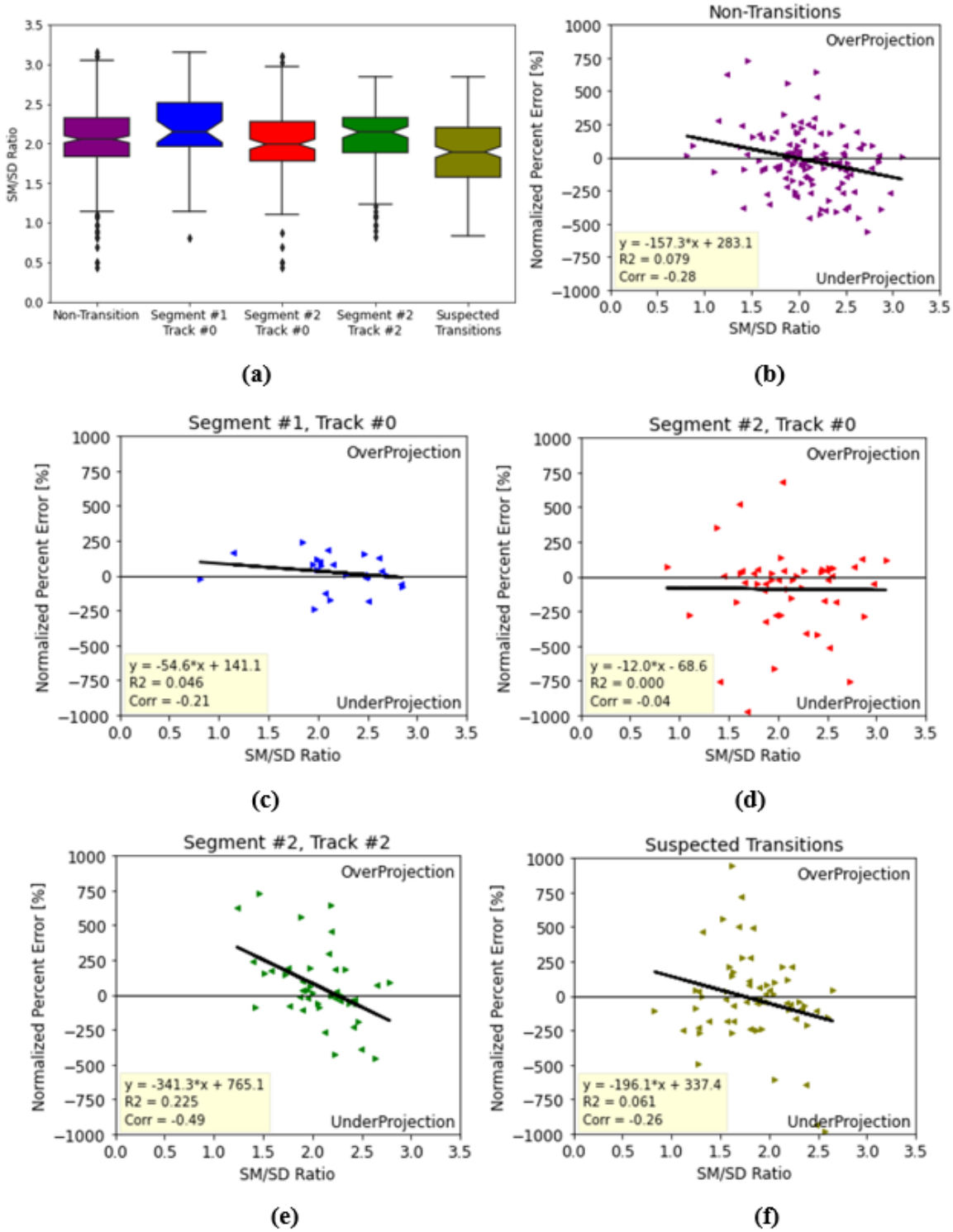

Figure 71: SM/SD Ratio Plots Showing Range of Values (a) and Regression Curves (b–f) with the NPE at Various Track Segments

To further emphasize the SM/SD Ratio and NPE relationship at Segment #2, Track #2 (Figure 71e, green), Figure 72 shows the BFI-dSM plot broken up into quartiles with the green (top left box) showing the lowest quartile and the red (bottom right box) showing the highest quartile. It can be observed that most high BFI locations that have lower than anticipated dSM values are in the first quartile. On the other hand, most locations above the curve are in the fourth quartile.

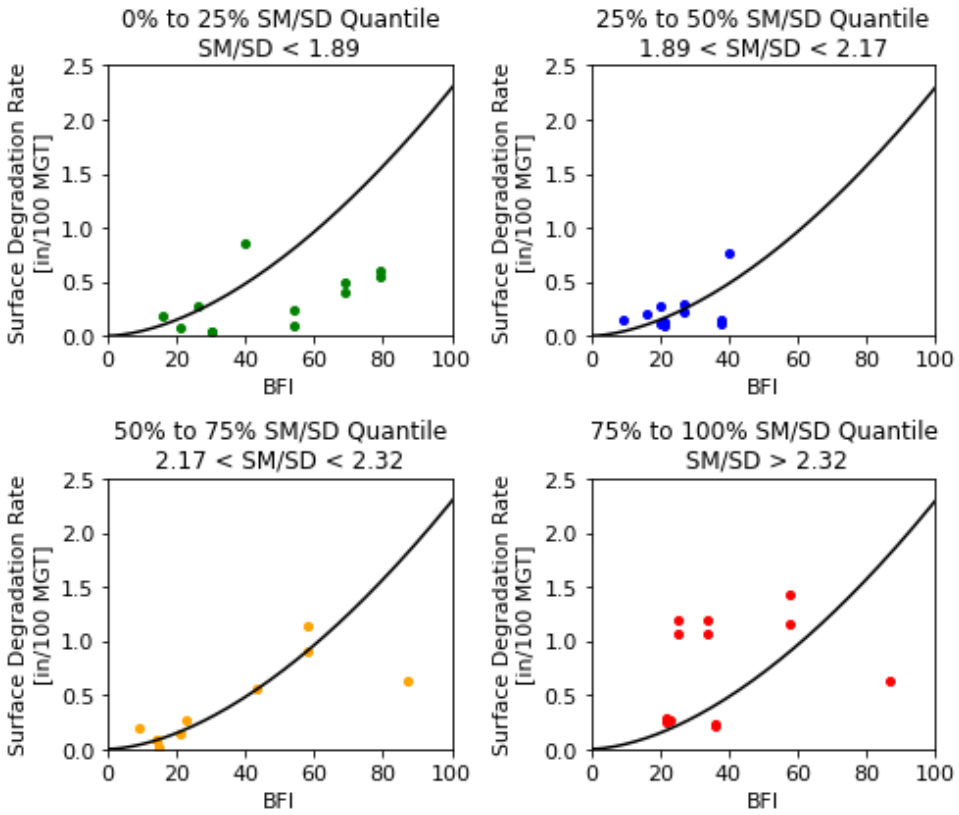

Figure 72: BFI-dSM Plot for Segment #2, Track #2 Split Up by SM/SD Quartiles

dSM/dSD:

A second roughness parameter is the dSM/dSD ratio. Section 3.2.4 also introduces this parameter and it is indicative of where the highest degradation occurred within the track geometry deviation. For high dSM/dSD values, the maximum location of degradation will generally be the location of maximum deviation (SM). For low dSM/dSD values, locations surrounding the location of maximum deviation are likely degrading at the faster rate. This concept should be explored to a greater degree, but can give some indications about the particularities of the track geometry shape and where the degradation occurred.

If this parameter is influential, an inverse correlation with the NPE is also anticipated. High dSM/dSD values should produce greater dSM values than anticipated, and therefore, the BFI projections would underproject the actual dSM value (negative NPE). Low dSM/dSD values should produce lower dSM values than anticipated, and therefore, the BFI projections would overproject the actual dSM value (positive NPE).

Figure 73 presents multiple aspects of the dSM/dSD ratio. Figure 73a shows a box plot of the non-transition, all three segments, and the suspected transition locations. The results again show

generally similar values, and it is not apparent that one track section has consistently higher values than another. The suspected transitions do show a wider range than the non-transition locations. Figure 73b–f plot the dSM/dSD Ratio against the NPE for the various track sections. Segment #2, Track #2 (Figure 73e in green) again shows the strongest relationship. While there is scatter, it is apparent that the highest dSM/dSD values generally show an underproject (higher dSM than anticipated based on the BFI) while the lower dSM/dSD do not show a strong trend.

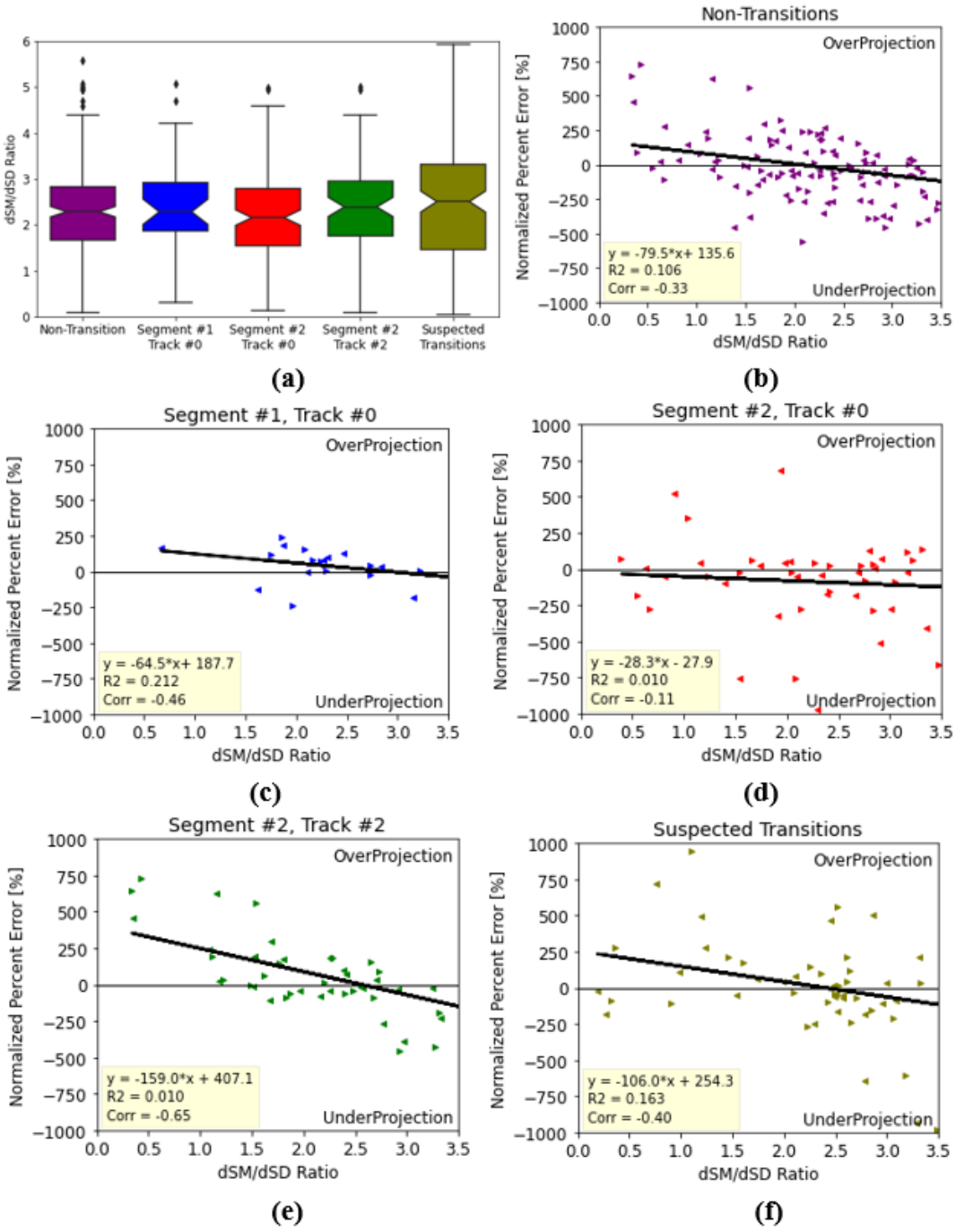

Figure 73: dSM/dSD Ratio Plots Showing Range of Values (a) and Regression Curves (b-f) with the NPE at Various Track Segments

To further emphasize the dSM/SD ratio and NPE relationship of Segment #2, Track #2 (Figure 73e, green), Figure 74 shows the BFI-dSM plot broken up into quartiles with the green (top left box) showing the lowest quartile and the red (bottom right box) showing the highest quartile. It can be observed that the first three quartiles (green, blue, yellow) all have majority values below the curve while most locations above the curve are in the fourth quartile (red).

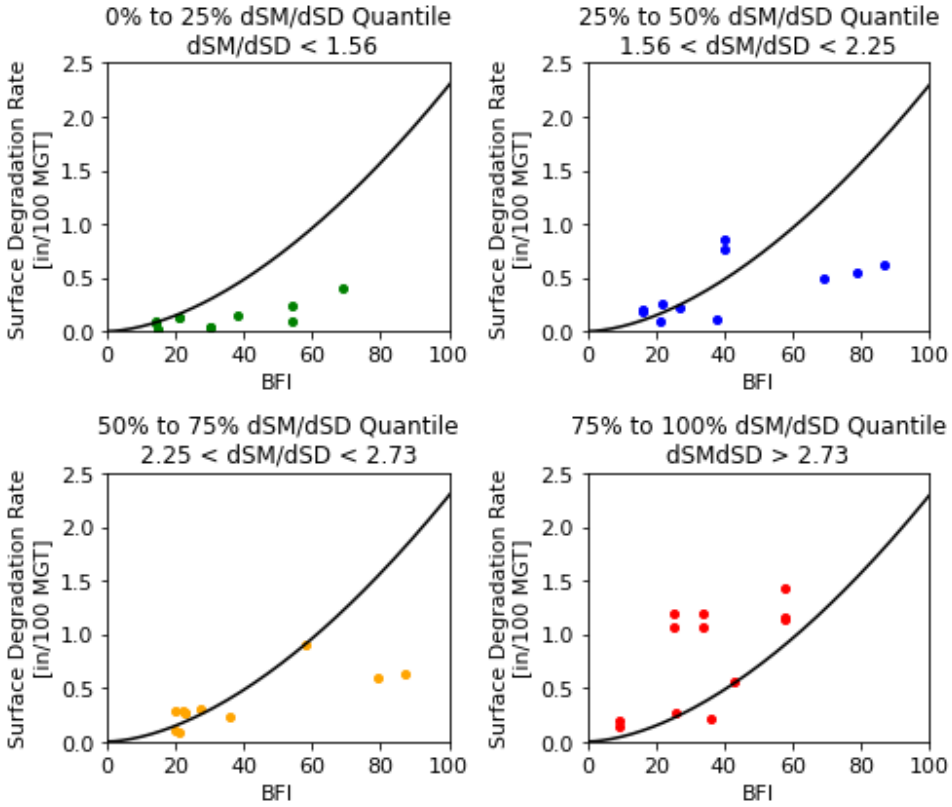

Figure 74: BFI-dSM Plot for Segment #2, Track #2 Split Up by dSM/dSD Quartiles

4.5.5 Summary of Correlation with Other Parameters

The goal of this analysis was to determine if additional parameters could be incorporated into a future forecasting model or at least be used to help explain scatter and outliers. No strong conclusions could be drawn based on the results drawn from the limited data, but these results did indicate that further studies should be conducted in the future. Some remarks are below:

- The influence of tie type and number of tracks was difficult to assess because these values are generally consistent along a segment of track. This lack of variation of these parameters in a single-track segment means that it is difficult to isolate the tie type and the number of tracks from the other variables, such as ballast maintenance history, subgrade, and drainage, which were anticipated to vary from track segment to track segment.
- Shoulder BFI should be further investigated in the future.

- Track roughness parameters (SM/SD and dSM/dSD ratio) appear to explain some outliers in track segments with a large amount of scatter. These parameters require additional study.
    - While both SM/SD and dSM/dSD ratios have physical meanings, these ratios may also be artifacts of the 62-foot surface profile chord.
    - If a particular location always tends to have high or low SM/SD ratios, this parameter may eventually be incorporated into a forecasting model if historical track geometry records are known.
- Based on the results of this preliminary study, no additional parameters are recommended to be incorporated into a forecasting model. This recommendation is mainly due to lack of data along with a solid understanding of why these parameters would affect the BFI-dSM curve. As larger datasets are analyzed, the use of additional parameters may eventually be used and recommended.

4.6 Pattern and Trending Analysis

The previous section plotted various additional parameters against the NPE of dSM projections based on BFI values to help explain scatter and over/underprojections. This section takes a deeper look into a few scenarios to summarize some commonalities exhibited by the data. These include typical behavior, influence of ballast maintenance, and a look into some representative outliers.

4.6.1 Typical Behavior

In general, some typical behaviors exhibited by the data were 1) a high correlation between high BFI regions and high track geometry deviation regions, 2) the BFI projection of maximum dSM values within a particular window, and 3) a linear degradation of track geometry.

Two field data locations that displayed typical behavior were BW# 308 and BW# 121. A deeper look into each of these locations is presented in Figure 75 and Figure 76, respectively. The graphs in this entire section (Section 4.6) are consistent with each other and should give a comprehensive view of the data. For all the graphs in this section, the upper left graph shows the data locations on the BFI-dSM curve for that particular track segment. The gray circles are the other data points from that segment not within the 1,500-foot section being analyzed. Additionally, only the left rail values are shown but the right rail values are similar. The upper right graph shows the track geometry degradation trends with the BFI values labeled manually along with the surfacing windows associated with the BFI values. The blue shaded region represents the surfacing window that corresponds with the 2017 BFI run while the orange shaded region represents e surfacing window that corresponds with the 2018 BFI run. The bottom plot shows the BFI, surface profile, and heatmap of the maximum surface profile (SM) along the track.

Excluding the suspected transition locations (black box regions), both datasets show dSM values that generally match the projections from BFI (upper left plot) and linear surface profile degradation trends (upper right plot). BW# 121 (Figure 76) has multiple surfacing cycles, and those can be observed in the data. The BFI records appear generally similar in 2017 and 2018 outside the suspected transition regions. The helps explain the consistent dSM behavior.

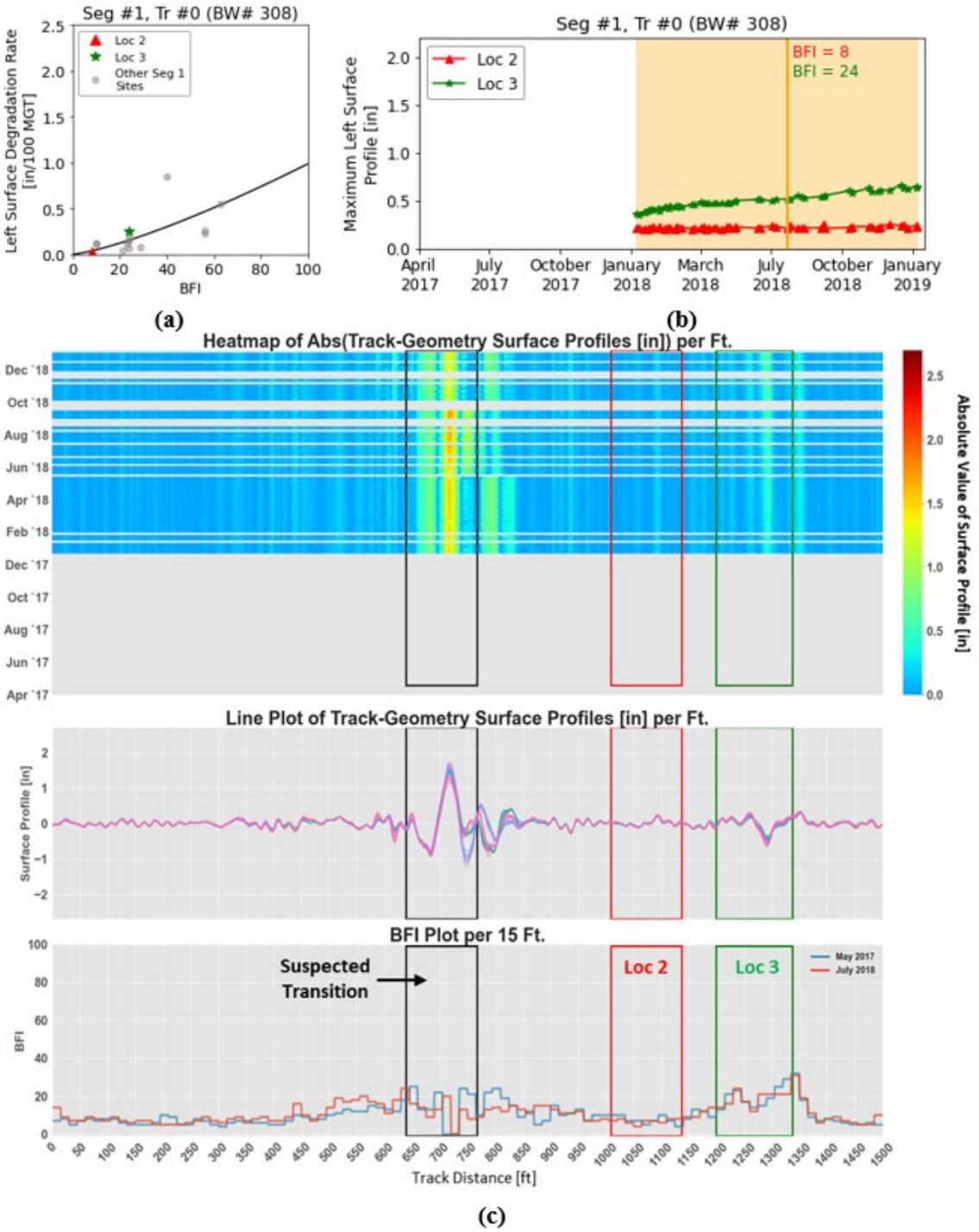

Figure 75: Deep Analysis of BW #308 (Segment #1, Track #0)

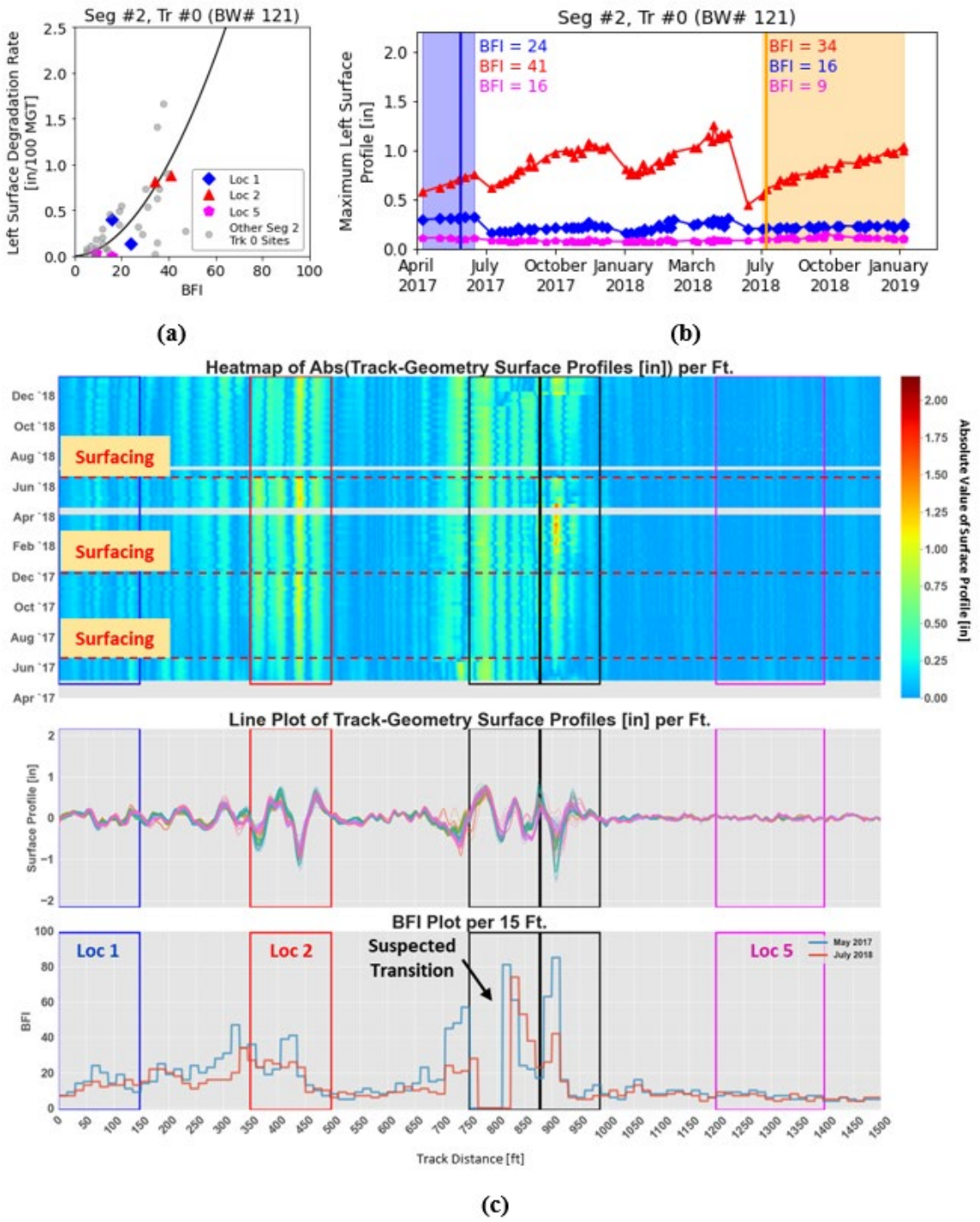

Figure 76**: Deep Analysis of BW #121 (Segment #2, Track #0)**

4.6.2 Ballast Maintenance Activities

Other than surfacing, ballast maintenance is one of the most common methods of remediating high BFI track that also displays high rates of track geometry degradation. This ballast maintenance that affects the center BFI can involve undercutting (UC) or track lifting (TLU). These two methods differ in that UC removes the top ballast layer and replaces it with clean

ballast while TLU involves lifting the track and adding clean ballast to separate the track from the high BFI region. Both these solutions should result in a lower center BFI, but the reduction will depend on the height of UC/TLU, the length of UC/TLU, and the center BFI prior to the UC/TLU. This means that a full 12-inch undercut should leave a BFI<5, but a spot undercut or a 6-inch track lift will likely leave a residual BFI. In addition, the GPR system may have experienced changes between the 2017 and 2018 runs, causing different interpretations on some regions between 2017 and 2018. The authors believe the very high 2017 BFI regions (BFI>50) were the most affected by the change. Between the various ballast maintenance methods and changes in GPR collection/processing, it is difficult to isolate the effects of specific maintenance activities, but some diagnosis can occur from analyzing the data. The remaining questions will be helpful for the planning of future tests intended to get a stronger dataset.

Figure 77 shows BW# 145, located on Segment #2, Track #0. The dSM could generally be projected based on the BFI. The main deviation is Loc 3 which is lower than the projection (overprojected, positive NPE). The track geometry degradation trends are generally linear, and two surfacing events are observed. The degradation rates between the 2017 GPR run (blue) and 2018 GPR run (orange) appear to be similar but are consistently lower for Loc 3, 4, and 5. The GPR values show a reduction in BFI in those regions, but this reduction involves a very high 2017 BFI to a more moderate 2018 BFI. It is likely that some sort of ballast maintenance occurred at these locations but most likely did not involve a full 12-inch undercut. If ballast maintenance had occurred, the track geometry response was slightly improved.

Figure 78 shows BW# 257, also located in Segment #2, Track #0. This location displays some of the highest dSM values in the study. Loc 1 through 3 show high levels of track geometry roughness along with very high BFI levels, especially from the 2017 run. The ballast waiver records show a repair on June 21, 2018, and it appears that the section was undercut or track lifted because of the reduction in BFI and the consistency of the 2018 record (Figure 78). The 2018 BFI between Loc 1 and Loc 3 is still between 20 and 30, so the ballast maintenance was not a full 12-inch undercut. The track geometry shows a significant reduction at Loc 1 but appeared not to have a significant effect on Loc 2 or Loc 3. FDL or some drainage would be interesting additions for this analysis.

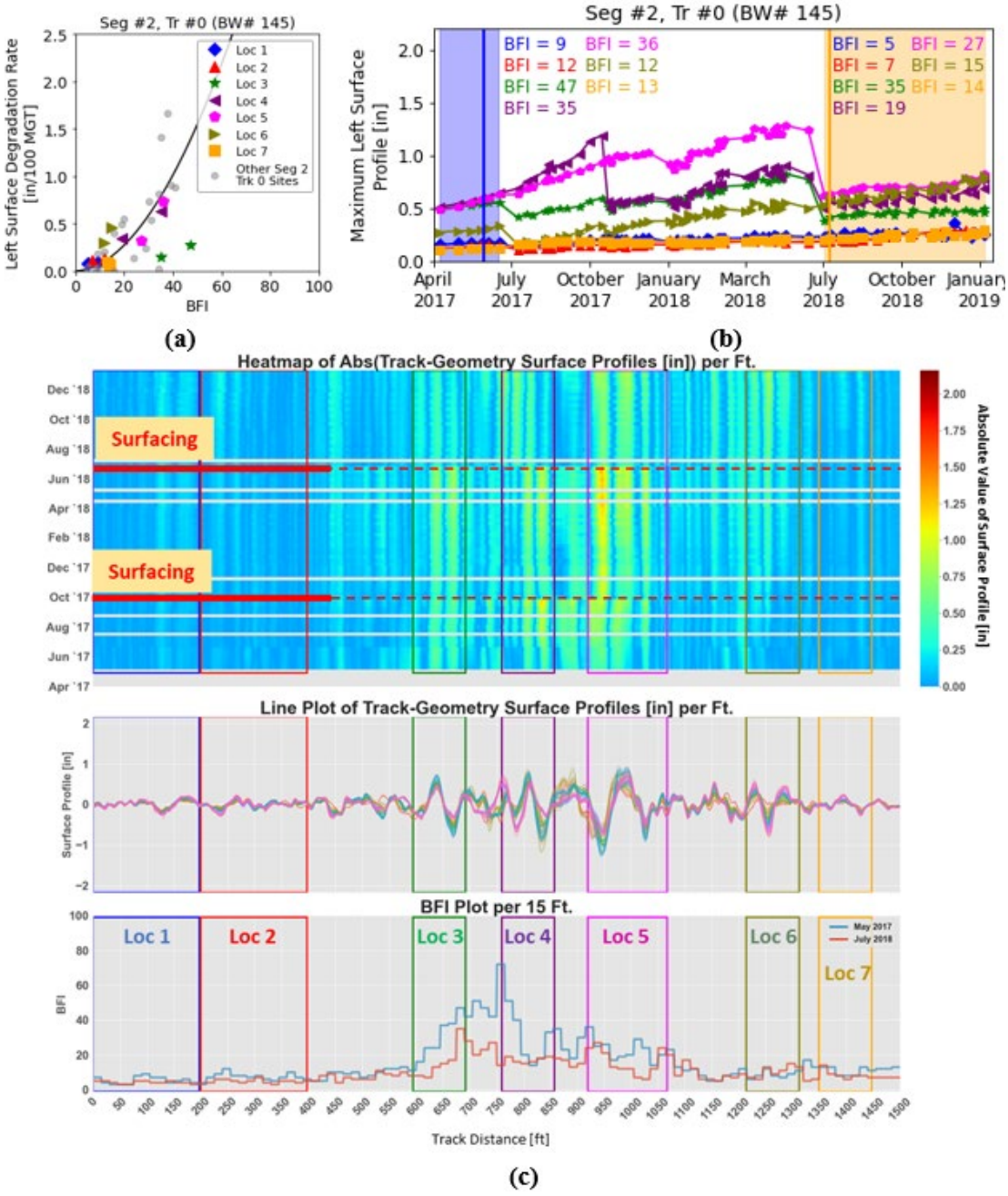

Figure 77: Deep Analysis of BW #145 (Segment #2, Track #0)

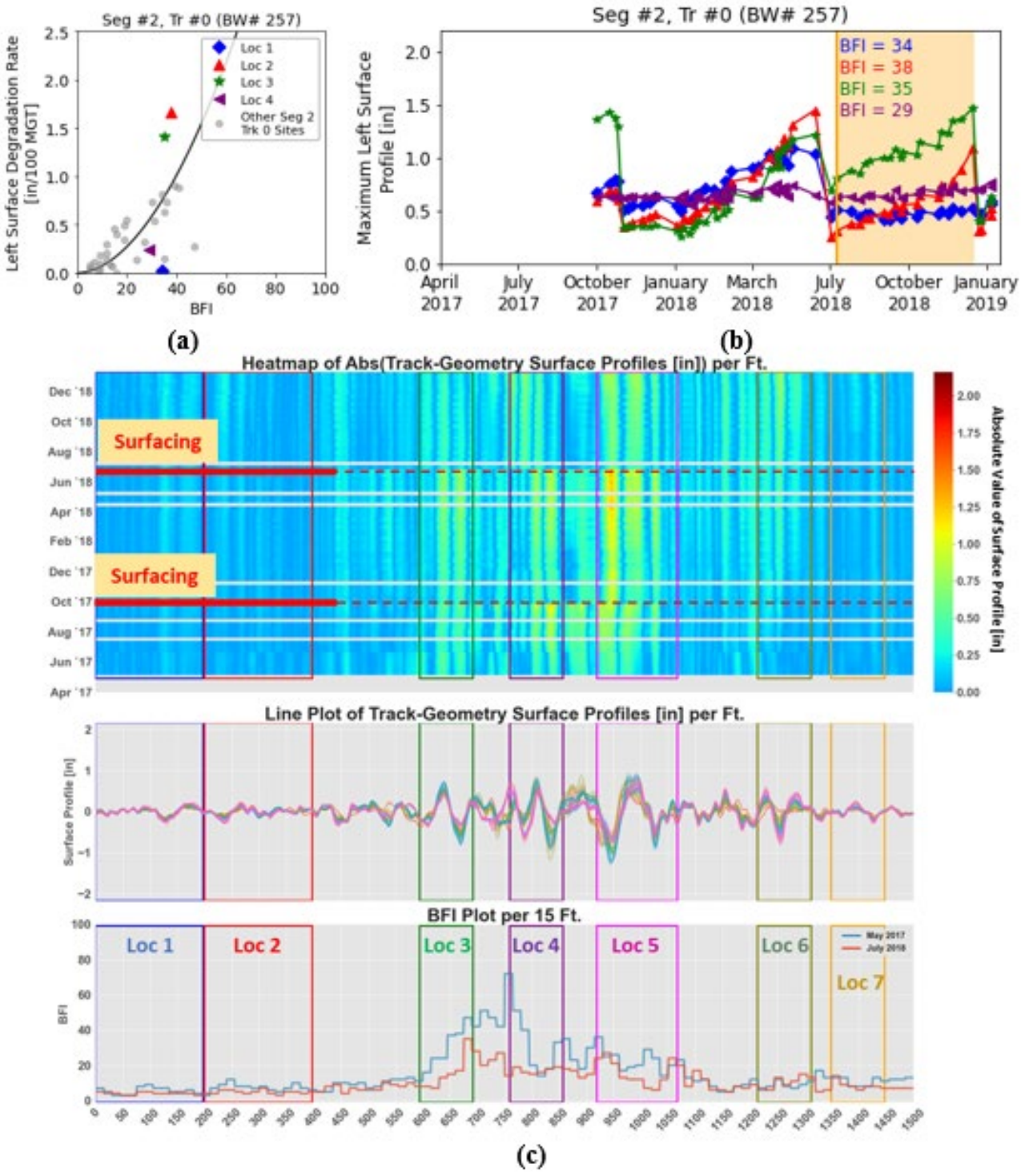

Figure 78: Deep Analysis of BW #257 (Segment #2, Track #0)

4.6.3 Outliers – Underprojected

BW# 375 shows a good example of location that is underprojected by the BFI-dSM curve. Figure 79 shows the data. At this dataset, a transition location is suspected between foot index 20

and 120. The BFI-dSM curve shows Loc 2 to be a good match while Loc 3 is higher than anticipated (underprojected). The heat map and surface profile show Loc 3 as a distinct single deviation where the bottom of the dip is degrading the quickest. The SM/SD value is 2.5 and the dSM/dSD value is 3.0, which is considered high and agrees with the general observations. Based on the parameter correlation analysis (Section 4.5), this behavior is common for underprojected locations. The peak in BFI at the 2017 run (blue) most likely indicates an isolated mudspot. The BFI reduction in 2018 could have explanations, including ballast maintenance (e.g., undercutting), same ballast condition but drier state, or a difference in the GPR algorithm.

The surface profile degradation with time shows linear behavior at Loc 2 while the degradation rate at Loc 3 has some non-linearity and slightly decreases over time. This non-linearity is not common and has multiple potential explanations. These explanations include a general reduction in settlement and degradation, ballast maintenance around April/May 2018, or some seasonality.

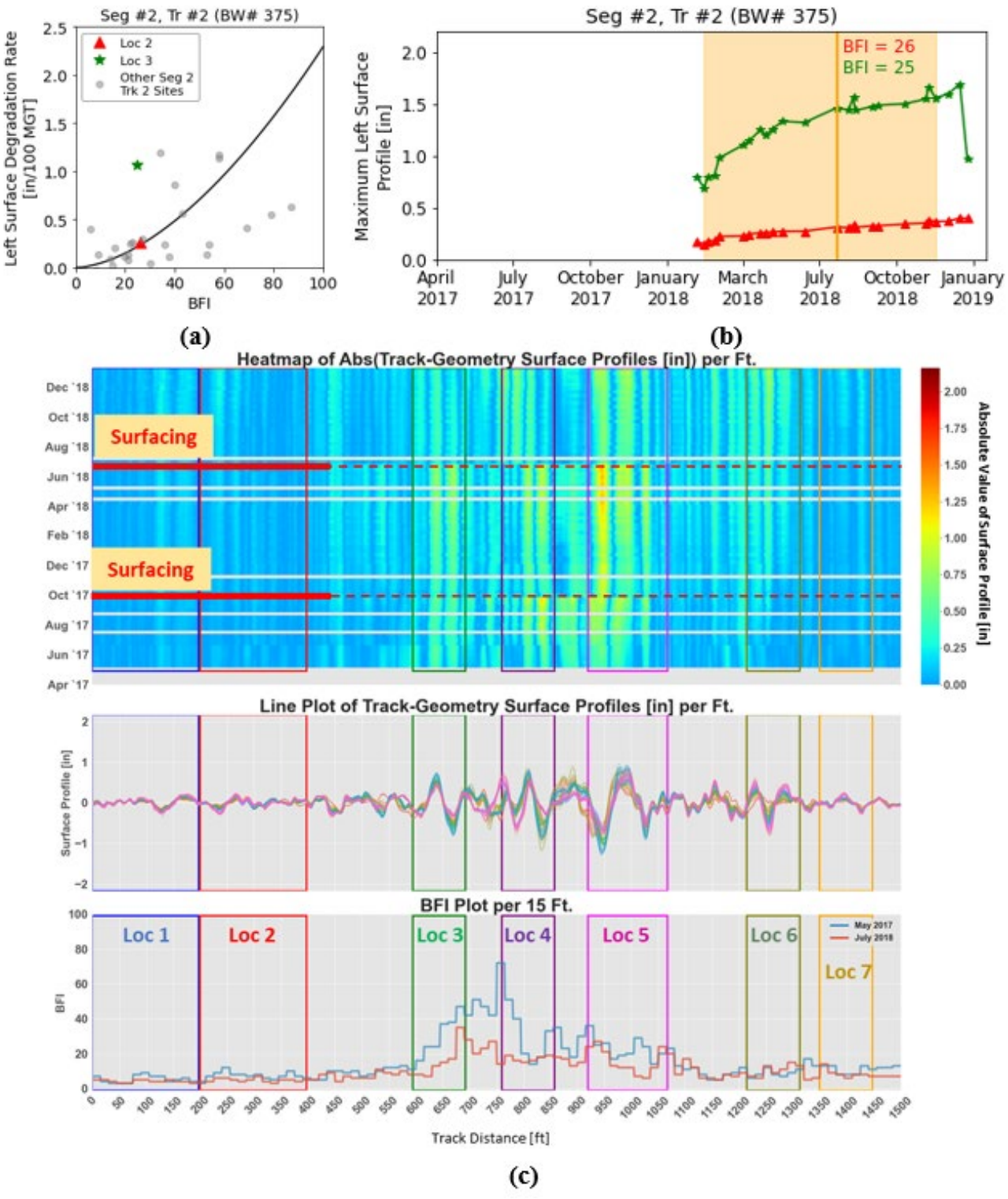

Figure 79: Deep Analysis of BW #375 (Segment #2, Track #2)

4.6.4 Outliers – Overprojection

Figure 80 shows BW# 118 which is located in Segment #2, Track #2. This site has a few locations, Loc 2 and Loc 3, in which the BFI overprojects the actual dSM value. Loc 3 shows fairly consistent behavior from 2017 to 2019 with a single surfacing event in October 2017. Loc 2 shows a significant change in behavior after that surfacing event with a decrease in dSM. The BFI plot shows a single reduction in Loc 2. This may be a spot undercut, but it is unclear from the data.

As for the indicators, both Loc 2 and Loc 3 have shoulder BFI values above 10. While this value is low for non-shoulder cleaned track, these values are unusually high for this dataset, which is routinely shoulder cleaned. The high shoulder BFI values in this dataset often result in overprojected SM values. In addition, the SM/SD and dSM/dSD values vary but are typically around 1.5 which is considered low. The track geometry records show Loc 2 to be fairly rough while Loc 3 shows a single deviation where the maximum positive surface values are similar the maximum negative surface value. Both conditions could explain the low SM/SD value.

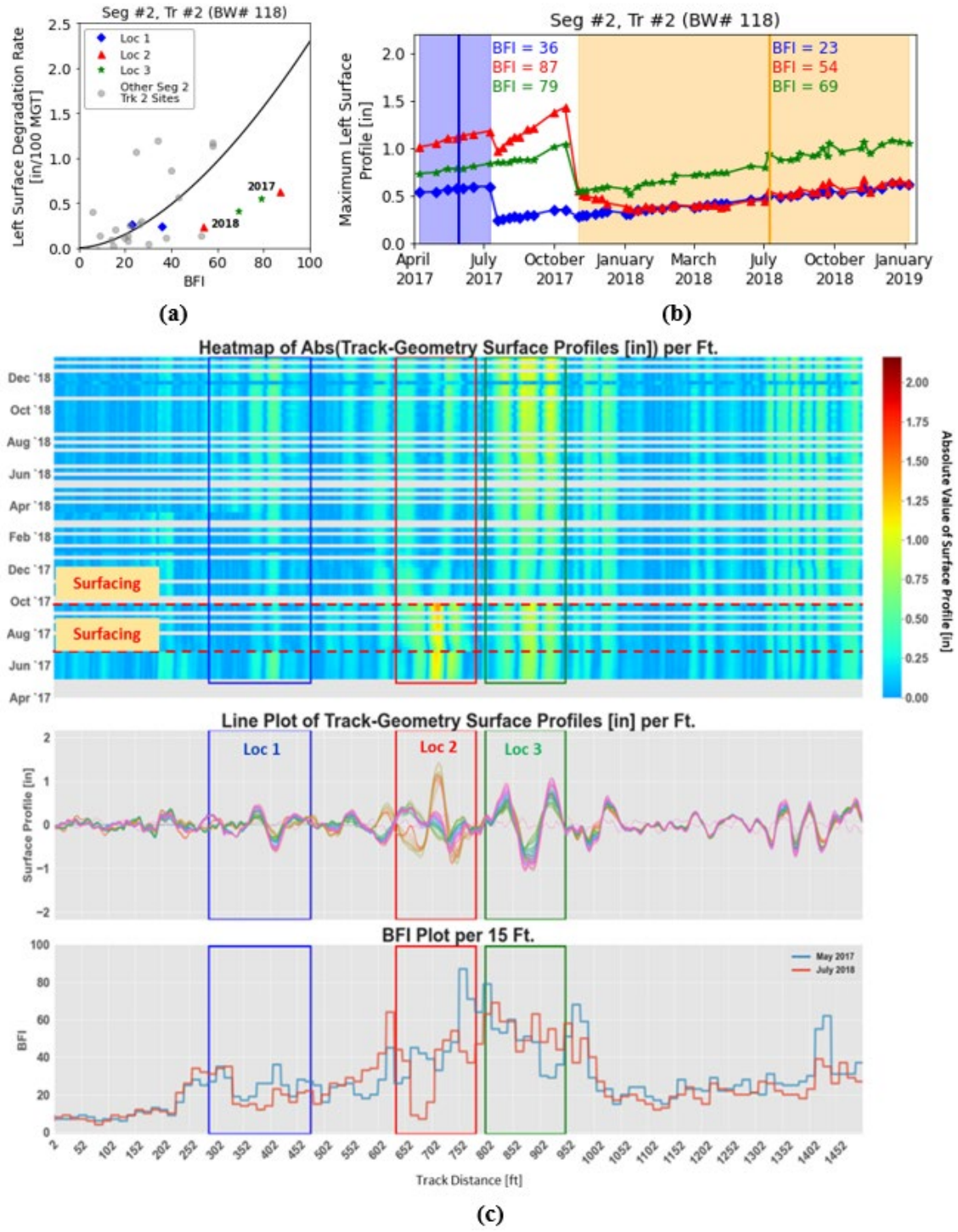

Figure 80: Deep Analysis of BW #118 (Segment #2, Track #2)

4.6.5 Pattern and Trending Analysis Summary

The outlier and pattern analysis provides a detailed look into the behavior of a few select regions of track. The results indicate that track behavior at any individual location is very complicated, and that it can be difficult to interpret what is happening from the data.

One of the surprising observations is that the track geometry degradation rates tend to be linear. This is a much different response than ballast settlement, which often has a distinct non-linearity and can often best fit a logarithmic curve with a continuously decreasing settlement rate. Without a direct comparison between settlement and dSM, it is unclear what is happening, but there are few possible explanations.

First, the SM/u Ratio may be changing over the surfacing cycle. In the beginning, the SM/u Ratio is close to zero because the entire ballast section will settle immediately after tamping. After consolidation, some regions will start settling more than others, causing a larger SM/u Ratio.

Second, the first track geometry record after tamping is likely collected in the "post-consolidation" ballast settlement stage and therefore does not include the initial high settlement rates in ballast consolidation. Therefore, the initial non-linearity may exist but, this information is not captured in the available track geometry records.

Third, the SM degradation may be non-linear for low dSM values and more linear for higher dSM values. Linear settlement trends has been observed for high BFI tests such as the Rainy Section model [34] and previous bridge approach studies [48], so it is possible that the logarithmic curve is relevant for cleaner ballast while linear behavior is more appropriate for high BFI tests. For the low dSM regions, the linear and logarithmic approximations will be similar and difficult to discern. For this reason, the linear trend is recommended.

4.7 Pre- vs. Post-Surfacing Track Geometry Deviations

Long-term track geometry degradation forecasting models will need to address surfacing events and the likely SM value that remains post-surfacing. To estimate the post-surfacing SM value, the pre- and post-surfacing SM value at each surfacing event was plotted against each other. As a note, the post-surfacing SM value is the first track geometry record after surfacing but not the SM immediately after surfacing. Typically, there is a gap in time between the surfacing event and the first post-surfacing track geometry run, so the ballast consolidation stage has likely already occurred.

Figure 81 shows the trend analysis. First, the results showed a bi-linear trend with a 1:1 ratio up to about 0.55 inches and then a slight increase in post-surfacing SM (y-axis) with increases in pre-surfacing SM (x-axis). Equations 30 and 31 present the fitting equation below:

$$SM_{post} = SM_{pre} \qquad if\ SM_{pre} \leq 0.55\ inches \qquad (30)$$

$$SM_{post} = 0.5114 + 0.0822 * SM_{pre} \qquad if\ SM_{pre} > 0.55\ inches \qquad (31)$$

This means that if the SM value is 0.55 inches or less pre-surfacing, the post-surfacing behavior will generally return to the pre-surfacing SM value. However, if the pre-surfacing SM value is greater than 0.55 inches, surfacing will generally leave an observable improvement in the SM value. A second observation is that a lot of scatter exists. Currently, it is unclear what causes the scatter.

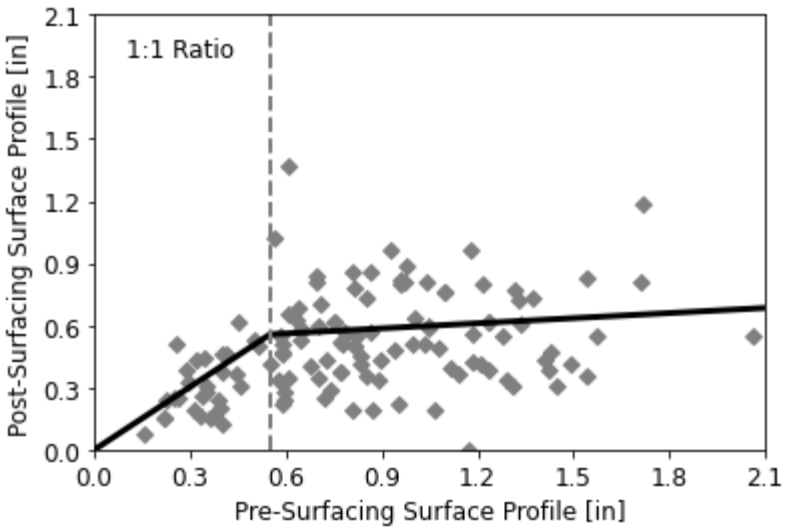

Figure 81: Relationship between Pre- and Post-Surfacing Surface Profile Values (SM)

This trend analysis now allows for an estimate of the post-surfacing SM value if a surfacing event is simulated in a track geometry forecasting model.

4.8 Summary and Future Recommendations

4.8.1 Field Data Analysis Summary

The field data analysis reviewed track geometry and GPR records at multiple locations within a single Class I track subdivision. This analysis was designed to 1) understand key parameters that affect track geometry degradation, 2) develop relationships for future projections, and 3) assess parameters and trends that could be incorporated into a forecasting model.

The results showed that relationships between track geometry degradation and BFI can be developed based on the collected field data. In addition, unique curves appear to exist for each track section. The unique curve for each track section was likely due to unique ballast maintenance history and possibly local variations in drainage, subgrade, tonnage, and tie type. Locations where the track geometry degradation was vastly over or underprojected from the BFI were able to be explained through parameters that characterize the track roughness, but more work is needed to investigate the meaning behind these potential trends. In addition, most of track geometry degradation trends were linear or close enough to linear to assume a linear trend and the post-surfacing track geometry state could be estimated based on the pre-surfacing track geometry state.

The field data analysis provided much useful information that can be used for the model demonstration. A few general remarks are as follows:

- BFI-dSM curves can be developed based on the collected field data.
    - Unique curves appear to exist for each track segment. The unique curve for each track section was likely due to unique ballast maintenance history as well as possible local variations in drainage, subgrade, tonnage, and tie type.

    - The curves used a power law fit which can be calculated by implementing a linear fit in a log-log scale.
- Other measurable parameters besides BFI are anticipated to have an influence on track geometry degradation, but no hard conclusions could be made from this dataset.
    - The current dataset did not allow for conclusions to be made on tie type, single/double track, or other parameters.
    - Most of the outliers were able to be explained through parameters that characterize the track roughness (i.e., SM/SD, dSM/dSD), but these parameters are not currently incorporated into any mechanistic track model.
- Most track geometry degradation trends were linear or close enough to linear to assume a linear trend.
    - One reason for this behavior is that the initial ballast settlement (consolidation stage) likely occurs prior to the first track geometry run after surfacing, and therefore, would not be captured.
    - Additional investigation is needed to define the track settlement and its relation to the 62-foot surface profile in various situations. It is possible that the behavior will vary based on the situation.
- The post-surfacing SM value could be estimated based on the pre-surfacing SM value.
    - There are many locations that deviate from these estimations and future work should look at additional parameters that may explain the deviations.

4.8.2 Recommendations for Future Analyses

While this analysis provided useful information, the sample size was relatively small with only hundreds of data points and improvements in the analysis could be made. Some of these improvements are listed below:

- As more data is regularly collected, larger dataset will improve correlations, improve BFI-dSM curves, and help identify additional parameters that will improve the analysis. Areas of interest are differences from axle loads, geographic region, and tie type.
- Additional recorded parameters could help the analysis. In regions with a lot of track lifting and undercutting, FDL would likely be helpful. GPR can also be used to measure the roughness of the ballast/subgrade interface, and that could be an additional indicator.
- Longer timeframes (three to four consecutive surfacing cycles) for the analysis would help determine if single locations regularly overproject or underproject the BFI level. If so, this could eventually allow for individualized correction factors.

5. Mechanistic Model Demonstration and Recommendations

The goal of this section is to determine the accuracy and capabilities of the track geometry deterioration models, namely the RTLM, by comparing the BFI-dSM relationship and the projections of track geometry degradation with MGT. This work is still in progress and is anticipated to be updated as more field data is collected and analyzed.

The goal of this analysis was to gain a current assessment of the ability of these models and determine how they can be improved in the future. The long-term goal is to develop track geometry forecasting models that could perform a wide variety of functions. These functions could include short-term risk assessments of a single location forecasting regarding when it will surpass a track geometry exception threshold or forecasting the amount of track geometry exceptions anticipated over a certain amount of track in a given timeframe. An additional application would be projecting how the track behavior may change depending on ballast maintenance methods, such as surfacing, ballast shoulder cleaning, or undercutting. A third group of applications would include forecasting how potential changes in track structure, tonnage, or climate would affect track performance. This information could be useful in determining how a change in tie type or tonnage would affect the anticipated maintenance, or how long-term changes in climate, via annual rainfall or the amount of high-intensity rain events, would affect track geometry degradation.

5.1 Model Assumptions

When comparing all the models, it is very important to understand the various assumptions and proper implementation so invalid comparisons are not made. A statement that can be applied to all the models:

- Each of the three previously developed models (i.e., Rainy Section model, RTLM, and K&H model) has settlement as its main output. As explored in Section 3.2, the relationship between settlement (u) and surface profile degradation (dSM) is likely complicated and not a linear 1:1 relationship.

Some comments on each individual model:

- The Rainy Section model was developed to explore the potential range in behavior due to moisture at a specific location. This means the Rainy Section model is more conceptual and can be used to check for scatter but should not be a predictive tool of the median response.
- The RTLM is the most comprehensive model and was designed to be used in a wide range of track conditions. As opposed to the Rainy Section model, the RTLM outputs the median response and did not incorporate scatter. However, this model incorporated many other factors beyond BFI, which, in theory, would account for some of the scatter shown between track geometry degradation and BFI in the previous sections.
- The K&H model is a statistical fit model that was developed in the northeastern United States for use on a wide range of traffic conditions. The ballast in that region was near the end of its life. This model only simulated a single regional response but was still helpful with comparisons to other BFI-dSM curves and was a median response similar to the RTLM.

Some additional comments regarding track inspection vehicles:

- Current inspection technologies can estimate most important parameters based on a review of fundamental ballast behavior. Most of the parameters (e.g., tie type, subgrade type, tonnage, etc.) will generally be constant over a period of a few years so they can be documented after a single inspection. However, the factors that change continuously (e.g., BFI and moisture) often have a greater influence on ballast performance and would require more frequent inspection.
- For the RTLM, current inspection technologies along with general track knowledge could estimate the axle load, BFI, climate, and track structure. However, ballast abrasion and track modulus are not typical measurements.

5.2 BFI-dSM Relationship

This section compares the BFI-dSM relationship calculated from the various mechanistic and statistical models. Section 3.3 introduced the equations used for the models. This section provides a high-level overview of the performance of the models against the field data analyzed in Section 4.

5.2.1 Comparison of All Models

The first comparison involves a very high-level overview of the various models. Figure 82 shows this comparison. Only one version of the Rainy Section model and RTLM is included as those will be expanded on later. One observation is that the general response of all models is similar for BFI<20 but deviates significantly for BFI>20. This is because the behavior of cleaner ballast has fewer influential parameters (e.g., ballast shape and subgrade) that affect its behavior than fine-filled ballast does (e.g., moisture, BFI, and FDL).

Expanding on varying responses for BFI>20, it is also apparent that there is no single appropriate BFI-dSM curve for all railroad track, and additional factors are needed to determine how steep or shallow the curve is. For example, the three models from the field data presented in Section 4, despite being in the same geographic region, had different maintenance histories. The K&H model, beyond being measured in a different geographic region and loading environment, measured locations that were highly degraded and near the end of their ballast life which agrees with the general trends.

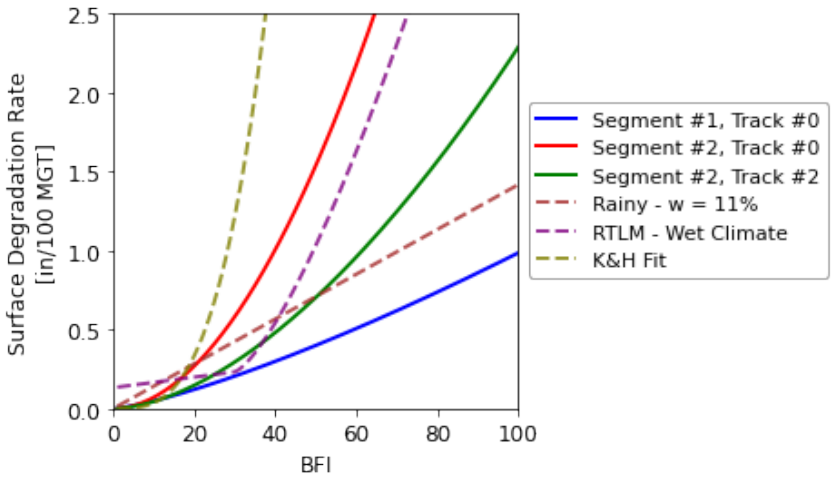

Figure 82: BFI-dSM Curve that Includes the Three Field Data Segments and Three Previously Introduced Models

5.2.2 Influence of Moisture/Climate

Both the Rainy Section model and RTLM included varying responses depending on the moisture levels, but each one represented a separate aspect of moisture. The Rainy Section model was designed to show the range in potential behaviors for a single location. The RTLM was designed to show the average response for a wide range of geographic regions. Therefore, while both models are used for comparison, the Rainy Section model should be used to inform the amount of scatter due to moisture levels from one particular geographic region while the RTLM is used to compare the fitted BFI-dSM curves.

To emphasize the different moisture representations, Figure 83 shows all the non-transition field data for the moisture/climate ranges from the Rainy Section model and RTLM. The Rainy Section model does a good job of incorporating the scatter while the RTLM appears to do well with a general data fit. These observations were unsurprising given the purpose of each model.

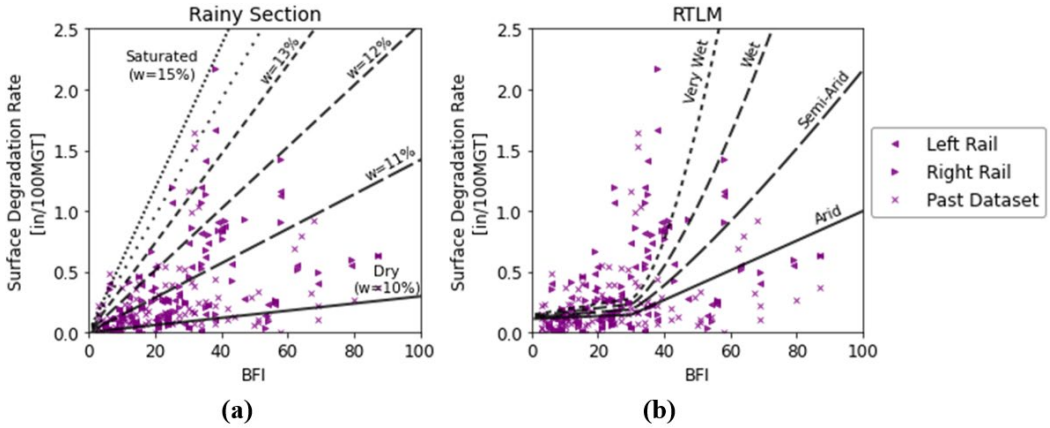

Figure 83: Field Data Points Plotted on Top of Ranges from Rainy Section Model (a) and RTLM (b)

Figure 84, on the other hand, plots the BFI-dSM curves on top of the moisture/climate ranges of the Rainy Section model and RTLM. The results showed a better match with the RTLM than the

Rainy Section model. Again, this is unsurprising when the purpose of each model is considered. For the field data power law fits and the RTLM fits, the range in behaviors is very similar even though they represent two different parameters. The RTLM varies due to climate conditions while the field data fit varies, likely due to ballast maintenance history. These variations suggest that both factors (i.e., median and scatter) should be incorporated in a forecasting model.

Another observation is that the RTLM shows a sharp change in behavior at a BFI = 30. This change in behavior is due to the assumption that ballast voids are filled with fine material at a BFI of 30. The power law fit and data (Figure 83) suggest this change starts to occur at bit earlier at BFI of 20.

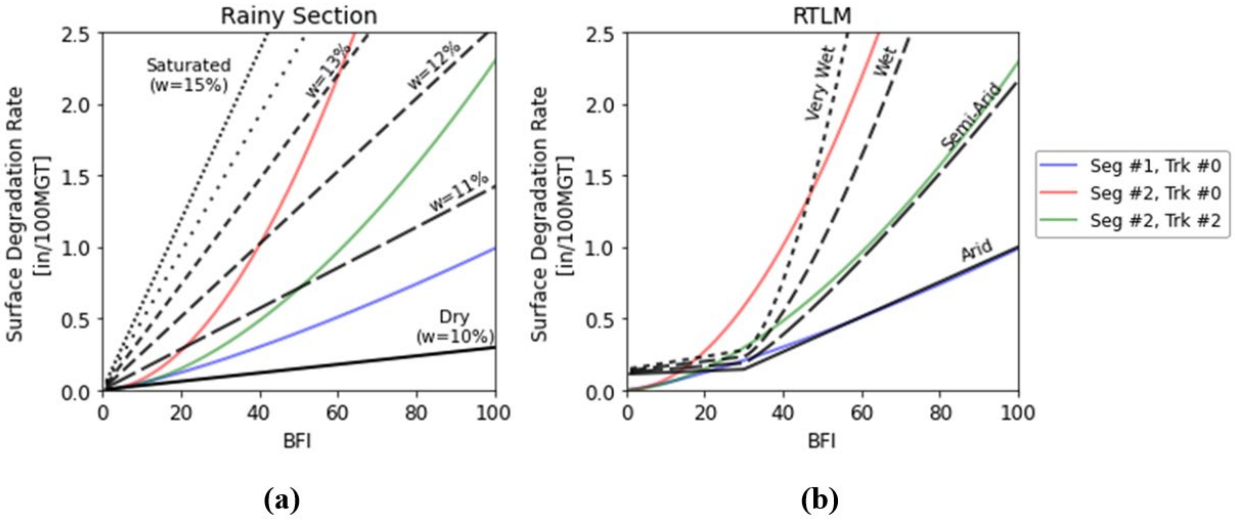

Figure 84: Field Data BFI-dSM Curves Plotted on Top of Ranges from Rainy Section Model (a) and RTLM (b)

5.2.3 Influence of Tie Type

An additional factor included in the RTLM is the tie type. Concrete ties are assumed to have higher degradation rates due to how the tie stiffness affects the interface stresses between the bottom of the tie and top of the ballast. Numerical modeling suggests the combination of stiff concrete and ballast causes higher stress concentrations near the top of the ballast layer around concrete ties than with the softer wood tie [20].

Figure 85 shows the RTLM response in track with assumed concrete ties or wood ties. For instance, Segment #2, Track #2 (green) should be a mostly wood tie track so that fit is separated from the two concrete tie track sections. This suggests that, based on the RTLM assumptions, most differences between Segment #2, Track #0 (red) and Track #2 (green) could potentially be explained by tie type. The RTLM assumption has not yet been verified, while this is an interesting observation, additional verification is needed before this explanation can be used with any degree of regularity.

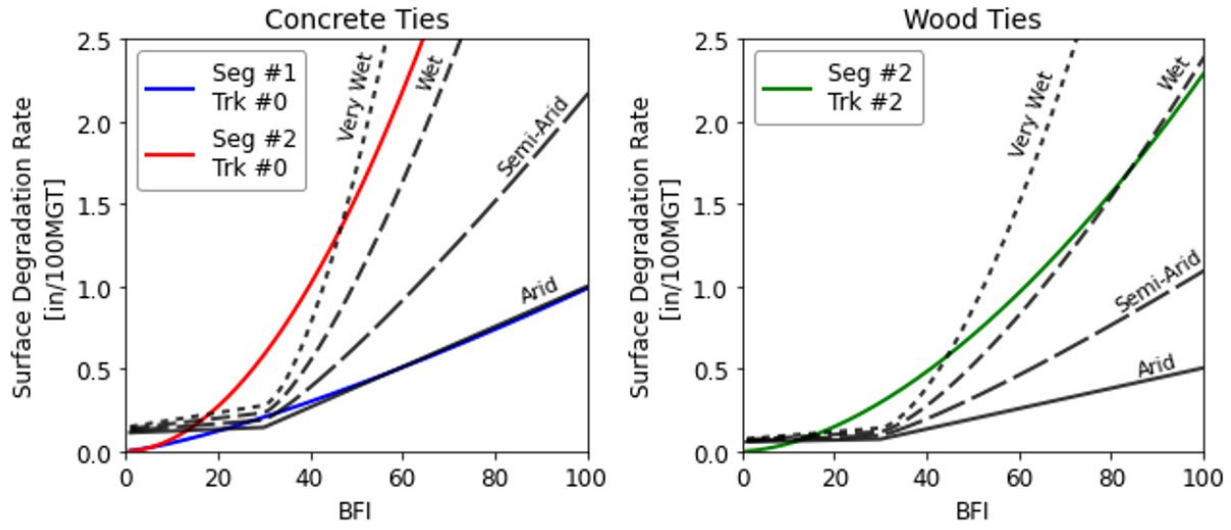

Figure 85: Comparison of RTLM and Field Data BFI-dSM Curves Incorporating Concrete Ties (a) and Wood Ties (b)

5.2.4 BFI-dSM Fit Comparison

The last aspect of model demonstration is to perform a detailed comparison between the BFI-dSM curves from the RTLM and power law fits. As a note, the RTLM uses two equations and must be manually calculated while the ballast waiver power law can be calculated using fitting methods.

The data and best fit from all three segments are shown in Figure 86 in both linear and log-log form with the closest corresponding RTLM curve. Segment #1 (Figure 86a and Figure 86b (blue)) assumes concrete ties and arid climate. Segment #2, Track #0 (Figure 86c and Figure 86d (red)) assumes concrete ties and a very wet climate. Segment #2, Track #2 (Figure 86e, Figure 86f (green)) assumes wood ties and a wet climate.

The plots show a good fit for both plots at BFI>30 but greater deviation at BFI<30. The data suggest the power law fits the data to a better degree. An explanation for the RTLM curve is that the RTLM is designed to output settlement and was modified to fit SM data for this study. For all ballast, clean or fine-filled, some amount of settlement was anticipated so settlement data would likely fit the RTLM data better. The overprojection at BFI<20 also suggests that the SM/u Ratio assumption of 0.3 is likely not appropriate for BFI<20 track and is potentially lower because clean ballast will settle fairly uniformly during the initial consolidation and then show low amounts of variation afterward. High BFI track will show more variation after the consolidation phase, resulting in higher SM values.

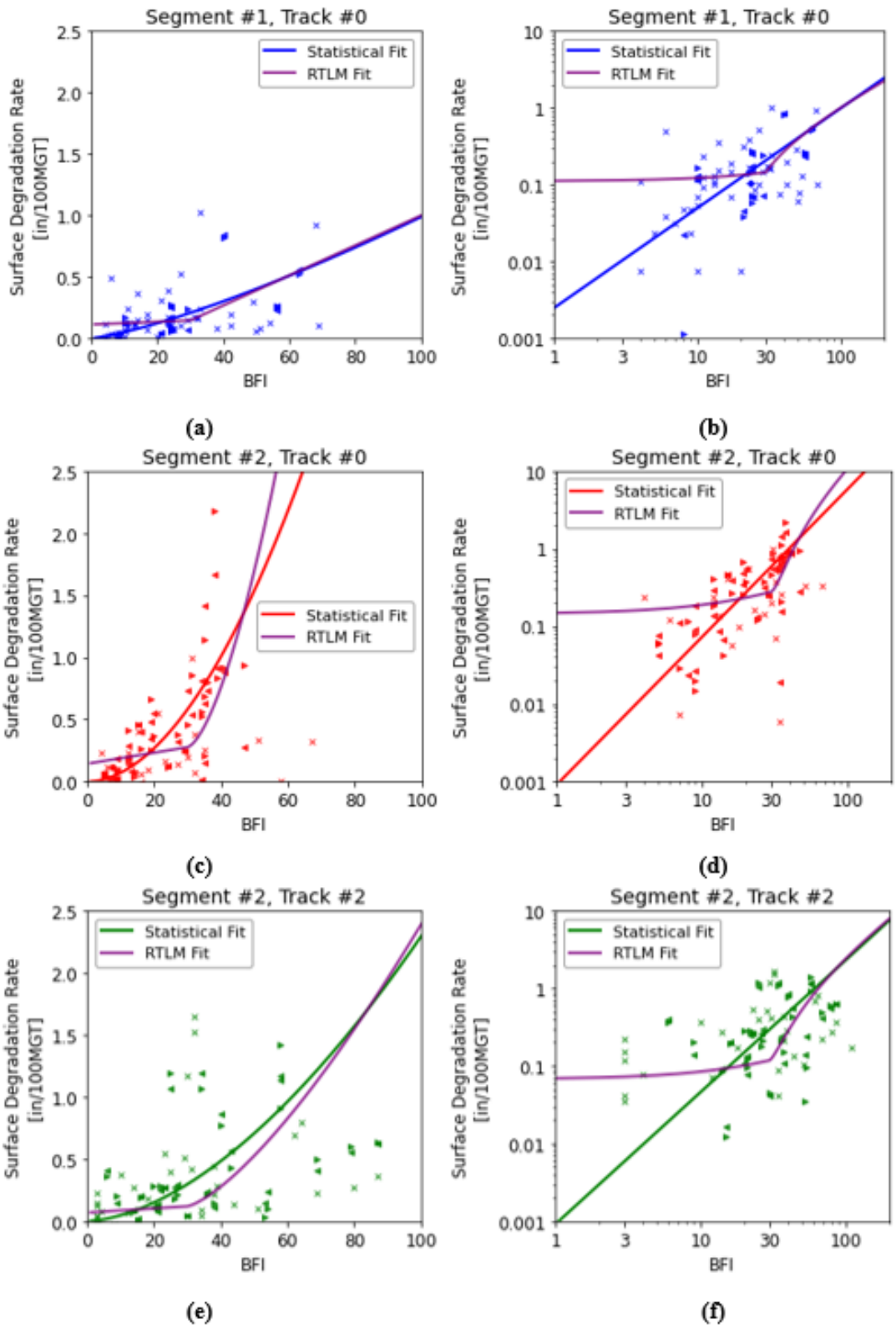

Figure 86: Comparison of BFI-dSM Curve in Linear and Log-Log Form for Segment #1, Track #0 (a, b), Segment #2, Track #0 (c, d), and Segment #2, Track #2 (e, f)

5.3 Track Geometry Degradation with MGT

The last aspect of the model demonstration is to compare the assumed SM degradation with MGT. The BFI-dSM plots assume changes over 100 MGT. The Field Data Fit assumes a linear change with MGT while the RTLM assumes a logarithmic fit. Once again, this difference is due to the RTLM originally representing settlement and then being modified to fit SM data for this study.

Figure 87 and Figure 88 shows two examples of the Field Data and RTLM projections against field data. For these datasets, the initial SM value (SM at 0 MGT) is set to zero to eliminate the variation of initial SM values and better isolate the degradation trends.

Figure 87 shows all the track geometry degradation locations with BFI 20 to 24 in Segment #1, Track #0 against the field data and RTLM projections assuming a BFI of 22. The two projections are similar because of the low degradation rate and match well with the field data in gray. Based on the field data (gray lines), it does seem that there are some locations display linear behavior while other locations display logarithmic behavior. Whether the location shows linear or logarithmic behavior is likely due to how uniformly the track is settling and how quickly a track geometry record was taken after surfacing (whether it was still in the consolidation stage or not).

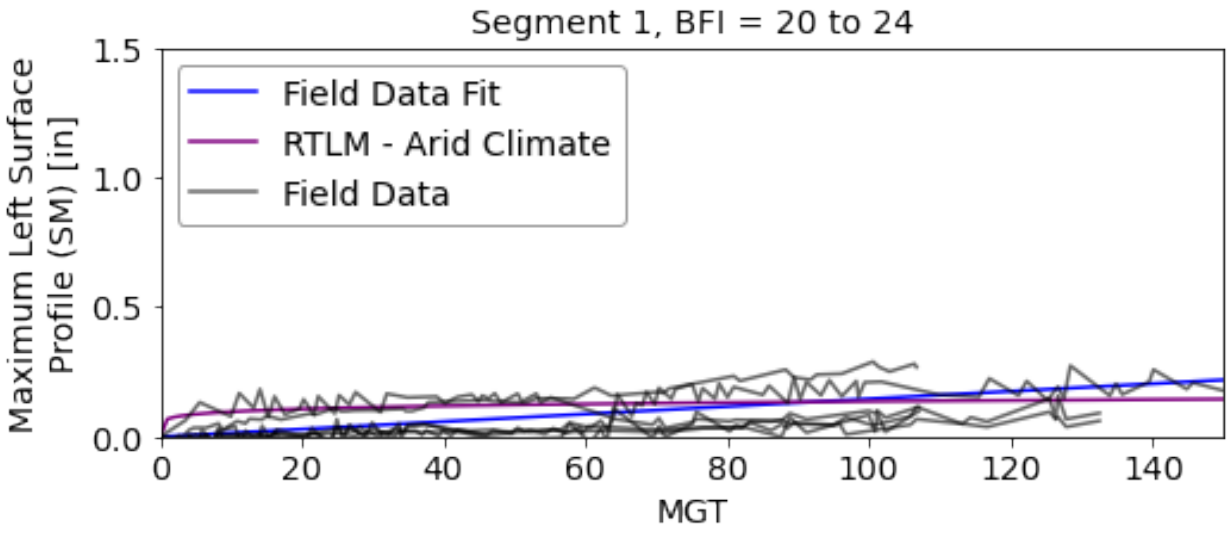

Figure 87: Comparison of Linear and Logarithmic (RTLM) Trends for SM Degradation with MGT for Segment #1 with BFI from 20 to 24

Figure 87 shows all the track geometry degradation locations with a BFI 35 to 39 in Segment #2, Track #0 against the field data and RTLM projections assuming a BFI of 37. The two projections are significantly different with the RTLM showing very high settlement rates in the first few MGT. Then, the degradation become very flat. The Field Data (gray lines), while scatter exists, fits the Linear Data fit trend much better than the logarithmic RTLM . This observation suggests that for high BFI track, the track geometry will generally be linear.

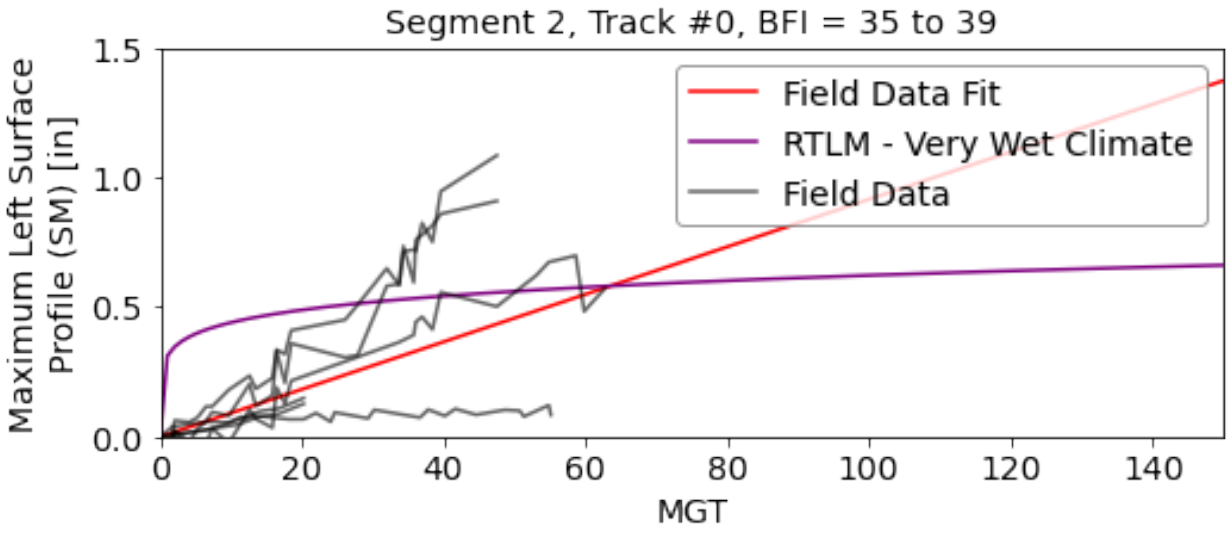

Figure 88: Comparison of Linear and Logarithmic (RTLM) Trends for SM Degradation with MGT for Segment #2 Track #0 with BFI from 35 to 39

One major finding from this analysis is that a linear trend is more reasonably suited than a logarithmic fit for representing SM degradation. There will be instances when the data will show non-linear behavior but suggests that most is represented by the linear trend. The linear representation of track geometry degradation will be recommended for future forecasting models.

5.4 Model Performance and Inputs

As mentioned, the RTLM is the most comprehensive mechanistic model and should be used as a framework for developing a forecasting model that is more aligned with outputs from track inspection vehicles. The current dataset reinforces the view that BFI should be a primary input and that the BFI-dSM curve can vary based on track section. The authors suggest that other important loading and track structure aspects, such as axle load and tie type, should be kept but used cautiously until data agrees or disagrees with the trends. However, if site specific trends are developed, the climate/axle load/tie type will only be a stand-in until a section-specific curve can be developed.

Track Modulus could be useful as a starting point on a location-by-location basis to help explain scatter. High track modulus locations would lead to lower dSM projections, and low Track Modulus locations would lead to higher dSM projections. The authors do not envision Track Modulus being widely used because it is rarely measured but could be helpful for detailed site investigations and as a possible “correction factor” of individual locations.

AN is recommended to be discarded from the forecasting model because it is rarely measured, and high frequency BFI measurements can better represent degrading ballast than an AN.

Based on the current dataset, no additional variables are recommended because very few relevant parameters are currently measured by track inspection systems. However, as more parameters are included, they may be useful as “correcting factors” to modify the initial projection based on BFI, especially if they show consistent trends at explaining over and under projections. These “correcting” factors could include moisture, track roughness characteristics, or even tie-ballast interface or tie deflections.

5.5 Forecasting Model Recommendations

The results from Data Collection and model demonstration have led to multiple recommendations for developing a forecasting model. The scope of Phase I of this project is to develop recommendations. Future phases will work on incorporating the following recommendations into a model:

- The RTLM can be used as an initial framework that is modified as needed. The modified forecasting model is envisioned as a mechanistic-statistical hybrid model that will eventually fit site-specific track sections and location-specific trends into an existing mechanistic framework.
- Two modifications to the RTLM are recommended regarding the underlying framework:
  - Switch the RTLM BFI curve from a manual fit to a power law fit. The power law fit better fits the SM data and is easier to calculate than the current manual approach.
  - Track geometry degradation (SM) should trend linearly with MGT instead of with the current non-linear logarithmic fit based on settlement. The field data showed linear trends better represents the high dSM data locations and will be easier from a calculation standpoint.
- The RTLM adjustment factors are recommended to be modified and re-categorized as follows:
  - Abrasion Number correction factor should be discarded as a direct input parameter because it is rarely measured.
  - Climate, Tie Type, and Axle load can be recategorized as "track-section-specific" adjustment factors. Ballast maintenance history may also be included. The purpose of these adjustment factors is to project the BFI-dSM curve prior to any track geometry data analysis. This BFI-dSM curve will eventually be replaced with a site-specific curve developed from field data.
  - Track Modulus can be recategorized as a "location-specific" adjustment factor. This would not just include track modulus but could eventually incorporate track roughness characteristics (SM/SD), tie displacement, or even manually adjusted due to currently uncharacterizable parameters (e.g., ballast pocket or flooded region). Each specific location (200-foot track region) may eventually be assigned a value through a back-calculation process if enough data is available.
- Due to inevitable variation and scatter, some sort of uncertainty or statistical distribution should eventually be included to move from a deterministic analysis to a risk-based statistical analysis.
- The influence of ballast maintenance should eventually be incorporated as a better understanding of the effects.

5.6 Forecasting Model Preliminary Framework

The forecasting model will have an envisioned framework as the following:

$$SM_{MGT} = SM_i + dSM_{1\kappa_2} * MGT \quad (32)$$

$$dSM = e^{b} * BFI^{a} \quad (33)$$

SM_{MGT} = Projected maximum 62-foot surface profile (SM) at a given MGT after surfacing

SM_i = Post-surfacing SM (assumes after ballast consolidation)

MGT = MGT after surfacing

κ_2 = Site-specific adjustment factor

a,b = constant for section BFI-dSM curve

The details would be worked out in future phases, but this framework should include the major features and be robust enough to incorporate a wide range of track behaviors.

In general, the model would proceed as follows:

- Track segments with limited data would make assumptions about the a,b, and κ_2 values. Recommended values may eventually be provided.
- Once historical data is available, the a- and b-constants would be statistically fit for a track segment based on the datasets. This fit should represent the median value for that track section.
- The site-specific adjustment factor (κ_2) would be based on historical data and try to address the scatter at individual locations. This factor would assume that individual locations consistently over- or underproject the median response.

5.7 Summary

The mechanics-based model development aspect involved compiling existing track geometry deterioration models and demonstrating how these models project future track geometry conditions by comparing the projections versus the field data results. The goal of this analysis was to gain a current assessment of the ability of these models and how they could be improved in the future. The long-term goal is to develop track geometry forecasting models that can perform short-term risk assessments on track risk, projections on how track behavior may change depending on ballast maintenance, along with long-term forecasts to incorporate potential changes in track structure, tonnage, or climate.

The results showed that each of the three previously developed models were significantly different from each other in terms of ability and scope. These differences included projecting the range of behavior at one location due to moisture in one instance to projecting the range in median response of the entire track section based on different climate regions. The future forecasting model would aim to incorporate both of those factors along with others. It is envisioned that a forecasting model could initially give broad projections based on track structure, tonnage, climate, and other potential factors. This could be used as a forecast at locations with little data or to explore how changes of these factors would affect track geometry degradation. Then, eventually, as track data was collected and analyzed, the model could eventually be developed into a site-specific model based on statistic fits of the track section and even potentially used at highly localized high-risk locations.

Detailed conclusions from the mechanistic forecasting model data analysis are as follows:

- Each of the three previously developed models (Rainy Section model, RTLM, and K&H model) have settlement as its main output. As explored in Section 3.2, the relationship between settlement (u) and surface profile degradation (dSM) is likely complicated and not a linear 1:1 relationship.
- The Rainy Section model was developed to explore the potential range in behavior due to moisture at a specific location. This means the Rainy Section model was more conceptual and could be used as a check for scatter but should not be a predictive tool of the median response.
- The RTLM is the most comprehensive model and was designed to be used in a wide range of track conditions. Opposite of the Rainy Section model, the RTLM outputs the median response and does not incorporate scatter. However, this model incorporates many other factors beyond BFI which, in theory, would account for some of the scattering shown in the previous sections between track geometry degradation and BFI.
- The K&H model is a statistical fit model that was developed in the northeastern United States using a wide range of traffic conditions. The ballast in that region was near the end of its life. This model only simulates a single regional response, but it is still helpful with comparisons to other BFI-dSM curves and is a median response similar to the RTLM.
- The RTLM can be used as an initial framework that is modified as needed. The modified forecasting model is envisioned as a mechanistic-statistical hybrid model that will eventually fit a site-specific track section and location-specific trend into an existing mechanistic framework.
- Two modifications are recommended regarding the underlying framework:
    - Switch the RTLM BFI curve from a manual fit to a power law fit. The power law fit better fits the SM data and is easier to calculate than the current manual approach.
    - Track geometry degradation (SM) should trend linearly with MGT instead of with the current non-linear logarithmic fit based on settlement. The field data showed linear trends that better represent the high dSM data locations and is easier from a calculation standpoint.
- The RTLM adjustment factors are recommended to be modified and re-categorized.
    - Abrasion Number correction factor is recommended to be discarded as a direct input parameter because it is rarely measured, but it will be considered as part of the statistical element based on the historic data.
    - Climate, Tie Type, and Axle load can be recategorized as “track-section-specific” adjustment factors. Ballast maintenance history may be included as well. The purpose of these adjustment factors is to project the BFI-dSM curve prior to any track geometry data analysis. This BFI-dSM curve will eventually be replaced with a site-specific curve that is developed from field data.
    - Track Modulus can be recategorized as a “location-specific” adjustment factor. This would not just include track modulus but could eventually incorporate track roughness characteristics (SM/SD) or even be manually adjusted due to uncharacterizable parameters (e.g., ballast pocket or flooded region). Each specific

location (200-foot track region) may eventually be assigned a value through a back-calculation process if enough data is available.

  - Based on the current dataset, no additional variables are recommended because very few relevant parameters are currently measured by track inspection systems. However, as more parameters are included, these may be useful as "correcting factors" to modify the initial projection based on BFI, especially if they show consistent trends at explaining over and underprojections. These parameters could include moisture, track roughness characteristics, even tie-ballast interface, or tie deflections.

- Due to inevitable variation and scatter, some sort of uncertainty, or statistical distribution should be eventually included to move from a deterministic analysis to a risk-based statistical analysis.
- The influence of ballast maintenance should eventually be incorporated as a better understanding of the effects of ballast maintenance are understood.

6. Conclusions

FRA requested that researchers build on and extend earlier work on mechanics-based ballast condition forecasting models to support improved safety and reliability of ballast tracks. The conclusions drawn from the Phase I report are considered preliminary and subject to change in the Phase II final report.

6.1 Lateral Ballast Behavior

This study produced multiple observations and conclusions that are listed below:

- Multiple parameters including, but not necessarily limited to, ballast density, ballast shape characteristics, ballast shoulder width, ballast crib height, tie type, tie-ballast interface, and maintenance influenced the lateral tie strength of clean ballast
    - Based on the current study and historical tests, a change in the 6-inch shoulder width, 1-inch crib height, heavier ties, and more angular ballast are roughly equivalent in their influence on lateral tie strength
    - Ballast shape characteristics (angularity) were found to be a potential variable that could have significant effects on lateral tie strength because more angular ballast particles would engage the ballast to a greater degree than rounded ballast particles
    - The long-term increase in lateral tie resistance over time was generally proportional to the initial 0 MGT lateral tie resistance. This was because the increase in tie resistance from ballast density had even greater influence on sections with more ballast.
    - Risk-based assessments can be made with general knowledge of the ballast parameters, but more work is required before forecasting models can be used with high confidence
    - Slow order tonnage appeared to increase lateral resistance by 10 to 20 percent
    - Higher tamp lift heights resulted in lower lateral resistance at 0 MGT
- Small- and large-displacement lateral resistance metrics such as peak lateral resistance (large-displacement) and initial lateral stiffness (small-displacement) were strongly related, suggesting the shape of the pre-peak force-displacement curve remains similar but is scaled upwards depending on the peak resistance
- Statistical distributions of the lateral resistance did not confirm normal distributions for all tests, and it was unclear if non-normal distributions could be used. Reasons for tests not confirming to normal distributions included non-normal distributions, significant influence of outliers due to low statistical sample size, and varying ballast conditions (e.g., not fully isolating a single condition within the sample size).
- Fine-filled ballast appeared to have a significant influence on the lateral resistance with dry fine-filled ballast producing very high resistance values, likely due to the suction pressures in the shoulders. The wet condition resulted in lateral resistance values much lower than the dry counterparts but not lower than clean ballast. These results were anticipated to vary significantly by location depending on the fines and ballast conditions.

- The ballast regions resisting vertical and lateral tie movement were different and should be reflected with different inspection technology strategies to address risk analysis.
    - The ballast resisting lateral tie movements were closer to the surface so surface inspection technologies such as LiDAR or machine vision may be used for site characterization. The relevant characteristics could include tie type, ballast shoulder width, and ballast crib height.
    - The surface ballast was less confined, so particle shape characteristics had a greater influence on the ability of ballast particles to interlock than the vertical direction counterparts.
    - The ballast section (shoulder width and crib height) was more influential for resisting lateral movement than vertical direction.

6.2 LiDAR Field Data Analysis

The field data analysis provided information that can be used for the model demonstration. A few general remarks are as follows:

- BFI-dSM curves can be developed based on the collected field data.
    - Unique curves appear to exist for each track section. The unique curve for each track section is likely due to unique ballast maintenance history as well as possible local variations in drainage, subgrade, tonnage, and tie type.
    - The curves used a power law fit which can be calculated by implementing a linear fit in a log-log scale.
- Other measurable parameters besides BFI are anticipated to have an influence on track geometry degradation, but no hard conclusions could be made from this dataset.
    - The current dataset did not allow for conclusions to be made on tie type, single/double track, or other parameters.
    - Most of the outliers were able to be explained through parameters that characterize the track roughness (i.e., SM/SD, dSM/dSD), but these parameters are not currently incorporated into any mechanistic track model.
- Most of the track geometry degradation trends were linear or close enough to linear to assume a linear trend.
    - One reason for this behavior is that the initial ballast settlement (consolidation stage) likely occurs prior to the first track geometry run after surfacing, and therefore, would not be captured.
    - Additional investigation is needed to define the track settlement and its relation to the 62-foot surface profile in various situations. It is possible that the behavior will vary based on the situation.
    - The post-surfacing SM value could be estimated based on the pre-surfacing SM value.
    - There are many locations that deviate from these estimations and future work should look at additional parameters that may explain the deviations.

6.3 Mechanics-Based Forecasting Model Demonstration

Detailed conclusions from the mechanistic forecasting model data analysis are as follows:

- Each of the three previously developed models (i.e., Rainy Section model, RTLM, and K&H model) have settlement as its main output. As explored in Section 3.2, the relationship between settlement (u) and surface profile degradation (dSM) is likely complicated and not a linear 1:1 relationship.
- The Rainy Section model was developed to explore the potential range in behavior due to moisture at a specific location. This means the Rainy Section model was more conceptual and could be used as a check for scatter but should not be a predictive tool of the median response.
- The RTLM is the most comprehensive model and was designed to be used in a wide range of track conditions. Opposite of the Rainy Section model, the RTLM outputs the median response and does not incorporate scatter. However, this model incorporates many other factors beyond BFI which, in theory, would account for some of the scattering shown in the previous sections between track geometry degradation and BFI.
- The K&H model is a statistical fit model that was developed in the northeastern United States using a wide range of traffic conditions. The ballast in that region was near the end of its life. This model only simulates a single regional response, but it is still helpful with comparisons to other BFI-dSM curves and is a median response similar to the RTLM.
- The RTLM can be used as an initial framework that is modified as needed. The modified forecasting model is envisioned as a mechanistic-statistical hybrid model that will eventually fit aa site-specific track section and location-specific trend into an existing mechanistic framework.
- Two modifications are recommended regarding the underlying framework:
    - Switch the RTLM BFI curve from a manual fit to a power law fit. The power law fit better fits the SM data and is easier to calculate than the current manual approach.
    - Track geometry degradation (SM) should trend linearly with MGT instead of with the current non-linear logarithmic fit based on settlement. The field data showed linear trends better represents the high dSM data locations and is easier from a calculation standpoint.
- The RTLM adjustment factors are recommended to be modified and re-categorized.
    - Abrasion Number correction factor is recommended to be discarded as a direct input parameter because it is rarely measured, but it will be considered as part of the statistical element based on the historic data.
    - Climate, Tie Type, and Axle load can be recategorized as “track-section-specific” adjustment factors. Ballast maintenance history may be included as well. The purpose of these adjustment factors is to project the BFI-dSM curve prior to any track geometry data analysis. This BFI-dSM curve will eventually be replaced with a site-specific curve that is developed from field data.

- Track Modulus can be recategorized as a “location-specific” adjustment factor. This would not just include track modulus but could eventually incorporate track roughness characteristics (SM/SD) or even be manually adjusted due to uncharacterizable parameters (e.g., ballast pocket or flooded region). Each specific location (200-foot track region) may eventually be assigned a value through a back-calculation process if enough data is available.
- Based on the current dataset, no additional variables are recommended because very few relevant parameters are currently measured by track inspection systems. However, as more parameters are included, these may be useful as “correcting factors” to modify the initial projection based on BFI, especially if they show consistent trends at explaining over and underprojections. These parameters could include moisture, track roughness characteristics, even tie-ballast interface, or tie deflections.

- Due to inevitable variation and scatter, some sort of uncertainty, or statistical distribution should be eventually included to move from a deterministic analysis to a risk-based statistical analysis.
- The influence of ballast maintenance should eventually be incorporated as a better understanding of the effects of ballast maintenance are understood.

7. References

[1] Kish, A., "Ballast and Track Lateral Stability," AREMA Railway Roadbed and Ballast Symposium, Kansas, KS, 2020.

[2] Trevizo, M. C., "Restoration of Post-Tamp Stability," Association of American Railroads, Transportation Technology Center, Report No. WP-150, 1991.

[3] Kish, A., Sussmann, T., & Trosino, M., "Effects of Maintenance Operations on Track Buckling Potential," U.S. Department of Transportation, Washington, DC, 2003.

[4] McHenry, M., "Evaluation of Polymer Composite Tie Lateral Track Resistance at FAST," *Technology Digest,* 2017.

[5] Li, D., & Shust, W., "Investigation of Lateral Track Strength and Track Panel Shift Using AAR's Track Loading Vehicle," Association of American Railroads, Transportation Technology Center, Report No. R-917, Pueblo, CO, 1997.

[6] Li, D., & Shust, W., "Automated Measurements of Lateral Track Panel Strength and Examinations of Track Maintenance Effects Using AAR's Track Loading Vehicle," Association of American Railroads, Transportation Technology Center, Inc., Report No. R-918, Pueblo, CO, 1999.

[7] American Railway Engineering and Maintenance-of-Way Association, Manual of Railway Engineering, Landover, MD: AREMA, 2019.

[8] Selig, E. T., "Tensile zone effects on performance of layered systems," *Géotechnique,* vol. 37, no. 3, p. 247–254, 1987.

[9] Federal Railroad Admnistration, "Track Safety Standards Compliance Manual," Office of Safety Assurance and Compliance, U.S. Department of Transportation, Federal Railroad Administration, Washington, DC, 2019.

[10] Li, D., Hyslip, J., Sussmann, T., & Chrismer, S., Railway Geotechnics, CRC Press, 2015.

[11] Wilk, S. T., "Mitigation of differential movements at railroad bridge transition zones," University of Illinois at Urbana-Champaign, Urbana, IL, 2017.

[12] Mesri, G., & Vardhanabhuti, B., "Compression of granular materials," *Canadian Geotechnical Journal,* vol. 46, no. 4, p. 369–392, 2009.

[13] Jeffs, T., & Marich, S., "Ballast Characteristics in the Laboratory," in *Conference on Railway Engineering*, Perth, Australia, 1987.

[14] Sato, Y., "Japanese Studies on Deterioration of Ballasted Track," *International Journal of Vehicle Mechanics and Mobility,* vol. 24, no. 1995, p. 197–208, 2007.

[15] Shenton, M. J., "Ballast deformation and track deterioration," in *Track Technology*, University of Nottingham, 1984, p. 254–265.

[16] Dahlberg, T., "Some railroad settlement models—A critical review," in *Proceedings of the Institution of Mechanical Engineers, Part F: Journal of Rail and Rapid Transit*, 2001.

[17] Stark, T., Wilk, S., Thompson, H., Sussmann, T., Baker, M., & Ho, C., "Evaluating Fouled Ballast Using Seismic Surface Waves," in *2016 Joint Rail Conference*, Report No. V001T01A002, JRC2016-5714, Columbia, SC, 2016.

[18] Basye, C., & Li, D., "Evaluation of Falling Weight Deflectometer and Automatic Ballast Sampling Techniques for Track Substructure Investigation," *Railway Track and Structures,* vol. 110, no. 5, p. 15–17, 2014.

[19] Dyk Van, B., Edwards, J., Dersch, M., Ruppert, C., & Barkan, C., "Evaluation of dynamic and impact wheel load factors and their application in design processes," in *Proceedings of the Institution of Mechanical Engineers, Part F: Journal of Rail and Rapid Transit*, 2016.

[20] Chrismer, S., & Selig, E., "Mechanics-Based model to Predict Ballast-Related Maintenance Timing and Costs," University of Massachusetts Amherst, 1991.

[21] Klassen, M. J., Clifton, A. W., & Watters, B. R., "Track evaluation and ballast performance specifications," *Transportation Research Record,* no. 1131, 1987.

[22] Wnek, M. A., Tutumluer, E., Moaveni, M., & Gehringer, E., "Investigation of Aggregate Properties Influencing Railroad Ballast Performance," *Transportation Research Record,* vol. 2374, no. 1, p. 180–189, 2013.

[23] Selig, E., DelloRusso, V., & Laine, K., "Sources and causes of ballast fouling," Association of American Railroads, 1992.

[24] Qian, Y., Tutumluer, E., Hashash, Y., & Ghaboussi, J., "Effects of Ballast Degradation on Permanent Deformation Behavior from Large-Scale Triaxial Tests," in *Proceedings of the 2014 Joint Rail Conference*, Report No. JRC2014-3806, Colorado Springs, CO, 2014.

[25] Terzaghi, K., Peck, B., & Mesri, G., Soil Mechanics in Engineering Practice, Wiley, 1996.

[26] Bruzek, R., Stark, T., Wilk, S., Thompson, H., & Sussmann, T., "Fouled Ballast Definitions and Parameters," in *2016 Joint Rail Conference*, 2016.

[27] Read, D., Meddah, A., Li, D., Mui, W., TTCI, & Volpe Center, "Ground Penetrating Radar Technology Evaluation on the High Tonnage Loop: Phase 1," U.S. Department of Transportation, Federal Railroad Administration, Technical Report No. DOT/FRA/ORD-17/18, Washington, DC, 2017.

[28] Brown, M., & Li, D., "Ground Penetrating Radar Technology Evaluation and Implementation: Phase 2," U.S. Department of Transportation, Federal Railroad Administration, Technical Report No. DOT/FRA/ORD-17/19, Washington, DC, 2017.

[29] Basye, C., Sussmann, T., Thompson, H., Atherton, S., & Ericksen, A., "Ground Penetrating Radar (GPR) Technology Evaluation and Implementation on an FRA Research Car," in *Proceedings of 2018 American Railway Engineering and Maintentance-of-Way Association Conference*, Chicago, IL, 2018.

[30] Bankston, A., Wnek, M., & Wilk, S. T., "Implementation of BNSF Railway's Geometry Car-Based Ground Penetrating Radar Program," in *Proceedings of 2019 American Railway Engineering and Maintenance-of-Way Association Conference*, Minneapolis, MN, 2019.

[31] Feldman, F., & Nissen, D., "Alternative Testing Method for the Measurement of Ballast Fouling: Percentage Void Contamination," 2002.

[32] Indraratna, B., Su., L.-J., & Rujikiatkamjorn, C., "A new parameter for classification and evaluation of railway ballast fouling," *Canadian Geotechnical Journal,* vol. 48, p. 322–326, 2011.

[33] Tennakoon, N., Indraratna, B., Rujikiatkamjorn, C., & Nimbalkar, S. S., "The Role of Ballast-Fouling Characteristics on the Drainage Capacity of Rail Substructure," *Geotechnical Testing Journal,* vol. 35, no. 4, p. 1–12, 2012.

[34] Wilk, S. T., Basye, C., Brice, M., & Baillargeon, J., "Influence of rain events on performance of fine-contaminated ballast," in *Proceedings of the International Heavy Haul Conference*, Narvik, Norway, 2019.

[35] Wilk, S. T., Basye, C., Li, D., & Kerchof, B., "Use of Geosynthetics in Diverse Railroad Applications," in *Proceedings of Geo-Structural Aspects of Pavements, Railways, and Airfields (GAP 2019)*, Colorado Springs, CO, 2019.

[36] Ebrahimi, A., Tinjum, J. M., & Edil, T. B., "Large-Scale, Cyclic Triaxial Testing of Rail Ballast," University of Wisconsin-Madison, 2010.

[37] Han, X., & Selig, E., "Effects of fouling on ballast settlement," in *Proceedings of the 6th International Heavy Haul Railway Conference*, 1997.

[38] Kashani, H. F., & Hyslip, J. P., "Ballast Life and Effective Parameters," in *2018 Joint Rail Conference*, Report No. JRC2018-6264, V001T01A023, Pittsburge, PA, 2018.

[39] Nicks, J. E., "The Bump at the End of the Railway Bridge," Office of Graduate Studies of Texas A&M University, College Station, TX, 2009.

[40] Lackenberry, J., Indraratna, B., McDowell, G., & Christie, D., "Effect of confining pressure on ballast degradation and deformation under cyclic triaxial loading," *Géotechnique,* vol. 57, no. 6, p. 527–536, 2007.

[41] Anderson, W. F., & Fair, P., "Behavior of Railroad Ballast under Monotonic and Cyclic Loading," *Journal of Geotechnical and Geoenvironmental Engineering,* vol. 134, no. 3, p. 316–327, 2008.

[42] Thakur, P. K., Vinod, J. S., & Indraratna, B., "Effect of confining pressure and frequency on the deformation of ballast," *Géotechnique,* vol. 63, no. 9, p. 786–790, 2013.

[43] Stark, T. D., Wilk, S. T., & Rose, J. G., "Design and Performance of Well-Performing Railway Transitions," *Transportation Research Record: Journal of the Transportation Research Board,* vol. 2545, no. 1, p. 20–26, 2016.

[44] Indraratna, B., Thakur, P., & Vinod, J. S., "Experimental and Numerical Study of Railway Ballast Behavior under Cyclic Loading," *International Journal of Geomechanics,* vol. 10, no. 4, p. 136–144, 2010.

[45] Sun. Q. D., Indraratna, B., & Nimbalkar, S. S., "Deformation and Degradation Mechanisms of Railway Ballast under High Frequency Cyclic Loading," *Journal of Geotechnical and Geoenvironmental Engineering,* vol. 142, no. 1, 2015.

[46] Li, D., & Davis, D., "Transition of Railroad Bridge Approaches," *Journal of Geotechnical and Geoenvironmental Engineering,* vol. 131, no. 11, p. 1392–1398, 2005.

[47] Selig, E. T., & Waters, J. M., Track geotechnology and substructure management, Thomas Telford, 1994.

[48] Stark, T. D., & Wilk, S. T., "Root cause of differential movement at bridge transition zones," in *Proceedings of the Institution of Mechanical Engineers Part F Journal of Rail and Rapid Transit*.

[49] Schneider, P., Bolmsvik, & Nielsen, J., "In situ performance of a ballasted railway track with under sleeper pads," in *Proceedings of the Institution of Mechanical Engineers Part F Journal of Rail and Rapid Transit*, 2011.

[50] Hyslip, J., Kashani, H., & Trosino, M., "Ballast State of Good Repair," in *Proceedings of 2017 American Railway Engineering and Maintenance-of-Way Association Conference*, Indianapolis, IN, 2017.

[51] Bruzek, R., Thompson, H., & Banister, R., "Operation under a Fouled Ballast Waiver," in *Proceedings of 2018 American Railway Engineering and Maintenance-of-Way Association Conference*, Chicago, IL, 2019.

[52] "Bankston, A., & Wilk, S.," in *Proceedings of 2021 American Railway Engineering and Maintenance-of-Way Association Conference*, 2021.

[53] Kish, A., Clark, D., & Thompson, W., "Recent Investigations on the Lateral Stability of Wood and Concrete Tie Tracks," *AREMA Bulletin,* vol. 752, p. 248–265, 1995.

[54] Read, D., Thompson, R., Clark, D., & Gehringer, E., "Results of Union Pacific Concrete Tie Track Panel Shift Tests," *Technology Digest,* 2011.

Abbreviations and Acronyms

ACRONYMS	EXPLANATION
AN	Abrasion Number
SM	Absolute value of 62-foot surface profile (Surface Magnitude)
AREMA	American Railway Engineering and Maintenance-of-Way Association
AI	Angularity Index
AAR	Association of American Railroads
BFI	Ballast Fouling Index
CP	Canadian Pacific Railroad
CV	Coefficient of Variation
CWR	Continuously welded rail
DTS	Dynamic Track Stabilizer
FRA	Federal Railroad Administration
F&E Ratio	Flat and Elongated Ratio
FDL	Free Draining Layer
GPR	Ground Penetrating Radar
KDE	Kernel Density Estimate
MCO	Mid-chord Offset
MGT	Million Gross Tons
MAA	Modified Mill Abrasion
PVC	Percentage Void Contamination
RNT	Rail Neutral Temperature
RTLM	Railway Track Life-Cycle Model
SeiBIT	Seismic Ballast Inspection Tool
FI	Selig's Fouling Index
STPT	Single Tie Push Test
SD	Standard Deviation
SRI	Strategic Research Initiatives (AAR)
STI	Surface Texture Index
TOR	Top-of-Rail Survey Measurement
TLV	Track Loading Vehicle

ACRONYMS	EXPLANATION
TTC	Transportation Technology Center
TTCI	Transportation Technology Center, Inc.
UTP	Under Tie Pad
UIAIA	University of Illinois Aggregate Image Analyzer
VCI	Void Contamination Index
WILD	Wheel Impact Load Detector